

1 **Copernicus Atmosphere Monitoring Service - Regional Air Quality Production System v1.0**

2 Augustin Colette¹, Gaëlle Collin², François Besson², Etienne Blot², Vincent Guidard^{2,14}, Frédéric Meleux¹, Adrien Royer²,
3 Valentin Petiot^{2,14}, Claire Miller², Oihana Fermond², Alizé Jeant², Mario Adani^{5,16}, Joaquim Arteta¹⁴, Anna Benedictow¹⁰,
4 Robert Bergström¹¹, Dene Bowdalo⁸, Jorgen Brandt⁴, Gino Briganti⁵, Ana. C. Carvalho¹¹, Jesper Heile Christensen⁴, Florian
5 Couvidat¹, Ilaria D’Elia⁵, Massimo D’Isidoro⁵, Hugo Denier van der Gon¹², Gaël Descombes¹, Enza Di Tomaso^{3, 8}, John
6 Douros¹³, Jeronimo Escribano⁸, Henk Eskes¹³, Hilde Fagerli¹⁰, Yalda Fatahi⁹, Johannes Flemming³, Elmar Friese⁶, Lise Frohn⁴,
7 Michael Gauss¹⁰, Camilla. Geels⁴, Guido Guarnieri⁵, Marc Guevara⁸, Antoine Guion¹, Jonathan Guth¹⁴, Risto Hänninen⁹, Kaj
8 Hansen⁴, Ulas Im⁴, Ruud Janssen¹², Marine Jeoffrion², Mathieu Joly¹⁴, Luke Jones³, Oriol Jorba⁸, Evgeni Kadantsev⁹, Michael
9 Kahnert¹¹, Jacek W. Kaminski⁷, Rostislav Kouznetsov⁹, Richard Kranenburg¹², Jeroen Kuenen¹², Anne Caroline Lange⁶,
10 Joachim Langner¹¹, Victor Lannuque¹, Francesca Macchia⁸, Astrid Manders¹², Mihaela Mircea⁵, Agnes Nyiri¹⁰, Miriam Olid⁸,
11 Carlos Pérez García-Pando^{8,15}, Julia Palamarchuk⁹, Antonio Piersanti⁵, Blandine Raux¹, Miha Razinger³, Lennard Robertson¹¹,
12 Arjo Segers¹², Martijn Schaap¹², Pilvi Siljamo⁹, David Simpson¹⁰, Mikhail Sofiev⁹, Anders Stangel⁹, Joanna Struzewska⁷,
13 Carles Tena⁸, Renske Timmermans¹², Thanos Tsikerdekis¹³, Svetlana Tsyro¹⁰, Svyatoslav Tyuryakov⁹, Anthony Ung¹,
14 Andreas Uppstu⁹, Alvaro Valdebenito¹⁰, Peter van Velthoven¹³, Lina Vitali⁵, Zhuyun Ye⁴, Vincent-Henri Peuch³, Laurence
15 Rouil^{1, ^a}

16 ¹INERIS: Institut National de l’Environnement Industriel et des Risques, Verneuil en Halatte, 60550, France

17 ²Météo-France, Saint-Mandé, 94165, France

18 ³ECMWF: European Centre for Medium-Range Weather Forecasts, Reading, RG2 9AX, United Kingdom

19 ⁴Aarhus University: Roskilde, 4000, Denmark

20 ⁵ENEA: Italian National Agency for New Technologies, Energy and Sustainable Economic Development, Bologna, 40129,
21 Italy

22 ⁶Forschungszentrum Jülich GmbH, ICE-3, Institute of Climate and Energy Systems - Troposphere, 52428 Jülich, Germany

23 ⁷IEP-NRI: Institute of Environmental Protection - National Research Institute, Warsaw, 00-001, Poland

24 ⁸BSC: Barcelona Supercomputing Center, Barcelona, 08034, Spain

25 ⁹FMI, Finnish Meteorological Institute, Helsinki, 00-001, Finland

26 ¹⁰MET Norway: Norwegian Meteorological Institute, Oslo, 0372, Norway

27 ¹¹SMHI: Swedish Meteorological and Hydrological Institute. Norrköping, SE-601 76, Sweden

28 ¹²TNO: Netherlands Organisation for applied scientific research, Utrecht, 3584, The Netherlands

29 ¹³ KNMI: Royal Netherlands Meteorological Institute, De Bilt, 3730, The Netherlands

30 ¹⁴: Centre National de Recherches Météorologiques - UMR 3589 CNRS/Météo-France, Toulouse, 31000, France

31 ¹⁵. Catalan Institution for Research and Advanced Studies (ICREA), 08010, Barcelona, Spain

32 ¹⁶ Centro Euro-Mediterraneo sui Cambiamenti Climatici, 40127 Bologna, Italy

33 ^a: now at: ECMWF: European Centre for Medium-Range Weather Forecasts, Reading, RG2 9AX, United Kingdom

34 *Correspondence to:* Augustin Colette (augustin.colette@ineris.fr)

35

36 **Abstract**

37 The Copernicus Atmosphere Monitoring Service (CAMS) delivers a wide range of free and open products in relation to
38 atmospheric composition at global and regional scales. The CAMS Regional Service produces daily forecasts, analyses, and
39 reanalyses of air quality in Europe. This Service relies on a distributed modelling production by eleven teams in ten European
40 countries: CHIMERE (France), DEHM (Denmark), EMEP (Norway), EURAD-IM (Germany), GEM-AQ (Poland), LOTOS-
41 EUROS (The Netherlands), MATCH (Sweden), MINNI (Italy), MOCAGE (France), MONARCH (Spain), and SILAM
42 (Finland). The project management and coordination of the service is devoted to a Centralised Regional Production Unit. Each
43 model produces every day 24h analyses for the previous day and 97h forecasts for 19 chemical species over a spatial domain
44 at 0.1x0.1 degree resolution (approximately 10km x 10km) with 420 points in latitude and 700 in longitude and 10 vertical
45 levels. Six pollen species are also delivered for the surface forecasts. The eleven individual models are then combined into an
46 ENSEMBLE median. In total, more than 82 billion data points are made available for public use on a daily basis.

47 The design of the system follows clear technical requirements in terms of consistency in the model setup and forcing fields
48 (meteorology, surface anthropogenic emission fluxes, and chemical boundary conditions). But it also benefits from a diversity
49 in the description of atmospheric processes through the design of the eleven European Chemistry Transport Model (CTM)
50 involved.

51 The present article aims to provide a comprehensive technical documentation, both for the setup as well as for the diversity of
52 CTMs involved in the Service. We also include an overview of the main output products, their public dissemination and the
53 related evaluation and quality control strategy.

54 **1 Introduction**

55 The Copernicus Atmosphere Monitoring Service (CAMS, atmosphere.copernicus.eu/) is the core global and regional
56 atmospheric environmental service operated by the European Centre for Medium-Range Weather Forecast (ECMWF) within
57 the European Union Copernicus Earth Observation Programme. It provides a wide range of free, open, and quality assured
58 products in relation to global and regional air quality, inventory-based emissions, observation-based surface fluxes of
59 greenhouse gases and from biomass burning, solar energy, ozone and UV radiation, and climate forcings (Peuch et al., 2022).

60 We focus here on the regional production service (<https://atmosphere.copernicus.eu/european-air-quality-forecast-plots/>)
61 which provides daily 4-day forecasts of the main air quality species and analyses of the day before, as well as posterior re-
62 analyses using the latest observation datasets available for assimilation. It constitutes today the reference air quality forecasting
63 system at European scale by building upon a distributed production of eleven chemistry transport models operated in ten
64 European countries, with a Centralised Regional Production Unit to ensure a consistent implementation. Such a comprehensive
65 air quality forecasting system operated at continental scale has no equivalent in the world.

66 Air quality monitoring and forecasting constitute an essential activity to improve the knowledge of atmospheric composition
67 and air pollution patterns and identify short and long-term mitigation strategies. In the European legislation, the Directive (Ec,
68 2008) on ambient air quality and cleaner air for Europe of the European Parliament and of the European Council, defines limit
69 and target values for regulatory ambient air concentrations and improvement of ambient air quality to avoid, prevent or reduce
70 harmful effects on human health and the environment. To this end, it sets out the methodological requirements for the
71 assessment of ambient air quality in Member States which are based on the implementation of adequate monitoring systems,
72 typically relying on reference and standardised instruments operated at air quality monitoring stations whose data are reported
73 to the Air Quality e-reporting database maintained by the European Environment Agency (which subsequently makes the data
74 publicly available). A revision of the Ambient Air Quality Directive was adopted by the European Council in October 2024,
75 the revision includes amongst other features, a stronger emphasis on the use of air quality models as well as an explicit reference
76 to the Copernicus Atmosphere Monitoring Service as a trusted source of information products and supplementary tools to
77 support reporting activities in relation to forecasting and management of air pollution episodes.

78 Modelling comes as a complementary information on ambient air quality. Fitness for forecasting purposes of air quality
79 modelling has been widely documented (Zhang et al., 2012b, a), but air quality models are also essential to produce exposure
80 maps through data assimilation or data fusion. In such processes, the prior modelled estimates of surface air concentrations of
81 the main air pollutants are combined with in situ or remote sensing observations to produce improved mapping of air pollution,
82 typically for use in health impact assessment or epidemiological studies (Shaddick et al., 2020). Air quality modelling and
83 reanalyses are also typically used to anticipate ex-ante and assess ex-post the effectiveness of policy mitigation strategies. The

84 projections and hindcasts performed in the framework of the Convention on Long Range Transboundary Air Pollution
85 (CLRTAP) of the United Nations Economic Commission for Europe Geneva Air Convention and its Gothenburg Protocol
86 constitute a good example of atmospheric modelling activities in support of policy decisions at European scale (Maas and
87 Grennfelt 2016).

88 Whereas several European countries or selected metropolitan areas operate their own air quality modelling system, there is
89 also a need to produce air quality forecasts and analyses over the whole European continent: to provide background data for
90 those local systems (chemical boundary conditions), for the areas not covered by any national system, or just as complementary
91 information. The Copernicus Atmosphere Monitoring Service has played that role since 2015. It builds upon the earlier
92 research and development phases initiated since 2005 through European collaborative research and innovation projects: GEMS
93 (Hollingsworth, 2008) and MACC, MACC-II, and MACC-III (Marécal et al., 2015; Peuch et al., 2014).

94 The unique setup of the system allows it to reach an unprecedented level of quality and robustness by relying on a set of
95 stringent common requirements combined with a large variety of Chemistry-Transport Models (CTMs). Since 2022, an
96 ensemble of eleven CTMs have been used: CHIMERE (INERIS, France), DEHM (Aarhus Univ., Denmark), EMEP (Met
97 Norway), EURAD-IM (Forschungszentrum Juelich, Germany), GEM-AQ (IEP-NRI, Poland), LOTOS-EUROS (TNO and
98 KNMI, The Netherlands), MATCH (SMHI, Sweden), MINNI (ENEA, Italy), MOCAGE (Météo-France, France),
99 MONARCH (BSC, Spain), and SILAM (FMI, Finland). Using an ensemble of CTMs allows at the same time to minimize the
100 risk of failure in the daily operational production, and to increase the skill of the forecast (Galmarini et al., 2013). But
101 consistency in the implementation is key to ensure the continuous improvement of the system, hence the crucial role of the
102 CAMS Regional Central Production Unit led by Météo-France and INERIS.

103 Each model delivers every day 24h analyses and 97h forecast for 19 chemical species over a spatial domain at 0.1x0.1 degree
104 resolution (approximately 10km x 10km) with 420 points in latitude and 700 in longitude and 10 vertical levels. Additionally,
105 surface forecasts of six pollen species are delivered. With the 11 individual models and one ENSEMBLE median, it is a total
106 of almost 82 billion data point made available for public use every day.

107 The results of the CAMS Regional Service are made publicly available as quick looks on the website
108 atmosphere.copernicus.eu/european-air-quality-forecast-plots and the numerical outputs are disseminated on the Copernicus
109 Atmosphere Data Store (ADS): ads.atmosphere.copernicus.eu. The typical use of the forecasts is as background information
110 used by national and local air quality agencies, in addition to their knowledge about specific local air pollution sources. This
111 can be done either qualitatively by the consultation of available online viewers, or by using the numerical data to feed
112 downstream chemistry-transport, gaussian, or machine-learning models. The use of reanalyses is rather for policy applications

113 (for regulatory reporting obligations or to assess the impact policy interventions through trends analyses) or exposure
114 assessment in health impact studies.

115 The aim of the present article is to provide a transparent and detailed documentation to serve as a reference for the user of
116 CAMS Regional Air quality Products. It constitutes an update of the previous similar article devoted to the MACC regional
117 forecast system (Marécal et al., 2015), whereas the system was still in research mode at the time and not fully operational. A
118 focus on regional activities within the overall CAMS portfolio was also described in (Peuch et al., 2022). The CAMS Regional
119 production system has evolved continuously over the past. In the present article, we provide a detailed description of the system
120 as it stands in 2024. But since the near real time production of forecast and analysis remains available for public use with a 3-
121 year retention time, and reanalysis data remain available since the beginning of the production, we also provide some
122 information about the major evolutions in the recent past.

123 The main characteristics of the centralised production system are introduced in Section 2. This section covers the overall
124 production workflow, but also the common features and requirements which apply to the distributed production of individual
125 modelling teams such as the common external forcing data. Since the use of an ensemble of eleven different chemistry transport
126 models is an important specificity of the service, we devote a large part of the paper in Section 3 to summarize the formulation
127 of each model and how they adapt specifically to the requirement of the CAMS Regional Production System. The post-
128 processing as well as some elements regarding the evaluation and quality control or the main uses of the production are
129 presented in Section 4. In the conclusion (Section 5) we refer to the short and long-term development priorities to ensure the
130 performance and sustainability of the system over the long term.

131 **2 Centralised Regional Production Unit**

132 **2.1 Organisation of the production system**

133 The CAMS regional production relies on a quite unique ensemble of 11 individual models whose daily operation is distributed
134 amongst 11 modelling centres in ten European countries. The coordination is handled by the Central Regional Production Unit
135 (CRPU) which is led by Météo-France, with the support of INERIS for model development matters and reanalysis production
136 (Figure 1).

137 The CRPU defines the design of the regional production system under the auspices of ECMWF. This includes setting the
138 guidance and requirements for the implementation of individual models as well as continuous evolution in order to maintain
139 the system within the state of the art. The CRPU is also in charge of contractual matters and relations with the providers of
140 input data as well as the delivery of model results to the Atmosphere Data Store for public use (Section 4.3).

141 In earlier MACC phases and the first CAMS regional project, only 7 models were contributing to the distributed operational
142 production: CHIMERE, EMEP, EURAD-IM, LOTOS-EUROS, MATCH, MOCAGE, and SILAM. As of October 2019,
143 DEHM and GEM-AQ joined the operational system. As of June 2022, MINNI and MONARCH joined the production.

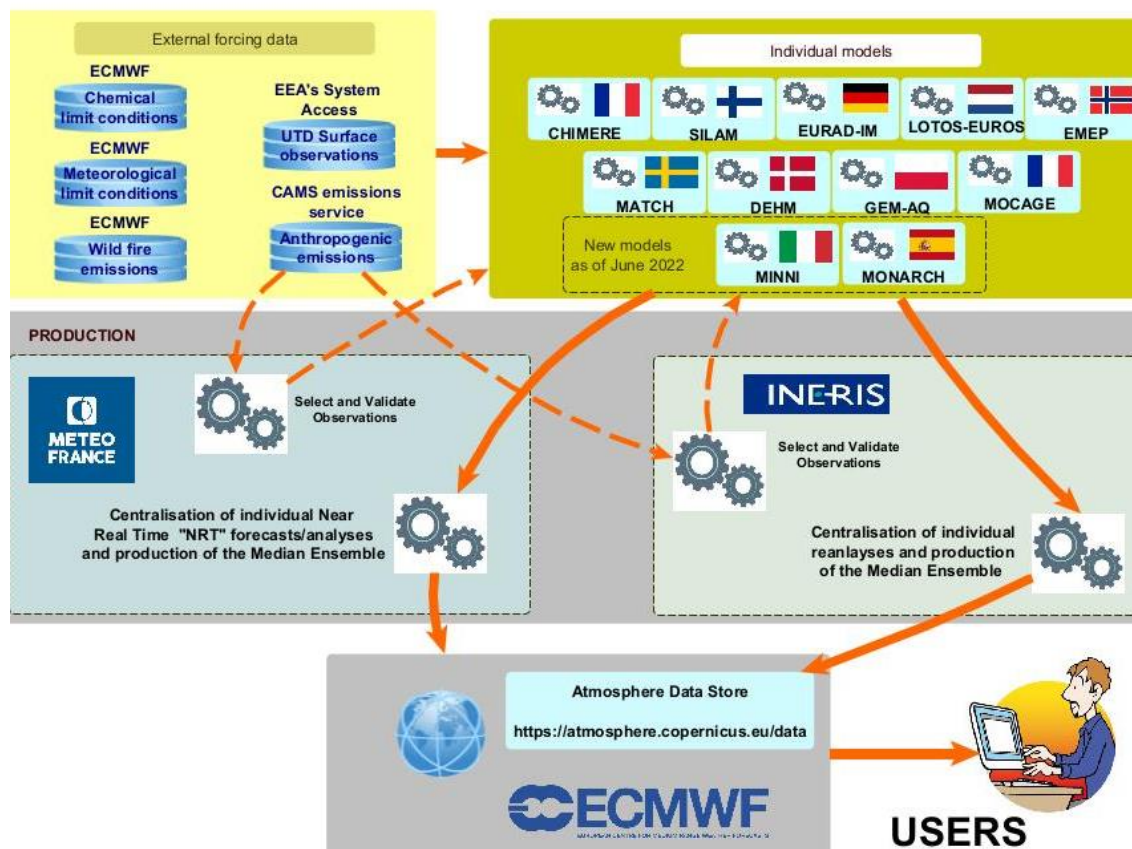


Figure 1: Schematic of the CAMS Regional Production workflow. Top-left the external forcings (anthropogenic emissions, meteorology, boundary conditions) and in-situ observations for assimilation and evaluation. Top right: eleven regional chemistry-transport model operated in ten European countries. Middle: Meteo-France (for the near real time) and INERIS (for the reanalysis) centralise the individual productions. Bottom: the results are disseminated to the Atmosphere Data Store.

2.2 Modelling products

The CAMS regional system includes both daily 4-days forecasts and several analysis products. All of them are provided from both eleven individual CTMs results and an ENSEMBLE product which is constituted by the median of individual models at each grid point (See also Section 4 on post-processing).

Hourly near-real time forecasts (NRT/FC) are released every day with a 4 days horizon (from 0 to 96hrs forecasts). They rely on chemistry-transport outputs, some of which are initialised on the basis of the previous analysis (see details in Section 3). The ENSEMBLE NRT/FC fields are made available publicly each day at 08:00 UTC for forecast horizon 0 to 48hrs (day 1

and day 2), and at 10:00 UTC for forecast horizon 49 to 96hrs (day 3 and days 4). All the forecasts are initiated at 00 UTC, the differentiated timing for the 48hr or 96hr lead time is only to account for longer production times.

The list of output species has been expanding gradually over the years. The choice of selected species accounts for user requests, especially with regards to downstream modelling needs (in the case where the CAMS regional system is used as forcing boundary conditions for smaller scale nested models), understanding air pollution episodes, and availability of observation data for evaluation and quality control (which is essentially focusing on PM₁₀, PM_{2.5}, NO₂, O₃ and pollens at present, but research grade measurement of the EMEP Monitoring Programme or the ACTRIS European Research Infrastructure are considered to strengthen the quality control procedures).

As of April 2025, the list of species in the NRT/FC includes the following gases: ozone (O₃), nitrogen oxide (NO), nitrogen dioxide (NO₂), carbon monoxide (CO), sulphur dioxide (SO₂), glyoxal (CHOCHO), formaldehyde (HCHO), ammonia (NH₃), total Non-Methane Volatile Organic Compounds (NMVOC, defined as the sum of the mass of the carbon atoms of all the VOC species of the chemical scheme of the model, excluding the methane and PANs species, and expressed in unit µg/m³ of carbon atoms), and total Peroxy-Acetyl Nitrates (PANs). Particulate matter (PM) are included as : PM_{2.5} (smaller than 2.5µm), PM₁₀ (smaller than 10µm). The following tracers in the PM_{2.5} fraction are also provided: sulphate (SO₄²⁻), nitrate (NO₃⁻), ammonium (NH₄⁺), total secondary inorganic aerosols (SIA), total elemental carbon (EC), EC fraction related to residential emissions, total organic matter. In the PM₁₀ fraction, the tracers include desert dust, sea salt and wildfires. In addition, six pollen species are included: birch, olive, grass, alder, mugwort and ragweed.

Hourly near-real time analysis (NRT/AN) are released each day by 12:00 UTC for the previous day. Here, each individual model is corrected to minimise error with observed air pollutant concentrations over Europe. For the latest reanalysis available on the ADS as of January 2024 (covering the year 2021), the list of species is: for O₃, NO, NO₂, CO, NH₃, NMVOC, PM₁₀, PM_{2.5}, PM₁₀ wildfires, PM₁₀ dust, EC total, EC residential, PAN, SIA, SO₂. For earlier years, not all of these species are available, and in the future the list will continue expanding to catch up with the full species set in the daily forecast production. Note that observations are available for assimilation only for NO₂, O₃, PM₁₀, and PM_{2.5}. Individual components contributing to the total PM₁₀ or PM_{2.5} mass are scaled according to the assimilation of total PM₁₀ or PM_{2.5} measurements, and pollen species are not assimilated.

The daily analyses products are supplemented by an interim reanalysis (IRA) and a validated reanalysis (VRA). Both rely on the same modelling tools as the NRT production, including assimilation strategy. But the observations taken into account differ. Acknowledging that for the NRT/AN production some observations can be missing or not validated, daily analyses are reproduced with a 20 days delay in the IRA. This time gap is considered sufficient to fix most failures in NRT data flows and maximise the number of available measurement data. The interim reanalysis is subsequently consolidated and delivered in the

186 first months of Y+1. Since all observations are only definitively validated by European member states by the end of the
187 following year (Y+1), the full year Y is reprocessed in Y+2 to produce the VRA of the corresponding year. As for NRT, the
188 production of IRA/VRA is also distributed across individual modelling teams which operate their own modelling system. The
189 CRPU (INERIS in the case of reanalyses) defines the common requirements in terms of model setup, input data (meteorology,
190 emissions, and assimilated observations) and centralised the verification and production of the ENSEMBLE product.

191 **2.3 Air quality observations**

192 The gathering, filtering and selection of observations is centralised by the CRPU and subsequently disseminated to individual
193 modelling teams which apply different assimilation algorithms even though the exact same stations are assimilated by each
194 model (see details in Section 3). All observation data are obtained from the Air Quality e-reporting database¹ maintained by
195 the European Environment Agency where near real time “up-to-date” (UTD) and validated observations are reported, in
196 particular for countries of the European Union which are expected to do so with respect to the European Directives.

197 An important step lies in the filtering and selection of data. For the NRT production (both FC and AN), the stations are clustered
198 using an objective classification which consists in building classes of stations which exhibit similar patterns of temporal
199 variability to differentiate background and proximity stations (Joly and Peuch, 2012). Originally (when the model had a
200 resolution of approximately 20x20km²), only the stations corresponding broadly to suburban and rural typologies were
201 included. But since November 2020, all stations falling in classes 1-7 of the Joly & Peuch classification are included, which
202 means broadly that urban background sites are taken into account while traffic and industrial sites are excluded. This way,
203 even if the spatial resolution of the CAMS Regional Production is 10x10km, we ensure the relevance of the modelling setup
204 to capture urban background air quality.

205 The design and use of this objective classification is particularly useful in NRT applications, which includes more outlying
206 data than the reanalyses. Such NRT applications are also less used for regulatory applications for which reanalyses are
207 preferred. This is why, the station classification in IRA and VRA follows the standard typology declared by the member states
208 in their reporting (even if it is admitted that it is not exempt from misclassification). In VRA and IRA, stations labelled as
209 traffic and industrial are strictly excluded and only background (urban, suburban, and rural) stations are included.

210 Approximately 2-third of the stations’ data are distributed by the CRPU for assimilation (both for NRT/AN and IRA&VRA),
211 while the rest of the data are kept for evaluation (see Section 4.2).

¹ <https://www.eea.europa.eu/data-and-maps/data/aqereporting-9>, last accessed 30/10/2024

212 This splitting is first performed using the station list used for VRA and IRA, therefore using only the sites for which member
213 states declared the typology as “background” that are available for the previous years (year-1 for IRA (Y-1) and year-2 for
214 VRA (Y-2)). Stations with less than 1 months of data are removed. The first prerequisite is to treat collocated stations together
215 for the pollutant pairs NO₂/O₃ and PM₁₀/PM_{2.5}. This prevents, for example, having the same station for NO₂ assimilation and
216 O₃ evaluation. The second prerequisite is to use a random selection process to ensure a good spatial coverage of stations in the
217 two listings. However, the construction of the assimilation and validation station sets is not entirely random: evaluation stations
218 are always selected near assimilation stations, while spatially isolated stations (typically in remote areas of Europe) are used
219 for assimilation. This classification is revised on an annual basis for each new production cycle of IRA and VRA to take into
220 account the evolution of the network.

221 The splitting obtained for the VRA and IRA production is subsequently translated for the NRT production. All the stations
222 from classes 1 to 7 belonging to the set of evaluation of VRA/IRA are tagged for NRT evaluation and all the stations that do
223 not belong to the evaluation of VRA/IRA are tagged for NRT assimilation (AN).

224 At present there is no centralisation of the dissemination of any satellite observation of atmospheric composition even if many
225 individual modelling teams already assimilate satellite data, and this is expected to further develop in the coming years (See
226 details in the presentation of individual models in Section 3).

227 **2.4 Modelling domain**

228 The modelling domain covers Europe within 25°W to 45°E longitude and 30°N to 72°N latitude at a 0.1°x0.1° resolution.
229 Whereas in earlier phases of the project some individual models were operating at slightly lower resolution (about 0.2°), today
230 all models operate on a native resolution of about 0.1°. Covering the whole region is a strong requirement, and all models
231 deliver data over the entire domain, which means that some of them perform the forecast on a slightly larger domain in order
232 to include a buffer area or cope with differing geographic projection (see details in Section 3). The spatial extent has evolved
233 marginally in recent years, it was only reaching up to 70°N until June 2019.

234 The strategy for the vertical discretisation is left open for individual contributing models, but there is a common requirement
235 in the delivery of model results on common vertical levels. As of January 2024, the complete list of vertical levels is: surface,
236 50m, 100m, 250m, 500m, 750m, 1000m, 2000m, 3000m, and 5000m above ground. This has evolved substantially in recent
237 years, only surface concentrations were provided in the earlier phases of CAMS, and different lists of vertical levels have been
238 archived in the past for near real time forecast, analyses, and reanalysis products.

239 **2.5 Meteorology and chemical boundary conditions**

240 The meteorological fields used to force the individual operational CTMs are from the European Centre for Medium-Range
241 Weather Forecasts (ECMWF) operational meteorological forecasts at high resolution based on the IFS model (Integrated
242 Forecasting System). The spatial resolution of the IFS forecast has increased in time, it is about 9km as of 2024. The exact list
243 of meteorological parameters used to drive the individual CTMs differs depending on the models (see details in Section 3).
244 Most of them use the forecast starting at 12:00 UTC on D–1 but there might also be some deviations to account for operational
245 constraints.

246 The chemical boundary conditions are also obtained from ECMWF but using the configuration including chemistry of the IFS:
247 IFS-COMPO referred to as CAMS-Global in this article (Flemming et al., 2015; Rémy et al., 2019) operating at approximately
248 40km spatial resolution. CAMS-Global runs forecasts twice daily from 00 and 12 UTC and the data are available every hour
249 (for surface fields) and every 3 hours (for above surface model- and pressure-level fields). The model results are made available
250 for further use as boundary conditions of regional models through different dissemination routes including the MARS archive
251 server of ECMWF, a dedicated ftp access for the regional CAMS operational models, and the atmosphere data store (ADS) of
252 Copernicus.

253 The list of species used as boundary conditions for the regional CAMS models is given in Table 2. Further details are available
254 through the CAMS User Support website² and (Morcrette et al., 2009). All aerosol species are provided as dry PM, except for
255 sea salt, whose mass and size is provided at a relative humidity of 80%. The mass of the corresponding dry sea salt is 1/4.3
256 smaller and the radius is half of the sea salt at relative humidity of 80%.

257 **2.6 Surface emissions**

258 **2.6.1 Anthropogenic emissions**

259 Using identical anthropogenic emissions in all the eleven individual models is essential for the consistency of the CAMS
260 Regional products. The so-called TNO-MACC-III (Kuenen et al., 2014) emission inventory was used for several years in the
261 past. Since June 2019, it has been replaced by the CAMS-REG emissions inventory, which is regularly updated (Kuenen et
262 al., 2022). The CAMS-REG inventory is based on official national totals of air pollutant emissions reported in compliance
263 with the European Directive on National Emission Reduction Commitments (2016/2284/EU) and the Gothenburg Protocol of
264 the LRTAP Convention. Additional processing is applied to ensure consistency in the dataset by making corrections and
265 performing some gap-filling where information is missing. A consistent spatial distribution for gridded emission datasets is

² <https://confluence.ecmwf.int/display/CKB/CAMS%3A+Global+atmospheric+composition+forecast+data+documentation>
(last accessed 30/10/2024)

266 applied at $0.05^\circ \times 0.1^\circ$ resolution. Since June 2021, the CAMS Regional production has used an improved version of the
267 CAMS-REG inventory which substituted national estimates of wood burning emission in order to cope with a well-established
268 inconsistency in the reporting of condensable emissions (Denier Van Der Gon et al., 2015).

269 The use of officially reported emissions induces a subsequent delay in the successive updates of the emission datasets. The
270 Emissions for year Y, are reported in March Y+2. Then they undergo verification, gap filling and spatialisation before being
271 considered for implementation in the CAMS Regional production. The emissions being used for the day-to-day forecasts are
272 thus generally based on national emissions reported about 3 years earlier. In order to cope with this limitation, the CAMS-
273 REG emission inventory developed a methodology to extrapolate the officially reported emissions to the most recent historical
274 year. The methodology basically consists in two steps. First, early available relevant activity data for different sectors are used
275 to extrapolate the trend in the activity, which are used to adjust future emissions. Second, for the historical years for which
276 emission data are available from CAMS-REG the trend in these is compared to the trend in the activities. If a significant trend
277 is found (here defined as $>3\%$ per year) the trend in the implied emission factor is determined by taking the ratio of the trend
278 in emissions and in activities, which is then projected into the future. The methodology has been validated for historical years
279 and overall works well, but such a method has also limitations, for instance it is not possible to predict sudden events such as
280 closure of power plants or industrial facilities, or implementation of emission reduction techniques in large facilities. This way,
281 the emission implemented in late 2024 in the regional production could be based on an estimate for the year 2023 (CAMS-
282 REG v7.1).

283 The common requirement to use CAMS-REG emissions in all CTMs is strictly enforced for the forecast. For the analysis, in
284 one of the models (Table 1) analysed concentrations are pulled away from the state that is physically related to the emissions
285 and therefore will not be strictly relatable anymore to specified required emissions. But none of the models use inverse
286 modelled emissions based on observation in the forecast.

287 Only the spatialised annual fluxes of NO_x , SO_x , NMVOCs, NH_3 , CO, PM_{10} and $\text{PM}_{2.5}$ emissions are prescribed for all models.
288 The subsequent disaggregation required in CTMs in terms of (i) hourly/daily/weekly/monthly profiles, (ii) vertical injection
289 height, and (iii) mapping towards model chemical species is left open for individual modelling teams. Default information is
290 nevertheless provided regarding the temporal disaggregation (Guevara et al., 2021) as well as the speciation of total VOC or
291 total PM on individual VOC species or aerosol species, respectively. NMVOC emissions in CAMS-REG are provided with
292 year-, sector- and country-dependent speciation profiles to breakdown total NMVOC to the 25 Global Emission Initiative
293 (GEIA) species, originally defined under the REanalysis of the TROpospheric chemical composition (RETRO) project
294 (Schultz et al., 2007). Each CAMS individual modelling team performs a remapping of the 25 GEIA NMVOC species to the
295 species of their corresponding gas phase chemical mechanism. Concerning PM, the default profiles provided in CAMS-REG
296 allow splitting coarse and fine PM emissions to primary organic carbon, elemental carbon, sulphates, sodium and others.

297 **2.6.2 Biogenic, natural and wildfire emissions**

298 Biogenic emissions are left to the choice of individual operational models, most of which include their own online calculation
299 of emissions from vegetation and other natural sources. They include soil emissions for (i) mineral dust resuspension, (ii) soil
300 NO_x or even (iii) sea salt within the European domain, but the agriculture related NH₃ emissions are issued from the
301 anthropogenic emission inventory.

302 The only coordination regarding ecosystem emissions concerns wildfires where all models are expected to use the Global Fire
303 Assimilation System (GFAS) product (Kaiser et al., 2012) provided by CAMS. GFAS is based on fire radiative power retrievals
304 from data of the Moderate Resolution Imaging Spectroradiometer (MODIS) instruments aboard the Terra and Aqua satellites.
305 GFAS provides hourly emission data with a 8-hr delay compared to real time. Each individual modelling team retrieves GFAS
306 emission when initiating their forecast. As the individual forecasts are initiated between 12:00 D-1 and 03:00 D+0 depending
307 on the regional systems, the only full day where GFAS wildfire emissions are available is D-2, and some systems also include
308 part of D-1 emissions. Each system therefore reconstructs a 24hr cycle of emission based either on D-2 only or also including
309 part of D-1 emissions. This cycle is used by all models for their analysis of D-1. For the forecast, persistence of this daily cycle
310 of emission is only maintained for D+0 and D+1 considering that the vast majority of wildfires in Europe are not persisting
311 for longer time periods.

312 **2.6.3 Pollen emission and dispersion**

313 The following pollen species are included in the CAMS Regional production: birch, grass, olive, ragweed, alder, and mugwort.
314 Their implementation in the individual operational CAMS models differ in terms of advection and deposition strategies, but
315 as for the anthropogenic air pollutants, the emission terms are coordinated following the original documentation of (Sofiev et
316 al., 2013) and subsequent updates for additional species. The pollen species differ in terms of their geographic distribution
317 (source masks), total amount of available pollen grains, start and end date of the season (heatsum thresholds), and the shape
318 of the season (source strength as function of time). The alder pollen emission model is similar to that of birch and olive, while
319 the mugwort source is a variation of the grass source. However, mugwort is implemented as five different sub-species, each
320 with its own spatially gridded start and end dates of the flowering season. Ragweed pollen follows the method described in
321 (Prank et al., 2013).

322 Once emitted, pollen species are advected in the model in the same way as other chemically inert species and are subject to
323 gravitational settling and wet scavenging over time.

3 Individual Model Description

3.1 CHIMERE

3.1.1 Model Overview

CHIMERE is a multi-scale CTM developed jointly by LMD, INERIS and LISA (Menut et al., 2021). Its development was initiated in the early 2000s (Menut et al., 2000; Honoré et al., 2000) and it has since then pioneered operational national air quality forecasting in France (Rouïl et al., 2009). It is also extensively used for long-term simulations for emission control scenarios (Colette et al., 2013; Meleux et al., 2007; Colette et al., 2015). It runs over a range of spatial scale from the hemispheric to the urban scale, with resolutions from 100km to 1km (Colette et al., 2014; Bessagnet et al., 2017). The exact model version used since June 2021 in the CAMS Regional Production is CHIMERE v2020r1.

3.1.2 Model geometry

For the CAMS regional forecasts, CHIMERE uses a regular latitude-longitude grid with a $0.1^\circ \times 0.1^\circ$ resolution which covers 25°W to 45°E and 30°N to 72°N and 9 vertical levels, extending from the surface up to 500 hPa, a lowermost layer about 20m deep and about 7 layers below 2 km. No vertical downscaling is applied and concentrations in the lowermost model layer are considered representative of the surface.

3.1.3 Forcing Meteorology

The forcing meteorology is retrieved from the IFS model vertical layers covering the CHIMERE vertical extent on a $0.1^\circ \times 0.1^\circ$ horizontal grid resolution with a temporal resolution of 3 hours. The forecast released at 00:00UTC of the previous days is used. The three-dimensional meteorological parameters included to force the CHIMERE forecast are horizontal wind components, temperature, specific humidity, orography, rain water/snow mixing ratios, cloud liquid and ice water contents. The 2D variables included are: surface temperature, surface pressure, large scale and convective precipitations, boundary layer height, sensible and latent heat fluxes at surface, surface solar radiation downwards, soil parameters (water and temperature) for 4 layers (0-7 cm, 7-28 cm, 28-100 cm, 100-255 cm), sea ice cover, and snow depth.

3.1.4 Chemical initial and boundary conditions

Lateral and top boundary conditions are taken from chemical species available in CAMS-Global forecast model of the previous day at 3hr temporal resolution. The full list of species used from CAMS-Global is given in Table 2. The forecasts are initialised by the CHIMERE forecasts of the previous day.

350

351 **3.1.5 Emissions**

352 The common annual anthropogenic emissions CAMS-REG are implemented as explained in Section 2.5.1. Temporal
353 disaggregation is based on TNO time profiles provided with CAMS-REG. Chemical disaggregation for VOCs is based on
354 (Passant, 2002). PM components are speciated using the splits provided with the CAMS-REG database.

355 Biogenic VOC emissions are computed online with the MEGAN 2.10 algorithm (Guenther et al., 2012) implemented in
356 CHIMERE and uses high spatiotemporal data LAI (30 arcsec every 8 days) generated from MODIS (Yuan et al., 2011).
357 Biogenic emission factors are estimated based on the 30 arcsec USGS (US Geophysical Survey) land-use database and the
358 emission factors provided for each functional type by (Guenther et al., 2012).

359 The hourly GFAS wildfire emission for D-2 (i.e. the last full day available when launching the forecast system) are used for
360 the analysis (D-1) and the first two days of the forecast (D+0 and D+1). Fire emissions are set to zero for the remainder of the
361 forecast horizon.

362 Dust production within the European domain is included. It is based on the dust production model optimised by (Menut et al.,
363 2005) using saltation (Marticorena and Bergametti, 1995) and cohesion kinetic energies scheme (Alfaro and Gomes, 2001).

364 **3.1.6 Solver, advection and mixing**

365 The numerical time solver is based on a splitting operator which solves separately transport (including deposition and
366 emissions), chemistry and aerosol formation.

367 Advection is based on the Piecewise Parabolic Method 3d order scheme (Colella and Woodward, 1984). Vertical turbulent
368 mixing takes place only in the boundary layer. The formulation uses K-diffusion parameterisation (Troen and Mahrt, 1986),
369 without counter-gradient term.

370 **3.1.7 Deposition**

371 Dry deposition of gaseous and particle species is parameterised as a downward flux out of the lowest model layer where the
372 deposition velocity is described through a resistance analogy (Wesely, 1989). Wet deposition of particles and gases are
373 computed by using a polydisperse distribution of rain droplets based on (Willis and Tattelman, 1989) and by computing the
374 efficiency of the collision. Below-cloud scavenging of gases is assumed irreversible and is therefore only accounted for the
375 most soluble compounds (HNO_3 , H_2O_2 , HCl , SO_2 and NH_3). In-cloud scavenging is accounted for all gases by computing the
376 gaseous and aqueous phases partitioning based on Henry's law constants and the pH of the clouds. Scavenging by snow is also
377 accounted for and is based on (Chang, 1984) for gases and on (Wang et al., 2014) for particles.

378 **3.1.8 Chemistry and aerosols**

379 In order to optimise computing time, the reduced MELCHIOR2 mechanism with 44 species and about 120 reactions is derived
380 from the full mechanism MELCHIOR (Derognat et al., 2003). The sectional aerosol module accounts for 7 species and 10 bins
381 from 10nm to 40µm (primary particle material, nitrate, sulphate, ammonium, biogenic secondary organic aerosol SOA,
382 anthropogenic SOA and water). Photolytic rates are computed according to (Mailler et al., 2016). The aerosol module is
383 described in great details in (Couvidat et al., 2018) and accounts for condensation, nucleation, and condensation/evaporation.
384 Aerosol thermodynamic equilibrium is achieved using the ISORROPIA model version 2.1. The secondary organic aerosol
385 formation mechanism used in the operational forecasting version of CHIMERE is described in (Bessagnet et al., 2008).

386 **3.1.9 Assimilation system**

387 The CHIMERE assimilation for operational purposes relies on a kriging based approach to assimilate hourly concentration
388 values for correcting the raw model results. For the analysis period, linear regression between a selected set of observations
389 (excluding mountain and proximity sites) and the raw CHIMERE model is performed (in moving neighbourhood). The
390 experimental variogram of the regression residuals is then computed and a variogram model is fitted; the model adequacy is
391 checked by cross validation. Ultimately, observations are kriged with the CHIMERE model as external drift (in moving
392 neighbourhood). This method is applied for O₃ and NO₂. For PM₁₀ and PM_{2.5}, an ordinary co-kriging of the observations (main
393 variable) and CHIMERE (secondary variable) is applied to ensure consistency between both pollutants. Only in-situ surface
394 observations are used.

395 Further evolution of the CHIMERE assimilation system using an ensemble Kalman Filter approach is under development, in
396 particular to pave the way for assimilation of satellite data. It is has however not yet demonstrated to provide better skill score
397 than the geostatistical method.

398

399 **3.2 DEHM**

400 **3.2.1 Model Overview**

401 The Danish Eulerian Hemispheric Model (DEHM) is a 3-dimensional, offline, large-scale, Eulerian, atmospheric chemistry
402 transport model developed to study long-range transport of air pollution in the Northern Hemisphere. DEHM was originally
403 developed in the early 1990's in order to study the atmospheric transport of sulphur-dioxide and sulphate into the Arctic
404 (Christensen, 1997; Heidam et al., 2004). The model has been modified, extended and updated continuously since then and
405 now includes a flexible setup with the possibility for nested domains with higher resolutions over targeted areas (Brandt et al.,
406 2012; Geels et al., 2021). Apart from standard air pollution components and pollen, the DEHM model also includes mercury
407 (Christensen et al., 2004), CO₂ (Lansø et al., 2019) and POPs (Hansen et al., 2008).

408 **3.2.2 Model geometry**

409 The horizontal domain is defined on a regular latitude-longitude grid of 0.1° resolution with grid centre points covering
410 longitude 24.95°W to 44.95°E and latitude 30.05°N to 71.95°N. The vertical discretization is defined on 29 terrain-following
411 sigma levels up to about 100hPa. The 12 lowest layers are within the lowest 1 km of the atmosphere and the thickness of the
412 lowest layer is about 20m. The model includes an option for downscaling to the surface, but this is not applied in the operational
413 setup.

414 **3.2.3 Forcing Meteorology**

415 The forcing meteorology is retrieved from the IFS model vertical layers covering the DEHM vertical extent on a 0.2°x0.2°
416 horizontal grid resolution with a temporal resolution of 3 hours. The forecast released at 12:00 UTC of the previous days is
417 used. The meteorological parameters included to force the DEHM forecast are: 3D fields of the horizontal wind components
418 (U,V), temperature, specific humidity, cloud liquid water contents, cloud ice water contents, rain water contents, snow water
419 contents and fraction of cloud cover. The 2D fields are land-sea mask, surface pressure, geopotential height, skin temperature,
420 Ustar, large scale and convective rain, snow depth, sensible heat flux, latent heat flux, net solar radiation, boundary layer
421 height, 2 m temperature, 2 m dew point temperature, 10 m wind (U,V), albedo, sea ice area fraction and surface roughness.

422 **3.2.4 Chemical initial and boundary conditions**

423 Lateral and top boundary conditions are taken from chemical species available in CAMS-Global forecast model of the previous
424 day at 3 hr temporal resolution. The full list of species used from CAMS-Global is given in Table 2. The DEHM forecasts are
425 initialised by the DEHM forecasts of the previous day.

426 **3.2.5 Emissions**

427 The common annual anthropogenic emissions CAMS-REG are implemented as explained in Section 2.5.1. Originally the
428 temporal disaggregation was based on the GENEMIS tables, using a GNFR to SNAP matrix. From 2021 the new CAMS-
429 TEMPO (Guevara et al., 2021) profiles for annual, monthly, weekly and daily distribution of emissions have been included in
430 the operational version of DEHM. PM components are speciated using the splits provided with the CAMS-REG emissions.
431 The speciation of VOCs from the emission input of total non-methane VOCs is based on the global speciated NMVOC
432 emission database EDGAR 4.3.2 (Huang et al., 2017).

433 Natural emissions of the Biogenic Volatile Organic Compounds (BVOCs) isoprene and monoterpenes are estimated in the
434 DEHM model based on the MEGAN model (Zare et al., 2012). The production of sea salt aerosols at the ocean surface is
435 based on two parameterisation schemes describing the bubble-mediated sea spray production of smaller and larger aerosols.
436 In each time step, the production is calculated for 10 size bins and thereafter summed up to give an aggregated production of
437 fine (with dry diameters $<1.3 \mu\text{m}$) and coarse (with dry diameters ranging $1.3\text{--}6 \mu\text{m}$) aerosols (Soares et al., 2016). NO_x
438 emissions from soil are based on data from the Global Emissions Inventory Activity (Yienger and Levy, 1995) and from
439 lightning they are from (Price et al., 1997).

440 The hourly GFAS wildfire emissions are retrieved as soon as they are available (i.e. with a 8-hr delay from real time) in order
441 to obtain a recent 24hr cycle spanning over D-2 and D-1. This cycle is used for the analysis (D-1) and the first two days of the
442 forecast (D+0 and D+1). Fire emissions are set to zero for the remainder of the forecast horizon. Hourly injection heights are
443 calculated based on the hourly data of ‘Mean altitude of maximum injection’ and ‘Altitude of plume top’.

444 **3.2.6 Solver, advection and mixing**

445 The horizontal advection is solved numerically using the higher order Accurate Space Derivatives scheme, documented to be
446 very accurate (Dabdub and Seinfeld, 1994), especially when implemented in combination with a Forester filter (Forester,
447 1977). The vertical advection as well as the dispersion sub-models is solved using a finite elements scheme (Pepper et al.,
448 1979) for the spatial discretization. For the temporal integration of the dispersion, the q-method (Lambert, 1991) is applied and
449 the temporal integration of the 3-dimensional advection is carried out using a Taylor series expansion to third order. Time
450 integration of the advection is controlled by the Courant-Friedrich-Lewy (CFL) stability criterion. A wind adjustment is
451 included in order to ensure mass conservation.

452 The vertical diffusion is configured by K_z profiles (Hertel et al., 1995), based on Monin-Obukhov similarity theory for the
453 surface layer. This K_z profile is extended to the whole boundary layer by using a simple extrapolation, which ensures that K_z

454 is decreasing in the upper part of the boundary layer. The planetary boundary layer (PBL) height is obtained directly from the
455 IFS meteorology.

456 **3.2.7 Deposition**

457 Gaseous and aerosol dry-deposition velocities are calculated based on the resistance method for 16 different land-use types
458 and are configured similar to the EMEP model (Emberson et al., 2000b; Simpson et al., 2003), except for the dry deposition
459 of species on water surfaces, where the deposition depends on the solubility of the chemical species and the wind speed (Hertel
460 et al., 1995).

461 Wet deposition includes in-cloud and below-cloud scavenging and is calculated as the product of scavenging coefficients and
462 the concentration of gases and particles in air (Simpson et al., 2003). The in-cloud scavenging coefficients are dependent on
463 Henry's law constants and the rate at which precipitation is formed.

464 **3.2.8 Chemistry and aerosols**

465 The basic chemical scheme in DEHM now includes 74 different species and 158 reactions. It is based on the original scheme
466 by (Strand and Hov, 1994). The original Strand and Hov scheme has been modified in order to improve the description of,
467 amongst other things, the transformations of nitrogen containing compounds. The chemical scheme has been extended with a
468 detailed description of the ammonia chemistry through the inclusion of ammonia (NH_3) and related species: ammonium-nitrate
469 (NH_4NO_3), ammonium bisulphate (NH_4HSO_4), ammonium sulphate ($(\text{NH}_4)_2\text{SO}_4$) and particulate nitrate (NO_3) formed from
470 nitric acid (HNO_3) using an aerosol equilibrium approach with reaction rates dependent on the equilibrium (Frohn, 2004).
471 Furthermore, reactions concerning the wet-phase production of particulate sulphate have been included. The photolysis rates
472 are calculated by using a 2-stream version of the Phodis model (Kylling et al., 1995). The original rates for inorganic and
473 organic chemistry have been updated with rates from the chemical scheme applied in the EMEP model (Simpson et al., 2003).
474 SOA formation is included via a VBS-based approach (Bergström et al., 2012b; Zare et al., 2014). In total, DEHM includes
475 nine classes of particulate matter ($\text{PM}_{2.5}$, PM_{10} , TSP, seasalt < 2.5 mm, sea-salt > 2.5 mm, smoke from wood stoves, fresh black
476 carbon, aged black carbon, and organic carbon).

477 **3.2.9 Assimilation system**

478 Since the system upgrade in November 2020, the assimilation in DEHM has been based on an updated version of the
479 comprehensive 3D-var data assimilation scheme previously described in (Silver et al., 2016). The NMC method (Kahnert,
480 2008; Parrish and Derber, 1992) is used to estimate the background error covariance matrix. Two 1-year runs of DEHM using
481 analysed and forecasted ECMWF weather data are performed and their differences are used to estimate the background errors

482 in spectral space for O₃, NO₂, SO₂, CO, PM_{2.5}, and PM₁₀. For the analysis and reanalysis runs, surface in-situ observations of
483 the six species are assimilated at an hourly basis in DEHM.

484 **3.3 EMEP**

485 **3.3.1 Model Overview**

486 The EMEP MSC-W (European Monitoring and Evaluation Programme Meteorological Synthesizing Centre-West) model is a
487 chemical transport model developed at the Norwegian Meteorological Institute under the EMEP programme of the United
488 Nations Geneva Convention on Long-range Transboundary Air Pollution. The EMEP MSC-W model system allows several
489 options with regard to the chemical schemes used and the possibility of including aerosol dynamics. (Simpson et al., 2012)
490 described an early version of the EMEP MSC-W model in detail, while updates to the model since 2012 have been documented
491 and evaluated in the annual status reports of EMEP (see (Emep, 2023) and references therein). The forecast version of the
492 EMEP MSC-W model (EMEP-CWF) has been in operation since June 2006. The scheduled model updates in CAMS ensure
493 that the model version stays as close as possible to the official EMEP Open Source version³. Nevertheless, the EMEP-CWF
494 results and performances in CAMS might differ from those presented in the annual EMEP Status Reports, because of different
495 input data (emissions and meteorological driver) and model configurations (Forecast in EMEP-CWF versus Hindcast in EMEP
496 Status Reports).

497 **3.3.2 Model geometry**

498 The EMEP-CWF covers the European domain [30°N-76°N] x [30°W-45°E] on a geographic projection with a horizontal
499 resolution of 0.1° x 0.1° (longitude-latitude). Vertically the model uses 20 levels defined as hybrid coordinates. The 10 lowest
500 model levels are within the PBL, and the top of the model domain is at 100 hPa. The lowermost layer has a thickness of
501 approximately 50 meters. Vertical downscaling is used to derive surface concentrations at 3 meters altitude, as described in
502 (Simpson et al., 2012).

503 **3.3.3 Forcing Meteorology**

504 The forcing meteorology is retrieved from the IFS model vertical layers covering the EMEP vertical extent on a 0.1°x0.1°
505 horizontal grid resolution with a temporal resolution of 3 hours. The forecast released at 12:00UTC of the previous days is
506 used. The meteorological parameters included to force the EMEP forecast are: 3D fields of the horizontal wind components
507 (U,V), potential temperature, specific humidity, and cloud fraction. The 2D fields are land-sea mask, surface pressure, friction
508 velocity (u^*), large scale and convective precipitation, soil water, snow depth, fraction of snow cover, fraction of ice cover,
509 sensible heat flux, latent heat flux, sea surface temperature, 2m temperature and 2m relative humidity. The IFS forecasts do
510 not include 3D precipitation, which is needed by the EMEP-CWF model. Therefore, a 3D precipitation estimate is derived
511 from large-scale precipitation and convective precipitation (surface variables).

³ <https://github.com/metno/emep-ctm> (last accessed 30/10/2024)

512 **3.3.4 Chemical initial and boundary conditions**

513 Boundary conditions are taken from chemical species available in the CAMS-Global forecast model of the previous day at 3hr
514 temporal resolution (Table 2). In cases where CAMS-Global chemical boundary conditions are not available, default boundary
515 conditions are specified for O₃, CO, NO, NO₂, CH₄, HNO₃, PAN, SO₂, isoprene, C₂H₆, some VOCs, Sea salt, Saharan dust
516 and SO₄, as annual mean concentrations along with a set of parameters for each species describing seasonal, latitudinal and
517 vertical distributions. It should be noted however that unavailability of CAMS-Global is very exceptional (less than once a
518 year), and in general due to data transfer issues. The EMEP forecasts are initialised by the EMEP 3D VAR analysis of the
519 previous day.

520 **3.3.5 Emissions**

521 The common annual anthropogenic emissions CAMS-REG are implemented as explained in Section 2.5.1. Temporal
522 disaggregation is based on CAMS-REG-TEMPO v4.1. Chemical disaggregation for PM species follows the tables that come
523 with CAMS-REG while VOC emissions are speciated for each source-sector based on a lumped-species approach as described
524 in (Simpson et al., 2012; Bergström et al., 2022) .

525 The hourly GFAS wildfire emission for D-2 (i.e. the last full day available when launching the forecast system) are used for
526 the analysis (D-1) and the first two days of the forecast (D+0 and D+1). Fire emissions are set to zero for the remainder of the
527 forecast horizon.

528 The mineral dust source in the EMEP model is based on (Alfaro and Gomes, 2001; Fécan et al., 1998; Gomes et al., 2003;
529 Marticorena and Bergametti, 1995; Marticorena et al., 1997).

530 Natural emissions of Biogenic Volatile Organic Compounds (BVOCs) are based on Table 3 of (Simpson et al., 2012).

531 **3.3.6 Solver, advection and mixing**

532 The numerical solution of the advection terms of the continuity equation is based on the scheme of (Bott, 1989). The fourth
533 order scheme is utilized in the horizontal directions. In the vertical direction, a second order version applicable to variable grid
534 distances is employed.

535 The turbulent diffusion coefficients (K_z) are first calculated for the whole 3D model domain on the basis of local Richardson
536 numbers. The planetary boundary layer (PBL) height is then calculated using methods described in (Simpson et al., 2012). For
537 stable conditions, K_z values are retained. For unstable situations, new K_z values are calculated for layers below the mixing
538 height using the O'Brien interpolation.

539 **3.3.7 Deposition**

540 Parameterisation of dry deposition is based on a resistance formulation. The deposition module makes use of a stomatal
541 conductance algorithm which was originally developed for ozone fluxes, but which is now applied to all gaseous pollutants
542 when stomatal control is important (Emberson et al., 2000a; Simpson et al., 2003; Tuovinen et al., 2004). Non-stomatal
543 deposition for NH_3 is parameterised as a function of temperature, humidity, and the molar ratio SO_2/NH_3 .

544 Both gaseous and particulate nitrogen species are scavenged in the EMEP model according to their wet scavenging ratios and
545 collection efficiencies listed in Table S20 of (Simpson et al., 2012). In-cloud and sub-cloud scavenging ratios are considered
546 for gases and in-cloud scavenging ratios and sub-cloud scavenging efficiencies for particles.

547 **3.3.8 Chemistry and aerosols**

548 The EmChem19 chemical scheme couples the sulphur and nitrogen chemistry to the photochemistry and organic aerosol
549 formation using about 200 reactions between ca. 130 species (Bergström et al., 2022; Simpson et al., 2020b; Andersson-Sköld
550 and Simpson, 1999). The standard model version distinguishes 2 size fractions for aerosols, fine aerosol ($\text{PM}_{2.5}$) and coarse
551 aerosol ($\text{PM}_{2.5-10}$). The aerosol components presently accounted for are SO_4 , NO_3 , NH_4 , anthropogenic primary PM, organic
552 aerosols, and sea salt. Also aerosol water is calculated. Dry deposition parameterisation for aerosols follows standard
553 resistance-formulations, accounting for diffusion, impaction, interception, and sedimentation. Wet scavenging is treated with
554 simple scavenging ratios, taking into account in-cloud and sub-cloud processes. For secondary organic aerosol (SOA) a
555 volatility-basis set approach (Simpson et al., 2012) is used, which is a somewhat simplified version of the mechanisms
556 discussed in detail by (Bergström et al., 2012a). The EmChem19a scheme also has explicit toluene and benzene with different
557 SOA yields to the o-xylene surrogate that was used previously.

558 **3.3.9 Assimilation system**

559 The EMEP data assimilation system (EMEP-DAS) is based on the 3D-Var implementation for the MATCH model (Kahnert,
560 2008). The background error covariance matrix is estimated following the NMC method (Parrish and Derber, 1992). Recent
561 changes involved increased computational efficiency, tuning of model and observation representation uncertainties, and
562 improved impact of the assimilation in the vertical.

563 The EMEP-DAS delivers analyses of D-1 (driven by the operational IFS forecast of 00UTC of yesterday) assimilating O_3 ,
564 NO_2 , CO, $\text{PM}_{2.5}$, and PM_{10} surface observations.

565

566 **3.4 EURAD-IM**

567 **3.4.1 Model Overview**

568 The EURAD-IM (European Air pollution Dispersion - Inverse Model) system consists of 5 major parts: the meteorological
569 driver WRF (Weather Research and Forecasting⁴), the pre-processors EEP and PREP for preparation of anthropogenic
570 emission data and observations, the EURAD-IM Emission Model EEM, and the chemistry transport model EURAD (Hass et
571 al., 1995; Memmesheimer et al., 2004). EURAD-IM is a Eulerian meso-scale chemistry transport model involving advection,
572 diffusion, chemical transformation, wet and dry deposition and sedimentation of tropospheric trace gases and aerosols. It
573 includes 3d-var and 4d-var chemical data assimilation (Elbern et al., 2007) and is able to run in nesting mode.

574 **3.4.2 Model geometry**

575 To cover the CAMS domain from 25°E to 45°W and 30°N to 72°N, two lambert conformal projections subdomains with
576 respectively 45 km (199x166 grid boxes) and 9 km horizontal resolution (581x481 grid boxes) are used. The model domain
577 with the finer resolution covering the entire European part of the CAMS domain is nested within the halo domain with the
578 coarser resolution.

579 Variables are horizontally staggered using an Arakawa C grid. Vertically, the atmosphere is divided by 23 terrain-following
580 sigma coordinate layers between the surface and the 100 hPa pressure level. About 15 layers are within the first 2 km of the
581 atmosphere. The thickness of the lowest layer is about 35 m. No vertical downscaling is used to derive surface concentrations
582 from the first model level.

583 **3.4.3 Forcing Meteorology**

584 The meteorological forcing is obtained from 3-hourly IFS forecasts, but unlike the other models, the Weather Research and
585 Forecast (WRF) model is used to compute meteorological fields on the grid needed to drive the EURAD-IM CTM. This
586 intermediate processing is essentially for historical reasons as in the past the IFS temporal and spatial resolution required
587 interpolation for use in the CTM. A direct use of the IFS data to dynamically drive EURAD-IM has been developed and is
588 currently in the testing to enter the operational production in the near future.

589 **3.4.4 Chemical initial and boundary conditions**

590

⁴ <https://www.mmm.ucar.edu/models/wrf>, last accessed 30/10/2024

591 The CAMS-Global 00:00 UTC forecast for the previous day is extracted from the MARS archive at ECMWF using 36 model
592 levels with a temporal resolution of 3 hours. The full list of species used from the CAMS-Global model is given in Table 2.
593 Sea salt concentrations from CAMS-Global are divided by the constant 4.3 for the conversion from wet to dry mass.

594 **3.4.5 Emissions**

595 The common annual anthropogenic emissions CAMS-REG are implemented as explained in Section 2.5.1. The VOC and PM
596 split, the vertical distribution of area sources, and the emission strength per hour are calculated within the EURAD-IM CTM
597 with the distribution profiles provided with the CAMS-REG-AP_v6.1/2019 inventory (Kuenen et al., 2022). The VOC and
598 PM split depends on source category and country, the vertical distribution only depends on the source category. The CAMS-
599 TEMPO v4.1 (Guevara et al., 2021) profiles are used for the annual, monthly, weekly and daily distribution of emissions.

600 Biogenic emissions and NO_x emissions from soil are calculated within the EURAD-IM CTM with MEGAN (Guenther et al.,
601 2012). Fire emissions are taken into account using hourly data from GFASv1.2 product (Kaiser et al., 2012). Zero fire
602 emissions are assumed for D+2 and D+3 forecasts.

603 **3.4.6 Solver, advection and mixing**

604 The positive definite advection scheme of (Bott, 1989), implemented in a one-dimensional realisation, is used to solve the
605 advective transport. An operator splitting technique is employed (Mcrae et al., 1982) to handle the varying numerical
606 specificities of processes to be solved.

607 An Eddy diffusion approach is used to parameterize the vertical sub-grid-scale turbulent transport. The calculation of vertical
608 Eddy diffusion coefficients is based on the specific turbulent structure in the individual regimes of the planetary boundary
609 layer (PBL) according to the PBL height and the Monin-Obukhov length (Holtslag and Nieuwstadt, 1986). A semi-implicit
610 (Crank-Nicholson) scheme is used to solve the diffusion equation.

611 The sub-grid cloud scheme in EURAD-IM was derived from the cloud model in the EPA Models-3 Community Multiscale
612 Air Quality (CMAQ) modelling system (Roselle and Binkowski, 1999). Convective cloud effects on both gas phase species
613 and aerosols are considered.

614 **3.4.7 Deposition**

615 The gas phase dry deposition modelling follows the method proposed by (Zhang et al., 2003). Dry deposition of aerosol species
616 is treated size dependent, using the resistance model of (Petroff and Zhang, 2010) with consideration of the canopy. Dry
617 deposition is applied as lower boundary condition of the diffusion equation.

Wet deposition of gases and aerosols is derived from the cloud model in the CMAQ modelling system (Roselle and Binkowski, 1999). The wet deposition of pollen is treated according to (Baklanov and Sørensen, 2001).

Size dependent sedimentation velocities are calculated for aerosol and pollen species. The sedimentation process is parameterized with the vertical advective transport equation and solved using the fourth order positive definite advection scheme of (Bott, 1989).

3.4.8 Chemistry and aerosols

In the EURAD-IM CTM, the gas phase chemistry is represented by an extension of the Regional Atmospheric Chemistry Mechanism (RACM) (Stockwell et al., 1997) based on the Mainz Isoprene Mechanism (MIM) (Geiger et al., 2003). A 2-step Rosenbrock method is used to solve the set of stiff ordinary differentials equations (Sandu and Sander, 2006). Photolysis frequencies are derived using the FTUV model (fast TUV) according to (Tie et al., 2003). The radiative transfer model therein is based on the Tropospheric Ultraviolet-Visible Model (TUV) developed by (Madronich and Weller, 1990).

The modal aerosol dynamics model MADE (Ackermann et al., 1998) is used to provide information on the aerosol size distribution and chemical composition. To solve for the concentrations of the secondary inorganic aerosol components, a FEOM (fully equivalent operational model) version, using the HDMR (high dimensional model representation) technique (Nieradzik, 2005; Rabitz and Aliş, 1999), of an accurate mole fraction based thermodynamic model (Friese and Ebel, 2010) is used. The updated SORGAM module (Li et al., 2013) simulates secondary organic aerosol formation.

3.4.9 Assimilation system

The EURAD-IM assimilation system (Elbern et al., 2007) includes (i) the EURAD-IM CTM and its adjoint, (ii) the formulation of both background error covariance matrices for the initial states and the emission, and their treatment to precondition the minimisation problem, (iii) the observational basis and its related error covariance matrix, and (iv) the minimisation including the transformation for preconditioning. The quasi-Newton limited memory L-BFGS algorithm described in (Liu and Nocedal, 1989; Nocedal, 1980) is applied for the minimisation.

Currently assimilated in the EURAD-IM analysis and interim re-analysis are surface in-situ observations of O₃, NO₂, SO₂, CO, PM_{2.5}, PM₁₀.

644 **3.5 GEM-AQ**

645 **3.5.1 Model Overview**

646 GEM-AQ is a numerical weather prediction model where air quality processes (gas phase and aerosols) are implemented on-
647 line in the host meteorological model, the Global Environmental Multiscale (GEM) model, developed at Environment and
648 Climate Change Canada (Côté et al., 1998a). The model is used for operational air quality forecasting in Poland. Also, it is
649 used in a research project to investigate air quality in different environmental conditions (Struzewska and Kaminski, 2008,
650 2012; Struzewska et al., 2015; Struzewska et al., 2016).

651 **3.5.2 Model geometry**

652 The GEM-AQ model can be configured to simulate atmospheric processes over a broad range of scales, from the global scale
653 down to the meso-gamma scale. An arbitrarily rotated latitude-longitude mesh focuses resolution on any part of the globe. In
654 the CAMS regional production, the model is run in the limited area mode with a resolution of $0.1^\circ \times 0.1^\circ$ on a spherical
655 coordinate system. The coordinates are the following: lower-left ($17.4^\circ\text{N} / 22.1^\circ\text{W}$), upper-right ($58.6^\circ\text{N} / 86.6^\circ\text{E}$). In the
656 vertical, GEM-AQ uses the generalised sigma vertical coordinate system. It has terrain-following sigma surfaces near the
657 ground that transform to pressure surfaces higher in the atmosphere. The model top is set at 10 hPa.

658 **3.5.3 Forcing Meteorology**

659 The operational IFS model provides meteorological fields for the initial and boundary conditions used by the meteorological
660 part of the GEM-AQ model. The GEM-AQ model is started using the 12-hour forecast (valid at 00:00 UT of the following
661 day) as the initial conditions. The IFS data are used as boundary conditions with a nesting interval of 3 hours. The IFS
662 meteorological fields are computed from spectral coefficients for the target GEM-AQ grid. Meteorological fields, in the GEM-
663 AQ model domain, are constrained within the nesting zone (absorber), which is defined over 10 grid points on each lateral
664 boundary of the limited area domain.

665

666 **3.5.4 Chemical initial and boundary conditions**

667 Chemical species of the CAMS-Global forecast for the previous day are used with a temporal resolution of 3 hours (Table 2).
668 For dust aerosols, the three available size bins from the CAMS-Global model are distributed uniformly over the 10
669 corresponding bins in GEM-AQ. For organic matter aerosol, black carbon and sulphates, the same log-normal based profile
670 was applied. For organic aerosol and black carbon, hydrophobic and hydrophilic components were summed as “total organic
671 aerosol” and “total black carbon aerosol” before applying size-bin distribution profiles.

672 **3.5.5 Emissions**

673 The common annual anthropogenic emissions CAMS-REG are implemented as explained in Section 2.5.1. Based on this
674 information, emission fluxes for 15 gaseous species (9 hydrocarbons and 6 inorganics) and 4 aerosol components (primary
675 organic aerosol, black carbon, sulphates, nitrates) are derived using factors provided by TNO. Total emission fluxes for each
676 aerosol component are distributed into 12 bins in the GEM-AQ aerosol module.

677 Anthropogenic emissions are distributed within the 7 lowest model layers (up to 1350 m) with injection height profiles for
678 each of the GNFR sectors re-mapped for the GEM-AQ levels (Bieser et al., 2011). Temporal profiles modulating annual and
679 diurnal variation of emission fluxes for each GNFR are used.

680 For biogenic emissions, a temperature-dependent, monthly averaged MEGAN-MACC (Sindelarova et al., 2014) dataset for
681 the year 2010 was used specifically to avoid the short-term variability of reactive biogenic VOCs that would otherwise be
682 generated in an online approach. In contrast to the online method, this approach provides an anticipated variability range,
683 particularly by reducing the influence of online factors such as meteorological errors and extreme values.

684 **3.5.6 Solver, advection and mixing**

685 The set of non-hydrostatic Eulerian equations (with a switch to revert to the hydrostatic primitive equations) maintains the
686 model's dynamical validity right down to the meso-gamma scales. The time discretization of the model dynamics is fully
687 implicit, 2 time-level (Côté et al., 1998b; Côté et al., 1998a). The spatial discretization for the adjustment step employs a
688 staggered Arakawa C grid that is spatially offset by half a mesh length in the meridional direction. It is second-order accurate,
689 whereas the interpolations for the semi-Lagrangian advection are of fourth-order accuracy.

690 Deep convective processes are handled by Kain-Fritsch convection parameterisation (Kain and Fritsch, 1990). The vertical
691 diffusion of momentum, heat and tracers is a fully implicit scheme based on turbulent kinetic energy (TKE) theory.

692 **3.5.7 Deposition**

693 The effects of dry deposition are included as a flux boundary condition in the vertical diffusion equation. Dry deposition
694 velocities are calculated from a 'big leaf' multiple resistance model (Wesely, 1989; Aamaas et al., 2013) with aerodynamic,
695 quasi-laminar layer, and surface resistances acting in series. The process assumes 15 land-use types and takes snow cover into
696 account. Wet deposition takes into account cloud scavenging for soluble gas species and aerosols.

697 **3.5.8 Chemistry and aerosols**

698 The gas-phase chemistry mechanism currently used in the GEM-AQ model is based on a modification of version 2 of the Acid
699 Deposition and Oxidants Model (ADOM) (Venkatram et al., 1988), derived from the condensed mechanism of (Lurmann et
700 al., 1986). The ADOM-II mechanism comprises 47 species, 98 chemical reactions and 16 photolysis reactions. In order to
701 account for background tropospheric chemistry, 4 species (CH_3OOH , CH_3OH , CH_3O_2 , and $\text{CH}_3\text{CO}_3\text{H}$) and 22 reactions were
702 added. All species are solved using a mass-conserving implicit time stepping discretization, with the solution obtained using
703 Newton's method. Heterogeneous hydrolysis of N_2O_5 is calculated using the on-line distribution of aerosol. Although the model
704 meteorology is calculated up to 10 hPa, the focus of the chemistry is in the troposphere where all species are transported
705 throughout the domain. To avoid the overhead of stratospheric chemistry, the ozone and NO_y fields are replaced above 100
706 hPa with those from the CAMS-Global model. Additionally, stratospheric columns for absorbing species used in photolysis
707 calculations (cf., ozone) are taken from the CAMS-Global model. Photolysis rates (J values) are calculated on-line every
708 chemical time step using the method described in (Landgraf and Crutzen, 1998). In this method, radiative transfer calculations
709 are done using a delta-two stream approximation for 8 spectral intervals in the UV and visible applying pre-calculated effective
710 absorption cross sections. This method also allows for scattering by cloud droplets and for clouds to be presented over a
711 fraction of a grid cell. The host meteorological model provides both cloud cover and water content. The J value package used
712 was developed for MESSy (Jöckel et al., 2006) and is implemented in GEM-AQ.

713 The current version of GEM-AQ has 5 size-resolved aerosol types, viz. sea salt, sulphate, black carbon, organic carbon and
714 dust as well as nitrates. The microphysical processes that describe the formation and transformation of aerosols are calculated
715 by a sectional aerosol module (Gong et al., 2003). The particle mass is distributed into 12 logarithmically spaced bins from
716 0.005 to 10.24-micron radius. This size distribution leads to an additional 60 advected tracers. The following aerosol processes
717 are accounted for in the aerosol module: nucleation, condensation, coagulation, sedimentation and dry deposition, in-cloud
718 oxidation of SO_2 , in-cloud scavenging, and below-cloud scavenging by rain and snow.

719 **3.5.9 Assimilation system**

720 Data assimilation in the GEM-AQ modelling system is done with Optimal Interpolation method (Robichaud and Ménard,
721 2014) and is applied to the forecast. Error statistics are computed with the Hollingsworth - Lönnberg (HL) method
722 (Hollingsworth and Lönnberg, 1986). It estimates the correlation length and the ratio of observation to model error variances
723 by a least-square fit of a correlation model against the sample of the spatial autocorrelation of observation-minus-model
724 residuals.

725 Currently, data assimilation is done at each forecast hour for O_3 , NO_2 , SO_2 , CO, PM_{10} and $\text{PM}_{2.5}$, using surface observations.

726

727 **3.6 LOTOS-EUROS**

728 **3.6.1 Model Overview**

729 The LOTOS-EUROS model is a 3D chemistry transport model aimed to simulate air pollution in the lower troposphere. The
730 model has been used in a large number of studies for the assessment of particulate air pollution and trace gases (e.g. O₃, NO₂)
731 (Hendriks et al., 2016; Schaap et al., 2013; Thürkow et al., 2021; Timmermans et al., 2022). A detailed description of the
732 model is given in (Manders et al., 2017). At present the version used in the production is v2.2.009.

733 **3.6.2 Model geometry**

734 The domain of LOTOS-EUROS is the CAMS regional domain from 25°W to 45°E and 30°N to 72°N. The projection is regular
735 longitude-latitude, at 0.1°x0.1° grid spacing. In the vertical and for the forecasts there are currently 12 model layers and 2 more
736 reservoir layers at the top, defined by coarsening in a mass conservative way the first 77 model levels of the IFS. For output
737 purposes, the concentrations at measuring height (usually 2.5 m) are diagnosed by assuming that the flux is constant with
738 height and equal to the deposition velocity times the concentration at height z (taken as average over the grid cell). This applies
739 for several of the gaseous species, namely O₃, NO, NO₂, HNO₃, N₂O₅, H₂O₂, CO, SO₂ and NH₃. For aerosols, the same
740 approach is utilized, only sedimentation velocity is used instead of deposition velocity.

741 **3.6.3 Forcing Meteorology**

742 The forcing meteorology is retrieved from the 00:00 and 12:00 UTC runs of the IFS model at hourly (surface fields) or 3-
743 hourly temporal resolution (model layer fields). The meteorological data is retrieved on a regular horizontal resolution of about
744 9 km and for all layers covered by the model's vertical extent. The meteorological variables included are 3-hourly 3D fields
745 for wind direction, wind speed, temperature, humidity and density, augmented by hourly 2D gridded fields of mixing layer
746 height, surface wind and temperature, precipitation rates, heat fluxes, cloud cover and surface variables snow depth, sea ice
747 cover and volumetric soil water.

748 **3.6.4 Chemical initial and boundary conditions**

749 The lateral and top boundary conditions for trace gases and aerosols are obtained from the CAMS-Global daily forecasts (see
750 Table 2). LOTOS-EUROS uses a bulk approach for the aerosol size distribution differentiating between a fine and a coarse
751 fraction, but for dust and sea salt there are 5 distinct size classes: ff: 0.1-1 µm, f:1-2.5 µm, ccc: 2.5-4 µm, cc: 4-7 µm, c:7-10
752 µm. When the chemical boundary conditions from CAMS-Global are missing (which is very rare, typically less than once a
753 year, and can, e.g., be due to delays in the file transfer or other serious technical issues at ECMWF), the model uses
754 climatological boundary concentrations derived from CAMS-Global data. The forecasts are initialised with the LOTOS-
755 EUROS forecast of the previous day.

756 3.6.5 Emissions

757 The common annual anthropogenic emissions CAMS-REG are implemented as explained in Section 2.5.1. Injection height
758 distribution from the EuroDelta study is implemented, which is per SNAP (or more recently, GNFR) category. Time profiles
759 used are defined per country and GNFR emission category type.

760 Biogenic NMVOC emissions are calculated online using actual meteorological data and a detailed landuse and tree species
761 database including emission factors from (Köble and Seufert, 2001). The isoprene emissions follow the mathematical
762 description of the temperature and light dependence of the isoprene emissions, proposed by (Guenther et al., 1993). Sea salt
763 emissions are parameterised following (Martensson et al., 2003; Monahan, 1986) from the wind speed at 10-meter height.

764 The fire emissions are taken from the near real-time GFAS fire emissions database. For the forecast, we assume persistence,
765 so that the latest downloaded emission for the specific hour is used. When the hourly emission is more than 3 days old, it is
766 set to zero.

767 Mineral dust emissions within the modelling domain are calculated online based on the sand blasting approach by (Marticorena
768 and Bergametti, 1995) with soil moisture inhibition as described by (Fécan et al., 1998). Finally, a parameterization using land
769 cover and temperature is used for handling soil NO_x emissions, based on (Yienger and Levy, 1995).

770 3.6.6 Solver, advection and mixing

771 The transport consists of advection in 3 dimensions, horizontal and vertical diffusion, and entrainment/detrainment. The
772 advection is driven by meteorological fields (u, v), which are input every 3 hours. The vertical wind speed w is calculated by
773 the model as a result of the divergence of the horizontal wind fields. A linear advection scheme is used to ensure tracer mass
774 conservation, which also allows more efficient parallelization and reduced model complexity. This scheme uses piece-wise
775 linear functions to define sub-grid concentrations, which is sometimes referred to as MUSCL ("Monotonic Upwind-centered
776 Scheme for Conservation Laws") following (Van Leer, 1984).

777 Vertical diffusion is described using the standard K_z theory. Vertical exchange is calculated employing the new integral scheme
778 by (Yamartino et al., 2007). For the forecasting set-up with 12 layers, atmospheric stability values and functions, including K_z
779 values, are derived based on the surface heat fluxes from ECMWF meteorology and similarity profiles following the IFS
780 approach (Ecmwf, 2021) to adapt for land-use specific conditions. For the 5-layer version in the assimilation, a correction is
781 made for the vertical diffusion to correct for the height difference between surface and mixing layer.

782 **3.6.7 Deposition**

783 The dry deposition in LOTOS-EUROS is parameterised following the resistance approach. The laminar layer resistance and
784 the surface resistances for acidifying components are described following the EDACS system (Van Zanten et al., 2010), the
785 deposition velocities for particles are based on (Zhang et al., 2001). Wet deposition is divided between in-cloud and below-
786 cloud scavenging. The in-cloud scavenging module is based on the approach described in (Seinfeld and Pandis, 1998) and
787 (Banzhaf et al., 2012).

788 **3.6.8 Chemistry and aerosols**

789 LOTOS-EUROS uses the TNO CBM-IV scheme, which is a modified version of the original CBM-IV (Gery et al., 1989).
790 N₂O₅ hydrolysis is described explicitly based on the available (wet) aerosol surface area (using $\gamma = 0.05$) (Schaap et al., 2004).
791 Aqueous phase and heterogeneous formation of sulphate is described by a simple first order reaction constant (Barbu et al.,
792 2009; Schaap et al., 2004). Inorganic aerosol chemistry is represented using ISORROPIA II (Fountoukis and Nenes, 2007)
793 and secondary organic aerosols formation based on a VBS scheme (Bergström et al., 2012a; Zare et al., 2014) will be included
794 in the operational forecast version in the future.

795 **3.6.9 Assimilation system**

796 The LOTOS-EUROS model is equipped with a data assimilation package with the ensemble Kalman filter technique (Curier
797 et al., 2012). The ensemble is created by specification of uncertainties for emissions (NO_x, VOC, NH₃ and aerosol), ozone
798 deposition velocity, and ozone top boundary conditions. Currently, data assimilation is performed for O₃, NO₂, PM₁₀ and PM_{2.5}
799 surface observations, OMI NO₂ is also assimilated.

800

801 **3.7 MATCH**

802 **3.7.1 Model Overview**

803 The Multi-scale Atmospheric Transport and Chemistry model (MATCH) (Robertson et al., 1999) is an off-line chemical
804 transport model (CTM) with a flexible design, accommodating different weather data forcing on different resolutions and
805 projections, and a range of alternative schemes for deposition and chemistry.

806 **3.7.2 Model geometry**

807 The model's geometry is taken from the input weather data. To reduce computational costs, the vertical resolution is reduced
808 compared to the ECMWF operational model by merging pairs of IFS vertical layers, while retaining the use of hybrid vertical
809 coordinates. The horizontal resolution in the MATCH simulation matches that of the meteorological forcing, which is currently
810 provided on a 0.1° latitude–longitude grid. The lowest 78 layers of the ECMWF model are lumped in 39 levels, which then
811 are used for the air quality simulations. The model top is at about 8000 m height. The model domain covers the area between
812 28.8° W to 45.8° E and 29.2° N to 72.0° N. The grid is an Arakawa C-grid with staggered wind components.

813 **3.7.3 Forcing Meteorology**

814 The forcing meteorology for MATCH forecasts is retrieved from the 12:00 UTC run of the IFS modelling system on a
815 0.1°×0.1° spatial grid and with a temporal resolution of three hour. For the analyses, the 00:00 UTC analysis of the IFS is used
816 at 0.2°×0.2° resolution. The reason for applying a coarser resolution in the analysis is twofold: 1) the delivery time is rather
817 short from when the in-situ observations are available, 2) the analysis increments are on a larger scale. The meteorological
818 variables included are 3D fields of the horizontal wind components (U, V), temperature, specific humidity, cloud cover, cloud
819 water content, cloud ice water content, and surface fields of surface pressure, logarithm of surface pressure, surface
820 temperature, sea surface temperature, snow depth, albedo, roughness height, total cloud cover, precipitation, and volumetric
821 soil water at the surface.

822 **3.7.4 Chemical initial and boundary conditions**

823 The lateral boundary conditions for trace gases and aerosols are obtained from the CAMS-Global forecasts at 3-hourly
824 resolution for the following species: O₃, CO, HCHO, NO, NO₂, SO₂, HNO₃, PAN, CH₄, C₃H₈, o-xylene, sulphate and C₂H₆
825 (see Table 2). In the event that the chemical boundary conditions from CAMS-Global would be missing (which has never
826 happened in practice but could in theory happen due to corruption or other technical issues), the model uses seasonal
827 climatological boundary concentrations instead.

828 **3.7.5 Emissions**

829 The common annual anthropogenic emissions CAMS-REG are implemented as explained in Section 2.5.1. Temporal
830 disaggregation is based on the GENEMIS tables (Ebel et al., 1997), using a GNFR to SNAP matrix. The vertical distribution
831 of the emissions depends on the sector. Near-surface emission sources (SNAP 2,6,7,8,10) are distributed in the lowest 90 m;
832 for other sectors the emissions are allocated over varying model levels up to a maximum of about 1100 m height. According
833 to the sector, the anthropogenic VOC emissions are split into the MATCH chemical mechanism surrogate species: C₂H₆,
834 NC₄H₁₀, C₂H₄, C₃H₆, OXYLENE, BENZENE, TOLUENE, CH₃OH, C₂H₅OH, HCHO, CH₃CHO, CH₃COC₂H₅; the particulate
835 matter components elemental carbon, organic matter, anthropogenic dust (other than soil and road dust) are allocated to two
836 bins (PM_{2.5} and PM-coarse), as well as the road dust estimated according to (Schaap et al., 2009) and (Omstedt et al., 2005),
837 and the teluric dust calculated according to (Zender et al., 2003).

838 Biogenic emissions of isoprene, monoterpenes and sesquiterpenes are calculated following (Simpson et al., 2012; Simpson et
839 al., 1995; Bergström et al., 2012a), taking into account temperature at 2 m, radiation fluxes and the vegetation cover.

840 The dimethyl sulphide - DMS – emissions from the Ocean and Baltic Sea are also considered; whereas the particulate matters
841 from sea salt are calculated according to the parameterisation proposed by (Sofiev et al., 2011).

842 The GFAS biomass burning emissions are taken into the model mapping the following species into the MATCH chemical
843 mechanism: NO_x, SO₂, CO, CH₄, C₂H₄, C₂H₆, C₃H₆, C₄H₁₀, C₈H₁₀, benzene, toluene, CH₃OH, C₂H₅OH, formaldehyde,
844 acetaldehyde, OC, BC, PM_{2.5}, and PM₁₀. The vertical injection is made by a parabolic curve with central height taken from the
845 GFAS INJH parameter. In case the injection height is missing for a GFAS emission cell this is assigned from some neighbour
846 height present. The diurnal emission profile is based on the D-1 GFAS hourly data filled up with GFAS data for D-2 for the
847 not yet available hours in D-1. This diurnal hourly profile is repeated throughout the forecast.

848 **3.7.6 Solver, advection and mixing**

849 Mass conservative transport schemes are used for advection and turbulent transport. The advection is formulated as a Bott-like
850 scheme (Robertson et al., 1999). A second order transport scheme is used in the horizontal as well as the vertical. The vertical
851 diffusion is described by an implicit mass conservative first order scheme, where the exchange coefficients for neutral and
852 stable conditions are parameterized following (Holtslag and Nieuwstadt, 1986). In the convective case the turbulent Courant
853 number is directly determined from the turnover time in the boundary layer.

854 Part of the dynamical core is the initialisation and adjustment of the horizontal wind components. This is a very important step
855 to ensure mass conservative transport. The initialisation is based on a procedure proposed by (Heimann and Keeling, 1989),

856 where the horizontal winds are adjusted by means of the difference between the input surface pressure tendency, and the
857 calculated pressure tendency assumed to be an error in the divergent part of the wind field.

858 Boundary layer parameterisation is based on surface heat and water vapour fluxes as described by (Van Ulden and Holtslag,
859 1985) for land surfaces, and (Burridge, 1977) for sea surfaces. The boundary layer height is calculated from formulations
860 proposed by (Zilitinkevich and Mironov, 1996) for the neutral and stable case, and from (Holtslag et al., 1995) for the
861 convective case. These parameterisations drive the formulations for dry deposition and vertical diffusion.

862 **3.7.7 Deposition**

863 Dry deposition of gases and aerosols is modelled using a resistance approach (based on the scheme in (Simpson et al., 2012)),
864 which includes stomatal and non-stomatal pathways for vegetated surfaces. In the current operational system, the model applies
865 this scheme across various physiographic tiles derived from the CLC/SEI inventory⁵ (Simpson et al., 2012). MATCH uses 3D-
866 precipitation (estimated in the model, based on the surface precipitation and 3D cloud water information from the IFS forecast)
867 and separates wet scavenging into in-cloud and sub-cloud scavenging. For most gaseous components the scavenging is
868 assumed to be proportional to the precipitation intensity (with higher scavenging ratios in-cloud than sub-cloud). For the
869 particulate components in-cloud scavenging is also treated using simple scavenging ratios while the sub-cloud scavenging is
870 treated using a scheme based on (Berge, 1993) with size dependent collection efficiencies (as in (Simpson et al., 2012)).

871 **3.7.8 Chemistry and aerosols**

872 The photochemistry scheme is based on the EMEP MSC-W chemistry scheme (Simpson et al., 2012), with a modified scheme
873 for isoprene, based on the so-called Carter-1 mechanism (Carter, 1996; Langner et al., 1998). The standard MATCH setup
874 used in CAMS treats particles as bulk aerosol in two size classes, fine ($PM_{2.5}$) and coarse ($PM_{2.5-10}$) particles. Particle formation
875 from gases include secondary inorganic aerosol (ammonium sulphate and nitrate) and secondary organic aerosol. Ammonium
876 nitrate equilibrium is calculated according to (Mozurkewich, 1993). Coarse nitrate formation from gas-phase HNO_3 is also
877 included (Strand and Hov, 1994). Secondary organic aerosol formation from oxidation of volatile organic compounds is treated
878 using a volatility basis set scheme based on (Hodzic et al., 2016). Exception is made for the isoprene oxidation for which the
879 chain of reactions is following the Carter-1 chemical mechanism, which has proven to give the comparable results with fewer
880 reactions (Carter, 1996; Langner et al., 1998).

⁵ www.sei.org/projects/sei-european-land-cover-map (last accessed 30/10/2024)

881 **3.7.9 Assimilation system**

882 The model for data assimilation is an integrated part of the MATCH modelling system. The data assimilation scheme as such
883 is a variational spectral scheme (Kahnert, 2008), implying that the background covariance matrices are modelled in spectral
884 space. The limitation is that covariance structures are described as isotropic and homogeneous. The advantage is that the
885 background error matrix becomes block diagonal, and there are no scale separations as the covariance between spectral
886 components are explicitly handled. The block diagonal elements are the covariance between wave components at model layers
887 and chemical compounds.

888 Modelling the background error covariance matrices is the central part in data assimilation. This is conducted by means of the
889 so-called NMC approach (Parrish and Derber, 1992). The CTM (MATCH) is run for a 3-month period for photochemistry and
890 aerosols with analysed and forecasted ECMWF weather data. The differences are assumed to mimic the background errors,
891 and the statistics in spectral space are generated for different combinations of the model compounds: O₃, NO₂, NO, SO₂, CO,
892 PM_{2.5}, PM₁₀.

893 The scheme is fully intermittent in hour-by-hour steps and the above-listed components are assimilated from in-situ
894 measurements. The analysed components are propagated by chemistry and transport into unobserved components as
895 NMVOCs, PAN and NH₃.

896

897 **3.8 MINNI**

898 **3.8.1 Model Overview**

899 MINNI (Italian Integrated Assessment Modelling System for supporting the International Negotiation Process on Air Pollution
900 and assessing Air Quality Policies at national/local level; (D'elia et al., 2021; Mircea et al., 2014) has been developed to support
901 the Italian Ministry for Environment and Territory and Sea. The core of the modelling system is the 3-dimensional offline
902 Eulerian CTM FARM (Flexible Air quality Regional Model, (Silibello et al., 2008) that accounts for the transport, chemistry
903 and removal of atmospheric pollutants.

904 **3.8.2 Model geometry**

905 For the CAMS regional forecast, the model is configured with a regular latitude-longitude grid of $0.15^\circ \times 0.10^\circ$ resolution.
906 The domain spans from -25° to 45.05° degree East and from 30° to 72° degree North. The model uses z-level terrain following
907 mesh with the first central grid point at 20 m AGL (above ground level) and the last one at 6290 m AGL. No vertical
908 downscaling is applied to extrapolate concentrations from 20 meters above the ground to the surface.

909 **3.8.3 Forcing Meteorology**

910 The forcing meteorology is retrieved from the 12:00 UTC run of the IFS modelling system on a $0.1^\circ \times 0.1^\circ$ spatial grid and with
911 a temporal resolution of one hour. The meteorological variables included are 3D fields such as temperature, relative humidity,
912 pressure and wind velocity and 2D fields such as boundary layer height, roughness length, albedo, sea surface temperature,
913 total cloud cover and precipitation.

914 **3.8.4 Chemical initial and boundary conditions**

915 The lateral and top boundary conditions for trace gases and aerosols are obtained from the CAMS-Global daily forecasts with
916 a 3-hr temporal resolution (see Table 2). The initial condition is taken from the previous forecast of the MINNI model.

917 **3.8.5 Emissions**

918 The common annual anthropogenic emissions CAMS-REG are implemented as explained in Section 2.5.1. Point emissions
919 are summed up to gridded emissions for each GNFR sector, since no information was available about the characterization of
920 the point sources in terms of injection height. Conservative mass horizontal interpolation has been applied to map the emissions
921 on the actual model domain. Vertical splitting has been applied for each GNFR sector adapting the vertical injection profiles
922 provided by TNO to the actual model levels. Temporal emission profiles for each GNFR sector, as they were provided by
923 TNO, have been applied considering local hour (i.e. the time zones shift has been taken into account).

925 PM_{2.5} has been speciated following the TNO table as a function of country and sector and AERO3 (Binkowski and Shankar,
 926 1995; Binkowski, 1999) species size fractions below 2.5µm. The coarse component (PM₁₀-PM_{2.5}) was associated to non-
 927 speciated coarse mode since MINNI dispersion model considers all the secondary aerosol fraction as PM_{2.5}. This method leaves
 928 the detailed chemical speciation out but ensures mass conservation.

929 The NMVOC speciation originated from the TNO table as a function of country and sector obtaining the v01-v25 species. The
 930 mapping among the v01-v25 species to SAPRC99 species has been done in agreement with the choices made and tested in the
 931 frame of EURODELTA III intercomparison exercise (Colette et al., 2017).

932 Biogenic emissions are computed with the MEGAN model v.2.04 (Guenther et al., 2006), and NO_x emissions from soil
 933 following (Williams et al., 1992) approach.

934 Erosion and resuspension of the dust are calculated by means of method proposed by (Vautard et al., 2005). Road dust
 935 emissions are parameterized following (Zender et al., 2003).

936 Fire emissions are taken into account using hourly data from the GFAS database considering emissions from D-1 for AN (D-
 937 1) and FC (D+0 and D+1, zero for the remaining days).

938 **3.8.6 Solver, advection and mixing**

939 FARM is a 3-dimensional Eulerian model with first order turbulence closure. Physical and chemical processes influencing the
 940 concentration fields within the modelling domain are described by a system of partial differential equations (PDE). The
 941 numerical integration of the above system of PDEs is performed by a method that splits the multi-dimensional problem into
 942 time dependent one-dimensional problems, which are then solved sequentially over the time step.

943 Partial differential equations involved in horizontal and vertical advection-diffusion operators are solved in FARM using the
 944 schemes employed in CALGRID model (Yamartino et al., 1992). In particular, horizontal advection-diffusion operators are
 945 solved using a finite elements method based on Blackman cubic polynomials. The coefficients of a cell-centered cubic
 946 polynomial are constrained to maintain high-accuracy and low-diffusion characteristics and to avoid undesirable negative
 947 concentrations. In addition, a filter is used for filling undesired short wavelength minima. The numerical integration of the
 948 vertical diffusion equation is performed in a hybrid way employing a hybrid semi-implicit Crank-Nicholson / fully implicit
 949 scheme (Yamartino et al., 1992).

950 The calculation of horizontal diffusion coefficients is based on Stress tensor formulation of (Smagorinsky, 1963) also including
951 a dependence on the local stability class and wind speed. For the calculation of vertical diffusion coefficients, the (Lange,
952 1989) approach to boundary layer scaling regimes is used. Mixing due to deep convection is not explicitly taken into account.

953 Two different schemes to compute the PBL scaling parameters are used. In the daytime, the (Maul et al., 1980) version of
954 (Carson, 1973)encroachment method is used. During night-time, the minimum value between (Nieuwstadt, 1981) and
955 (Venkatram, 1980) is used.

956 **3.8.7 Deposition**

957 The dry deposition velocities are modelled following a resistance analogy approach, as an inverse sum of a series of 3
958 resistances: the aerodynamic resistance, the quasi-laminar layer resistance and the surface resistance. Aerodynamic resistance
959 is dependent on surface characteristics and atmospheric stability conditions (described through friction velocity and Monin-
960 Obukhov length). Quasi-laminar layer resistance is parameterised using (Hicks et al., 1987). Surface resistance is approximated
961 as a set of parallel resistance associated with leaf stomata, leaf cuticles, lower canopy and surface soil, litter and water (Wesely,
962 1989). Deposition to water surfaces is based on (Slinn et al., 1978).

963 The deposition velocity of particulate species also depends on particle size distribution and density because of gravitational
964 settling. Sedimentation velocity acts in parallel to the other resistances. Hygroscopic growth is considered over water for
965 particles less than 2 μm . For particles ranging from 0.1 to 1 μm deposition velocity is computed as the inverse of the resistance
966 computed from canopy height, friction velocity and Monin-Obukhov length.

967 The parameterization of wet deposition follows the (Simpson et al., 2012) approach, including in-cloud and below-cloud
968 scavenging of gas and particles.

969 **3.8.8 Chemistry and aerosols**

970 The gas-phase chemical mechanism used for CAMS forecast is SAPRC-99 with the inclusion of Polycyclic aromatic
971 hydrocarbons (PAHs) and Mercury chemistry; moreover, a simplified aqueous phase mechanism is included for SO_2 oxidation
972 and chemical processes involving Mercury in both gas and aqueous phases.

973 A simple approach is used to estimate photolysis rates based on look-up tables to calculate the rate constants for photolysis
974 reactions (Nenes et al., 1998). Photolysis rates are computed and adjusted according to local solar zenith angle using an
975 empirical formula based on (Peterson, 1976) data.

976 The aerosols module is AERO3 (Binkowski and Shankar, 1995; Binkowski, 1999). In AERO3 the representation of the particle
977 size is three-modal (Aitken, accumulation and coarse), following lognormal distributions. The aerosol species included are
978 sulphate, nitrate, ammonium, anthropogenic primary and secondary organic aerosol, biogenic secondary organic aerosol,
979 elemental carbon, sea-salt and dust. The aerosol dynamics takes into account nucleation, condensation and coagulation
980 processes. The gas/particle mass transfer is implemented by means of ISORROPIA v1.7 (Nenes et al., 1998) and SORGAM
981 (Schell et al., 2001a) for secondary inorganic and organic aerosol, respectively.

982 **3.8.9 Assimilation system**

983 The assimilation scheme used is optimal interpolation: the correlation function is factorized in vertical and horizontal
984 components. The horizontal component has pollutant dependent fixed correlation length with a terrain-following exponential
985 decay. The vertical component is modelled with a Cressman function dependent on the boundary layer height. The system
986 assimilates NO₂, O₃, SO₂, CO, PM₁₀ and PM_{2.5}. In case of aerosol components, the correction applied to each of them is
987 proportional to their content in PM. At present, only data from surface stations are assimilated. More details are available in
988 (Adani and Uboldi, 2023).

989

990 **3.9 MOCAGE**

991 **3.9.1 Model Overview**

992 The MOCAGE 3D multi-scale Chemistry and Transport Model has been designed for both research and operational
993 applications in the field of environmental modelling. Since 2000, MOCAGE has been allowing to cover a wide range of topical
994 issues ranging from chemical weather forecasting, tracking and backtracking of accidental point source releases, trans-
995 boundary pollution assessment, assimilation of remote sensing measurements of atmospheric composition, to studies of the
996 impact of anthropogenic emissions of pollutants on climate change (Guth et al., 2018; Cussac et al., 2020).

997 **3.9.2 Model geometry**

998 For the CAMS Regional Service, MOCAGE operates on a regular latitude-longitude grid at 0.1 resolution covering the 28° to
999 72° North and 26°W to 46°E domain, for both forecast and assimilation. The products delivered for the CAMS service are
1000 issued from the regional domain only. In the vertical, 47 hybrid levels go from the surface up to 5 hPa, with approximately 8
1001 levels in the Planetary Boundary Layer (i.e. below 2km), 16 in the free troposphere and 24 in the stratosphere. The thickness
1002 of the lowest layer is about 40 m. There is no downscaling applied to surface concentration.

1003 **3.9.3 Forcing Meteorology**

1004 The forcing meteorology is retrieved from the IFS model vertical layers covering the MOCAGE vertical extent on a 0.1°x0.1°
1005 horizontal grid resolution with a temporal resolution of one hour for the 3 first forecast days and 3 hours for the last forecast
1006 day. The forecast released at 12UTC of the previous days is used. The meteorological parameters used for the dynamics
1007 calculation in MOCAGE are: horizontal and vertical winds, temperature, humidity, cloud fraction, surface pressure, albedo,
1008 precipitations and incoming radiative flux. The variables relevant for the deposition module are soil humidity and temperature,
1009 wind speed and direction, specific humidity, pressure at ground level, and sensible heat flux.

1010 **3.9.4 Chemical initial and boundary conditions**

1011 Chemical initial values in the regional domain are provided by MOCAGE 24h forecast from the day before. The boundary
1012 conditions are taken from global CAMS operational suite for the species (chemical and aerosols) that are distributed (see Table
1013 2). For aerosols, the 2 or 3 bins from CAMS-Global are summed to get total concentration and then distributed onto the 6
1014 MOCAGE bins considering Mean CAMS-Global bin size as emission modes. A factor 4.3 is applied to convert Sea Salt from
1015 wet to dry fractions. Aerm03 (of diameter larger than 10µm) is only marginally distributed within MOCAGE PM₁₀ sea salt
1016 because of the matching between bins and log-normal modes. For the species not included in Table 2, the concentrations from
1017 the MOCAGE global domain are used, which helps to introduce smoothly, on the horizontal as well as on the vertical, these
1018 chemical boundary conditions into the CAMS regional domain.

1019 **3.9.5 Emissions**

1020 The common annual anthropogenic emissions CAMS-REG are implemented as explained in Section 3.2. Temporal
1021 disaggregation is based on the GENEMIS tables (Ebel et al., 1997), using a GNFR to SNAP matrix. Chemical disaggregation
1022 for PM species and VOCs is based on sector and country-dependent split factors proposed by TNO.

1023 Isoprene biogenic emissions are computed online using MEGAN model (Guenther et al., 2012), while other biogenic emissions
1024 are computed from CAMS global biogenic emission inventory (version 3.1). NO_x soil emissions are taken from the CAMS-
1025 GLOB-SOILv2.2 emission inventory.

1026 Concerning biomass burning sources, GFAS emissions are emitted according to an ‘umbrella’ profile, with a maximum
1027 injecting height climatologically determined. GFAS “near real time” observation-based fire emissions are made available with
1028 a 8-hr delay. So that when the forecast system is initiated, most GFAS emission cover Day-2 of the forecast to be produced.
1029 As a consequence, the 2-day persistence is interpreted in a way that fire emissions are only applied for D+0.

1030 **3.9.6 Solver, advection and mixing**

1031 The chemical solver used is a semi-implicit solver as presented in (Cariolle and Teyssedre, 2007).

1032 Concerning physical and chemical parameterisations, an operator splitting approach is used. Parameterisations are called
1033 alternatively in forward and reverse order, with the objective to reduce systematic errors.

1034 Meteorological forcings are read every 3 hours from IFS input data, and are linearly interpolated to yield hourly values, which
1035 is the time-step for advection; smaller time-steps are used for physical processes and chemistry, but the meteorological
1036 variables are kept constant over each hour. MOCAGE is based upon a semi-lagrangian advection scheme (Williamson and
1037 Rasch, 1989), using a cubic polynomial interpolation in all 3 directions.

1038 For sub-gridscale transport processes, vertical diffusion is treated following (Louis, 1979) and transport by convection is from
1039 (Bechtold et al., 2001). Scavenging within convective clouds is following (Mari et al., 2000), allowing to compute wet removal
1040 processes directly within the convective transport parameterisation.

1041 **3.9.7 Deposition**

1042 Wet deposition in stratiform clouds and below clouds follows (Giorgi and Chameides, 1986). A description of MOCAGE
1043 surface exchanges module is presented in (Michou et al., 2005). The dry deposition parameterisation relies on a fairly classical
1044 surface resistance approach (Wesely, 1989), but with a refined treatment of the stomatal resistance, similar to the one used in

1045 Meteo-France numerical weather prediction models (Noilhan and Planton, 1989). Sedimentation of aerosol follows (Nho-Kim
1046 et al., 2004).

1047 **3.9.8 Chemistry and aerosols**

1048 The MOCAGE configuration for CAMS comprises 118 species and over 300 reactions and photolysis. It is a merge of reactions
1049 of the RACM scheme (Stockwell et al., 1997) with the reactions relevant to the stratospheric chemistry of REPROBUS
1050 (Lefevre et al., 1994). Aqueous chemistry for the formation of sulphate is represented, following (Ménégoz et al., 2009).
1051 Detailed heterogeneous chemistry on Polar Stratospheric Clouds (types I, II) is accounted for, as described in (Lefevre et al.,
1052 1994). Other heterogeneous chemistry processes are currently not included.

1053 Photolysis is taken into account using a multi-entry look-up table computed off-line with the TUV software version 4.6
1054 (Madronich, 1987). Photolysis depends on month (including monthly aerosol climatologies), solar zenith angle, ozone column
1055 above each cell (as the model extends to the mid-stratosphere, it is actually the ozone profile computed by MOCAGE which
1056 is used at every time step), altitude and surface albedo in the UV. They are computed for clear-sky conditions and the impact
1057 of cloudiness on photolysis rates is applied afterwards.

1058 The aerosol module of MOCAGE includes the primary species dusts, black carbon, sea salts, organic carbon, and the secondary
1059 inorganic species sulphate, nitrate and ammonium. The formation and the multi-phasic equilibrium of inorganic secondary
1060 aerosols are modelled by the ISORROPIA-II module. Details on MOCAGE aerosol simulation evaluation can be found in
1061 (Martet et al., 2009) for dusts, in (Nho-Kim et al., 2005) for black carbon, and in (Sič et al., 2015) for the latest version of
1062 MOCAGE primary aerosol module. The implementation and the evaluation of secondary inorganic aerosols in MOCAGE are
1063 described by (Guth et al., 2016). Further improvements of the representation of aerosols in MOCAGE are expected in the
1064 future with on-going work regarding organic secondary aerosols.

1065 **3.9.9 Assimilation system**

1066 MOCAGE operations for CAMS use the assimilation system based upon MOCAGE and PALM (Lahoz et al., 2007). As a first
1067 approximation, background error standard deviations are prescribed as proportional to background amounts. In order to spread
1068 assimilation increments spatially, background error correlations are modelled using a generalized diffusion operator (Weaver
1069 and Courtier, 2001). Several assimilation strategies are available in PALM but for CAMS MOCAGE uses a 3D-VAR
1070 technique, with an assimilation window that is 1h every hour.

1071 For surface analyses (NRT, IRA and VRA), MOCAGE assimilates O₃, NO₂, CO, PM₁₀ and PM_{2.5} in-situ surface observations.
1072 The species are assimilated independently every hour without any cross-species covariances, and then the increments per

1073 species are added to the analysis that serves as initial condition for computing the background of the next hour of the
1074 assimilation process, in this reanalysis mode.

1075 An hourly assimilation cycle is also used to update the atmospheric state of aerosols, with the assimilation of French lidars
1076 (mini-MPL) and some ceilometers from the European network E-profile in the regional domain of MOCAGE. The quantity
1077 modified during the assimilation process is the 3D field of total mass of all aerosol types and all sizes all together. The split
1078 per aerosol type and particle size is not modified during the assimilation. This hourly assimilation cycle is the backbone and
1079 every day at 00 UTC, the +96h forecast is initialised from this assimilation cycle.
1080

1081 **3.10 MONARCH**

1082 **3.10.1 Model Overview**

1083 The MONARCH model is a fully online multiscale chemical weather prediction system for regional and global-scale
1084 applications (Badia and Jorba, 2015; Badia et al., 2017; Jorba et al., 2012; Klose et al., 2021; Pérez et al., 2011). The system
1085 is based on the meteorological Nonhydrostatic Multiscale Model on the B-grid (NMMB; (Janjic and Gall, 2012)), developed
1086 and widely verified at the National Center for Environmental Prediction (NCEP). The model couples online the NMMB with
1087 the gas-phase and aerosol continuity equations to solve the atmospheric chemistry processes in detail. The model is designed
1088 to account for the feedbacks among gases, aerosol particles and meteorology. Currently, it can consider the direct radiative
1089 effect of aerosols while ignoring cloud–aerosol interactions.

1090 **3.10.2 Model geometry**

1091 The hybrid pressure-sigma coordinate is used in the vertical direction and the Arakawa B-grid is applied in the horizontal
1092 direction. The regional model is formulated on a rotated longitude–latitude grid, with the Equator of the rotated system running
1093 through the middle of the integration domain, resulting in more uniform grid distances. In the operational regional CAMS
1094 forecasts, the model is configured for a regional domain covering Europe and part of northern Africa with a regular horizontal
1095 grid spacing on the rotated projection of 0.15° (lower-left corner at 16.37°N 22.14°W, upper-right corner at 58.56°N 88.18°E)
1096 and the top of the domain is set at 50hPa using 24 vertical layers. Surface concentrations of gases and aerosols are derived
1097 directly from the first model level; no particular vertical downscaling is implemented. The depth of the first vertical layer of
1098 the model is around 45 m and about 7 layers are set below 2 km.

1099 **3.10.3 Forcing Meteorology**

1100 The forcing meteorology is retrieved from the IFS model on a 0.125°x0.125° horizontal grid resolution (the native resolution
1101 is remapped as close as possible to the MONARCH grid to optimise transfer time) with a temporal resolution of 6 hours and
1102 dynamically interpolated to the final chemistry grid and time steps using the meteorological component of MONARCH. The
1103 IFS forecast released at 12:00UTC of the previous days is used. The meteorological variables obtained from IFS are: Skin
1104 temperature, Soil temperature, Soil moisture, Snow depth, Sea-ice mask, Sea-level pressure, U component of the wind, V
1105 component of the wind, Temperature, Geopotential height, Relative humidity or specific humidity, Cloud water content.

1106 **3.10.4 Chemical initial and boundary conditions**

1107 The variables used from chemical species available in the CAMS-Global forecast model are detailed in Table 2. Note that CH₄
1108 is not used from CAMS-Global because the MONARCH chemical mechanism considers a constant CH₄ concentration of 1.85

1109 ppmv. A remapping has been applied to couple the modal distribution of the CAMS-Global aerosols with the aerosols
 1110 distribution of the MONARCH model (see Table 2). The forecasts are initialised by the model results of the previous day.

1111 **3.10.5 Emissions**

1112 The common annual anthropogenic emissions CAMS-REG are implemented as explained in Section 2.5.1. The High-Elective
 1113 Resolution Modelling Emission System version 3 (HERMESv3; (Guevara et al., 2019)) is used to pre-process the
 1114 anthropogenic, ocean and biomass burning emissions for the MONARCH model. HERMESv3 is an open source, parallel and
 1115 stand-alone multiscale atmospheric emission modelling framework that processes gaseous and aerosol emissions for use in
 1116 atmospheric chemistry models.

1117 CAMS_REG-AP NMVOC and PM_{2.5} emissions are speciated using the sector and country-dependent split factors proposed
 1118 by TNO. In terms of NO_x, a fraction of 90% NO and 10% NO₂ is considered for all sectors except for road transport, in which
 1119 the following fractions are applied: (i) 95% NO, 4.2% NO₂ and 0.8 HONO for gasoline road transport and (ii) 70% NO, 28.3%
 1120 NO₂ and 1.7% HONO for diesel road transport (Rappenglück et al., 2013). The vertical distribution of anthropogenic emissions
 1121 is performed following the sector-dependent profiles proposed by TNO. The temporal distribution follows the gridded CAMS-
 1122 REG-TEMPO v4.1 profiles (Guevara et al., 2021).

1123 The biogenic emissions for NMVOC and NO are computed on-line within the MONARCH model using the Model of
 1124 Emissions of Gases and Aerosols from Nature version 2.04 (MEGANv2.04; (Guenther et al., 2006)), while monthly oceanic
 1125 emissions of DMS are obtained from the CAMS-GLOB-OCEA v3.1 dataset (Granier et al., 2019; Lana et al., 2011).

1126 Mineral dust emissions can be calculated online using one of the schemes described in (Klose et al., 2021). For sea salt aerosol
 1127 emissions, multiple source functions are available (Spada et al., 2013).

1128 Finally, biomass burning emissions (forest, grassland and agricultural waste fires) of organic carbon, black carbon, SO₂, and
 1129 DMS are taken from the GFASv1.4 dataset. This product reports hourly emissions at a horizontal gridded resolution of 0.1° x
 1130 0.1°. The vertical allocation of GFAS emissions is done using the maximum fire plume injection height and distributing
 1131 uniformly all the emissions across the layers below this height. The persistence of the fires in forecast mode is set to 2 days,
 1132 afterwards biomass burning emissions are set to zero.

1133 **3.10.6 Solver, advection and mixing**

1134 Different chemical processes were implemented following a modular operator splitting approach to solve the advection,
 1135 diffusion, emission, dry and wet deposition, and chemistry processes. In order to maintain consistency with the meteorological
 1136 solver, the chemical species are advected and mixed at the corresponding time step of the meteorological tracers following the

1137 principles described in (Janjic and Gall, 2012) and references therein. The advection scheme is Eulerian, positive definite and
1138 monotone, maintaining a consistent mass conservation of the chemical species within the domain of study. Lateral diffusion
1139 is formulated following the Smagorinsky non-linear approach, while vertical diffusion is based on the Mellor–Yamada–Janjic
1140 level 2.5 turbulence closure scheme.

1141 The convective mixing, however, is treated differently for aerosols and gases. The scheme implemented for aerosols is
1142 described in detail in (Pérez et al., 2011) and follows a relaxation approach similar to the Betts-Miller-Janjic convective
1143 parameterization of the NMMB. On the other hand, the convective mixing of gases is solved following the sub-grid cloud
1144 scheme of (Foley et al., 2010) as described in (Badia et al., 2017).

1145 **3.10.7 Deposition**

1146 The deposition processes implemented in the MONARCH model are dry deposition, in-cloud grid-scale, and in-cloud subgrid-
1147 scale scavenging for gases and aerosols, and below cloud scavenging for aerosols only.

1148 For gases, the dry deposition scheme follows the classical deposition velocity analogy, enabling the calculation of deposition
1149 fluxes from airborne concentrations. The canopy resistance is simulated following (Wesely, 1989). The cloud-chemistry
1150 processes are included in the system considering both the sub-grid and grid-scale scheme described in (Foley et al., 2010). The
1151 processes included are the scavenging, vertical mixing and wet-deposition. Only in-cloud scavenging is considered in the
1152 current implementation (Badia et al., 2017).

1153 Regarding aerosols, the parameterization of the aerosol dry deposition is based on (Zhang et al., 2001) which includes
1154 simplified empirical parameterizations for the deposition processes of Brownian diffusion, impaction, interception and
1155 gravitational settling. Wet scavenging of aerosols by precipitation is computed separately for convective and grid-scale
1156 (stratiform) precipitation. The model includes parameterizations for in-cloud scavenging, and for below cloud scavenging.
1157 Detailed description of the schemes can be found in (Pérez et al., 2011).

1158 **3.10.8 Chemistry and aerosols**

1159 A gas-phase module combined with a hybrid sectional-bulk mass-based aerosol module is implemented in the MONARCH
1160 model. The gas-phase chemical mechanism used is the Carbon Bond 2005 chemical mechanism (CB05; (Yarwood. G. et al.,
1161 2005)) extended with Chlorine chemistry (Sarwar et al., 2012). The rate constants were updated based on evaluations from
1162 (Atkinson et al., 2004; Sander et al., 2006). The photolysis scheme used is the Fast-J scheme (Wild et al., 2000). It is coupled
1163 with physics of each model layer (e.g., aerosols, clouds, absorbers as ozone) and it considers grid-scale clouds from the
1164 atmospheric driver.

1165 The aerosol module in MONARCH model solves the life cycle of sea salt, dust, organic matter (both primary and secondary),
1166 black carbon, sulphate, and nitrate aerosols. While a sectional approach is used for dust and sea salt, a bulk description of the
1167 other aerosol species is adopted. A simplified gas–aqueous–aerosol mechanism accounts for sulphur chemistry (Spada, 2015).
1168 The production of secondary nitrate–ammonium aerosol is solved using the thermodynamic equilibrium model EQSAM
1169 (Metzger et al., 2002). The coarse nitrate production is computed with an uptake reaction of HNO_3 on dust and sea salt coarse
1170 particles. The formation of SOA is considered using a simple non-volatile scheme accounting for the contribution of
1171 anthropogenic, biomass burning, and biogenic formation (Pai et al., 2020). Hygroscopic growth is considered for all aerosol
1172 components except mineral dust.

1173 **3.10.9 Assimilation system**

1174 The MONARCH assimilation system (MONARCH-DA) is based on a Local Ensemble Transform Kalman Filter (LETKF)
1175 scheme (Di Tomaso et al., 2022; Di Tomaso et al., 2017; Escribano et al., 2022; Hunt et al., 2007; Miyoshi and Yamane, 2007;
1176 Schutgens et al., 2010) coupled to the model through I/O routines. MONARCH ensemble is created by perturbing
1177 anthropogenic, biomass burning, soil and ocean emissions that are pre-processed by HERMESv3 or that are modelled by
1178 MONARCH via a physically-based scheme for dust aerosol. For analysis production in CAMS, MONARCH ensemble is run
1179 at a horizontal resolution of 0.2° latitude \times 0.2° longitude in a rotated grid and initialised by the ensemble forecast of the
1180 previous day.

1181 Hourly surface observations from in-situ measurements are currently assimilated operationally for O_3 , NO_2 , SO_2 , CO , PM_{10} ,
1182 $\text{PM}_{2.5}$. For near-real time operational analysis production, previous-day observations are combined with a MONARCH 24-
1183 hour ensemble forecast initialised at 12 UTC of the previous day.

1184

1185 **3.11 SILAM**

1186 **3.11.1 Model Overview**

1187 The System for Integrated modelLling of Atmospheric coMposition SILAM (silam.fmi.fi) is a global-to-sub-km chemistry
1188 transport model developed for a wide range of atmospheric composition and air quality assessment tasks (Sofiev et al., 2015b),
1189 emergency decision support applications (Sofiev et al., 2008), and data assimilation and source inversion problems (Vira and
1190 Sofiev, 2015; Sofiev et al., 2013). The model incorporates Eulerian and Lagrangian dispersion frameworks (the Eulerian
1191 transport routine is used for CAMS) and a set of chemical and physical transformation modules for the troposphere and the
1192 stratosphere (Carslaw et al., 1995; Damski et al., 2007; Yarwood. G. et al., 2005; Sofiev, 2000; Sofiev et al., 2010). Apart from
1193 the transport and physico-chemical cores described below, SILAM includes a set of supplementary tools including a
1194 meteorological pre-processor, input-output converters, reprojection and interpolation routines, etc. In the operational forecasts,
1195 these enabled direct forcing of the model by the ECMWF IFS meteorological fields.

1196 SILAM has been extensively evaluated in a variety of regional and global air quality projects (Brasseur et al., 2019; Huijnen
1197 et al., 2010; Kouznetsov et al., 2020; Petersen et al., 2019; Sofiev et al., 2015b; Xian et al., 2019) and health impact assessment
1198 studies (Korhonen et al., 2008; Kukkonen et al., 2020; Lehtomäki et al., 2018).

1199 **3.11.2 Model geometry**

1200 The centre points of the model grid cover 25.05°W to 44.95°E and 30.05°N to 71.95°N on a regular latitude longitude grid of
1201 0.1°resolution. Following (Sofiev, 2002), SILAM uses a multi-vertical approach with the meteorology-resolving grid
1202 corresponding to the tropospheric part of the IFS vertical: hybrid levels from 69 to 137. The chemical transformations and
1203 vertical fluxes are computed based on 10 thick staggered layers, with the thickness increasing from 25 m for the lowest layer
1204 to 1000-2000 m in the free troposphere. The layer tops are located at 25, 75, 175, 375, 775, 1500, 2700, 4700, 6700 and 8700m
1205 above the surface. Within the thick layers, the sub-grid information is used to evaluate the weighted averages of the high-
1206 resolution meteorological parameters and effective diffusion coefficients after (Sofiev, 2002).

1207 **3.11.3 Forcing Meteorology**

1208 Meteorological forcing is the ECMWF IFS operational forecasts taken from the 12:00UTC forecast of the previous day
1209 extracted at a resolution of 0.1° and temporal frequency of one hour for the first 72 hours and three hours for the last day of
1210 the forecast. The list of meteorological parameters extracted is: U and V components of 10m wind [m/s], 2m temperature [K],
1211 dew point temperature 2m [K] accumulated large scale rain [kg/m²], accumulated convective rain [kg/m²], surface roughness
1212 [m], total cloud cover [fract], convective available potential energy [J/kg], U and V -wind components at model levels [m/s],

1213 temperature at model levels [K], cloud water at model levels [kg/kg], cloud ice at model levels [kg/kg], specific humidity at
1214 model levels [kg/kg], cloud cover at model levels[fract], logarithm of surface pressure.

1215 **3.11.4 Chemical initial and boundary conditions**

1216 Boundary conditions are taken from the CAMS-Global (see Table 2). The full fields are imported every 3 hours; in-between,
1217 the linear interpolation is applied. The forecasts are initialised with the SILAM forecast of the previous day.

1218 **3.11.5 Emissions**

1219 The common annual anthropogenic emissions CAMS-REG are implemented as explained in Section 3.2. The PM_{2.5} emissions
1220 are split into EC, OC and mineral components, and OC is mapped to the volatility bins according to (Shrivastava et al., 2008).
1221 Emissions of biogenic VOCs, wind-blown dust, and sea salt are computed online in dedicated SILAM modules (Poupkou et
1222 al., 2010; Sofiev et al., 2011; Soares et al., 2016; Sofieva et al., 2022). GFAS hourly emissions from wild-land fires are
1223 replicated from D-2 to D+1 for forecast and shut down after; in the analysis mode it is used as is.

1224 Emissions of 6 pollen species are computed online following the heat-sum approach for trees (Sofiev et al., 2015b),
1225 climatological season for grasses and mugwort species, and multi-criteria hybrid model for ragweed (Prank et al., 2013).

1226 **3.11.6 Solver, advection and mixing**

1227 The SILAM Eulerian transport core (Sofiev et al., 2015a) is based on the coupled developments: refined advection scheme of
1228 (Galperin and Sofiev, 1994) and vertical diffusion and dry deposition algorithm of (Sofiev, 2002) and (Kouznetsov and Sofiev,
1229 2012). The methods are compatible, in a sense that both use the same set of variables to determine the sub-grid distribution of
1230 tracer mass. The approach, in particular, allows computing correct vertical exchange using high-resolution input data but low-
1231 resolution chemistry and diffusion grids. The later feature is used in the vertical setup with thick layers.

1232 Diffusion is parameterised following the first-order K-theory based closure. Horizontal diffusion is embedded into the
1233 advection routine, which itself has zero numerical viscosity, thus allowing full control over the diffusion fluxes. The vertical
1234 diffusivity parameterisation follows the approach suggested by (Groisman and Genikhovich, 1997) and (Sofiev et al., 2010).
1235 The procedure diagnoses all the similarity theory parameters using the profiles of the basic meteorological quantities: wind,
1236 temperature and humidity. Output includes the value of eddy diffusivity for scalars at some reference height (taken to be 1m).

1237 The model uses process-wise splitting and 1-D advection implementation flipping the order of processes every other time step.

1238 **3.11.7 Deposition**

1239 Dry deposition parameterisation for gases generally follows the resistive analogy of (Wesely, 1989). Deposition velocities for
1240 aerosols are evaluated using the original (Kouznetsov and Sofiev, 2012) algorithm. Wet deposition parameterisation is based
1241 on the scavenging coefficient after (Sofiev, 2000) for gas species and follows the generalised formulations of (Kouznetsov and
1242 Sofiev, 2012) for aerosols.

1243 **3.11.8 Chemistry and aerosols**

1244 The main gas-phase chemical mechanism is CB05 with additions for SO_x from (Sofiev, 2000) and organics from VBS
1245 (Volatility-Basis Set, (Shrivastava et al., 2008)). The heterogeneous scheme is an updated version of the DMAT model scheme
1246 (Sofiev, 2000). The formation pathways of secondary inorganic aerosols follow the VBS approach extended with the feedback
1247 to the main gas-phase chemical module. The aerosol size distribution is represented via sectional approach, with species-
1248 specific bin selections. Each bin is characterised with its lower and upper borders, as well as the mass-mean diameter, which
1249 is precomputed / predefined for each bin and species from its size spectrum. Primary anthropogenic aerosols are emitted into
1250 bins with mass-mean diameter of 0.5 µm (fine aerosol, dry size) and 6 µm (coarse aerosols, dry size). Secondary inorganic
1251 aerosols were put into 0.2 and 0.7 µm bins, plus a separate 3 µm bin for coarse nitrates formed on the sea salt surface. The
1252 dust size spectrum is described with 4 bins from 0.3 µm up to 20 µm. Finally, the seasalt spectrum is represented with 5 bins,
1253 from 0.05 µm up to 20 µm of mass-mean nominal diameter. Throughout computations, the particles are transported in
1254 accordance with their mass-mean diameter corrected with regard to actual humidity and the particle solubility. External mixing
1255 is assumed.

1256 **3.11.9 Assimilation system**

1257 The embedded data assimilation is based on the 3d- and 4d-dimensional variational approach, as well as with the EnKF (Vira
1258 and Sofiev, 2012, 2015). Tangent-linear (if needed) and adjoint formulations exist for the transport module, the transformation
1259 schemes and for the deposition modules. The assimilation procedure has been tested for both initialising the concentration
1260 fields and for refinement of the emission (Sofiev, 2019). The observation operators exist for in-situ observations and for the
1261 vertically integrated columns observed by the nadir-looking satellites. For the near-real time operational analyses in CAMS,
1262 the previous-day observations are used in a 3D-VAR data assimilation suite. That routine assimilates in-situ observations of
1263 NO₂, O₃ and PM_{2.5}, PM₁₀, SO₂ and CO.

1264

1265 4 Post-processing

1266 4.1 ENSEMBLE model

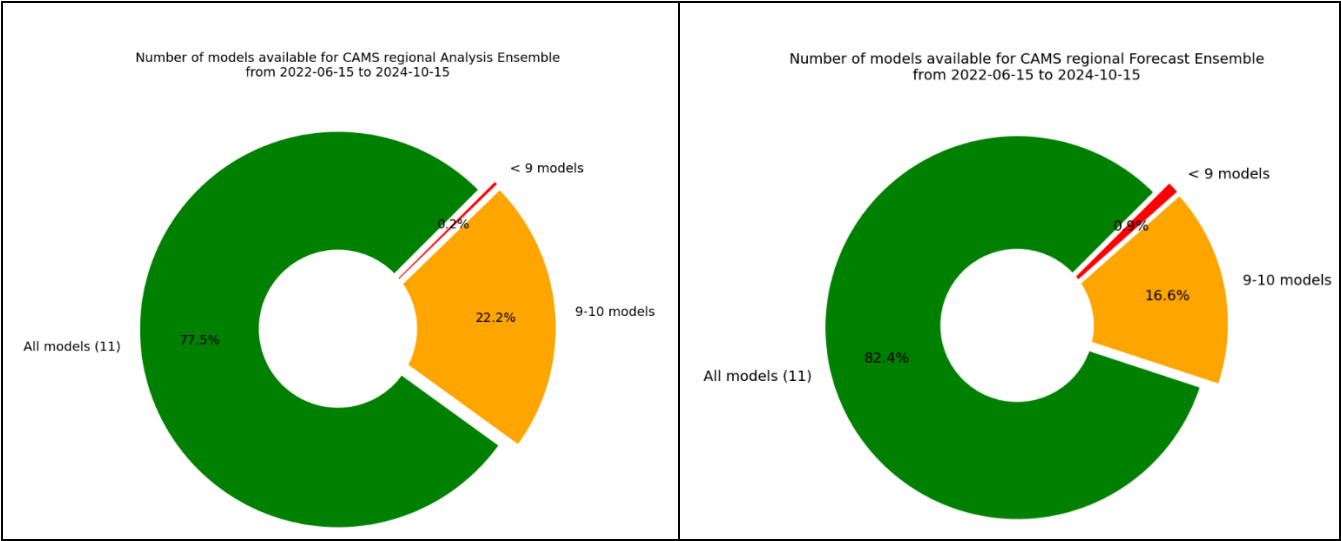
1267 All eleven individual operational model deliver their results to the CRPU (Météo-France for NRT/FC and NRT/AN, and
1268 INERIS for IRA and VRA, using the product definition introduced in Section 2.2). An ENSEMBLE model is subsequently
1269 computed as a median of all available operational models. As explicated in Section 3, there are slight differences in the
1270 individual model geometry even if they are as close as possible to the common grid. Five models are operated their forecasts
1271 directly on the target grid (CHIMERE, DEHM, EMEP, LOTOS-EUROS, and SILAM), one uses area-weighted interpolation
1272 of overlapping polygon (EURAD-IM), and the other models use a bilinear interpolation to deliver model output on the common
1273 grid. The ENSEMBLE is computed across all models at each horizontal and vertical grid point of the common grid. Each of
1274 the model deliver the full list of required species.

1275 Relying on 11 different models offers a very comprehensive view on the various possible representations of key atmospheric
1276 processes relevant to air quality (see the wide range of modelling design detailed in Section 3) and thus a characterisation of
1277 the intrinsic modelling uncertainty. The flipside of this diversity is a relatively higher risk of one model not being able to
1278 deliver in a timely basis. A median ENSEMBLE is computed everyday no matter how many models are successfully delivered
1279 for that given day. A Key Performance Indicator is documented to track the number of models which have delivered on time
1280 to be included in the ENSEMBLE for either the analyses or the forecasts (Figure 2). The fact that timeliness of forecast delivery
1281 is higher than for analyses might seem counterintuitive as forecast are expected earlier, but this is due to the fact that most
1282 analyses are produced later due to the late availability of assimilated observations, and not necessarily used at present as initial
1283 conditions of the forecast.

1284 Using the median to compute such an ensemble is a very robust approach to cope with potential missing members, and it has
1285 been shown to outperform individual models for average performances (Galmarini et al., 2004). It is however a very
1286 conservative approach and developments are ongoing, in particular to improve the skills of the system to capture air quality
1287 exceedance detections by making use of machine learning algorithm coupled to the raw CAMS regional forecasts. Firstly,
1288 optimised forecasts at observation sites are produced operationally for 4 pollutants (PM10, PM2.5, NO2 and O3) at thousands
1289 of AQ e-reporting stations throughout Europe on a daily basis and for the 96hr forecast period. This product is referred to as
1290 CAMS-MOS (Model Output Statistics)⁶. The underlying algorithm is a random forest using as predictor air pollutant
1291 concentration in the ENSEMBLE CTM as well as meteorological variables (temperature at 2m, relative humidity, wind speed
1292 and boundary layer height)(Bertrand et al., 2022). It is trained on a daily basis using the past 3 days of observations. As such,

⁶<https://confluence.ecmwf.int/display/CKB/CAMS+Regional%3A+European+Air+Quality+Forecast+Optimised+at+Observation+Sites+data+documentation> (accessed 24 April 2025)

1293 CAMS-MOS is a statistical model of the meteorological dependant ENSEMBLE error, which proved very effective in
 1294 improving the forecast skills in detecting exceedances of air quality information thresholds. Second, an weighted ensemble
 1295 forecast at the same resolution as the CTMs (10x10km2) has been developed. It consists of an optimum weighting of the 11
 1296 models calibrated on the past 7 days, but in this case the weights are constant and uniform and not dependent on meteorological
 1297 predictors. CAMS-MOS is already available in the ADS as an operational product. But the weighted ensemble is still
 1298 experimental. With the rapid development of machine learning and artificial intelligence, such experimental products will be
 1299 further developed in the future.



1300 *Figure 2: Distribution of the number of operational models having delivered on time to be included in the ENSEMBLE computation for the*
 1301 *period 15/06/2022-15/10/2024: left NRT/AN (analysis) and right: NRT/FC (forecasts).*

1302 **4.2 Evaluation and Quality Control (EQC)**

1303 Evaluation and quality control is an essential part of CAMS in order to ensure the reliability and transparency of the products.
 1304 For all the chemical species where a dense enough monitoring network allows a recurrent and statistically significant
 1305 evaluation, synthetic performance reports are produced and made available on the CAMS website⁷. These evaluations focus
 1306 primarily on the surface in-situ air quality regulatory monitoring networks for O₃, NO₂, PM₁₀, and PM_{2.5}. For the assimilated
 1307 products, the evaluation is performed on about one third of the stations, deliberately left out of the assimilation workflow
 1308 (Section 2.3). The forecasts are evaluated using all available surface stations whose spatial representativity ranges from rural
 1309 to urban background air quality. The skill scores are updated on a daily frequency and available publicly through an interactive
 1310 interface on the CAMS EQC pages for the ENSEMBLE and individual models. Quarterly summaries are produced in publicly

⁷ <https://atmosphere.copernicus.eu/regional-services>, last accessed 30/10/2024

1311 available reports. They also include an evaluation of the models in the troposphere against above-surface measurements
1312 (aircraft and space borne remote sensing and profiling). For the Interim and Validated reanalyses, the evaluation reports are
1313 produced on an annual basis.

1314 The present article is essentially a description of the system rather than a detailed analysis of its performance. Nevertheless,
1315 we present here several evaluation diagnostics for illustration purposes. Therefore, the performances of individual models
1316 contributing to the ENSEMBLE are anonymised as it would be too complex to enter here in the details of the performances of
1317 each model, which relate to intrinsic parametrisations. Such analysis is left for a dedicated future publication, but the interested
1318 user can also consult the interactive viewers and reference public reports on the Evaluation and Quality Control website to
1319 analyse the performances of individual models.

1320 In Figure 3 we show the root mean square error for surface ozone and PM_{10} taken as the median over each quarter since the
1321 beginning of the CAMS production at the end of 2014 and over hundreds of European air quality monitoring stations. The
1322 figure is divided in two parts as urban background stations were only included in the evaluation as of fall 2018 (note also that
1323 the vertical scales differ). It appears clearly that while the spread of the models was still substantial in the first part of the
1324 period, the system has reached a level of maturity since 2017 with more homogeneous performances between the various
1325 models and very few outliers. The ENSEMBLE model appears to give better scores overall. It can be surpassed in terms of
1326 RMSE in some occasions but not always by the same model, therefore still illustrating the added value of the multi-model
1327 ensemble approach. The range of performances is today about $12\text{--}18\mu\text{g}/\text{m}^3$ for the RMSE (root mean square error) of daily
1328 maxima ozone, so that the Key Performance Indicator of $18\mu\text{g}/\text{m}^3$ is not always met depending on the models and the season.
1329 For PM_{10} , the RMSE is between $5\text{ to }8\mu\text{g}/\text{m}^3$ so that the same KPI of $18\mu\text{g}/\text{m}^3$ is usually met. Without entering in a more
1330 detailed analysis, it is visible that the scores are still gradually improving over the 2018-2023 period. Over the recent years,
1331 the median ENSEMBLE seems to produce more systematically better performances and becomes more difficult to beat.

1332

1333

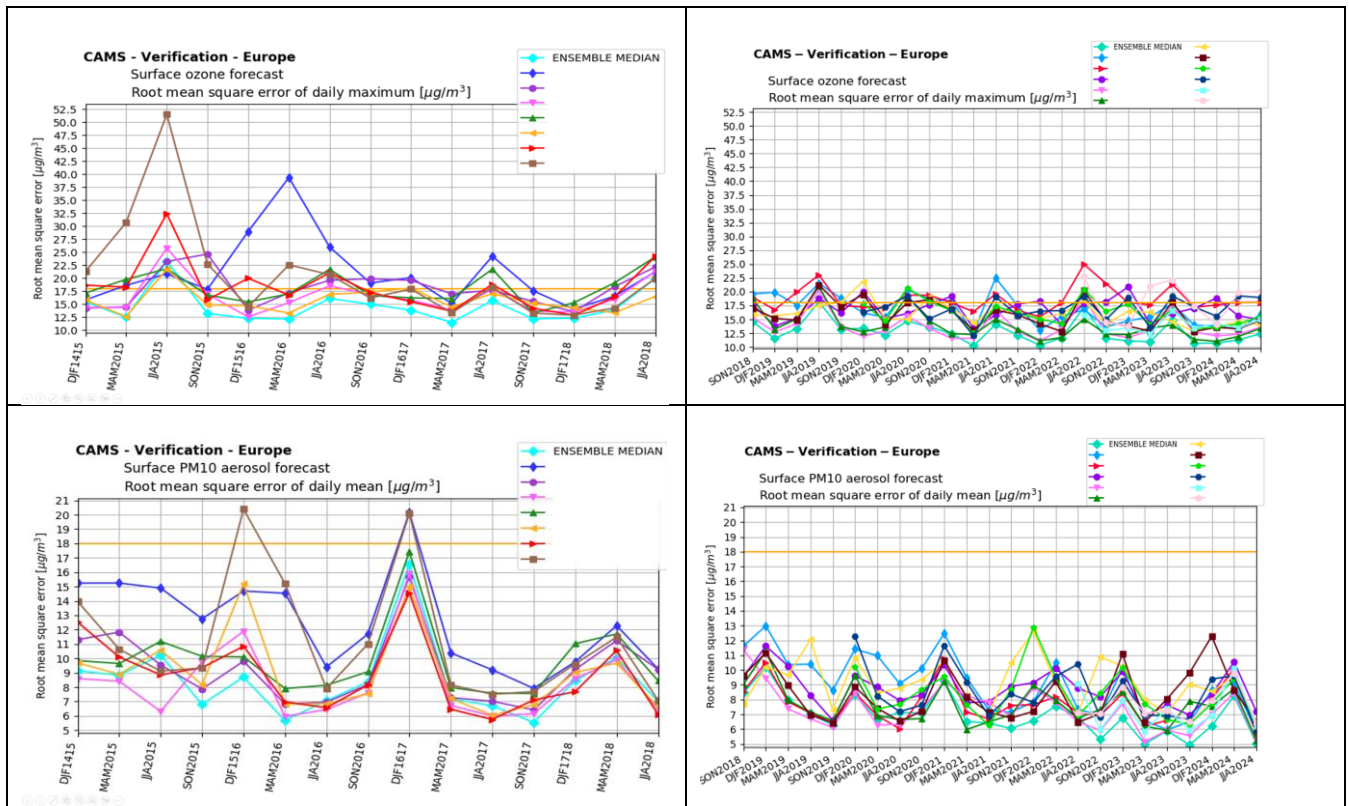
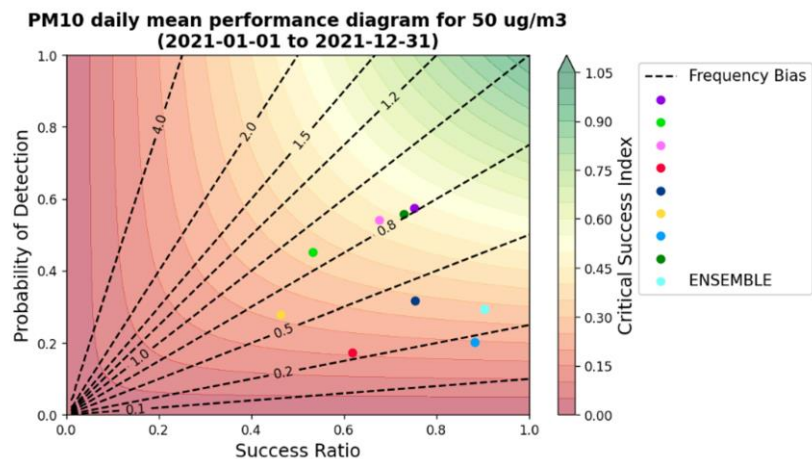


Figure 3: Evolution of the skill scores of the CAMS Regional Air Quality Forecasts (individual models and ENSEMBLE median) between 2014 and 2024 (divided in two parts: before and after 2018 as urban background stations were not included in the evaluation over the first period, and fewer models were available) Each point is the quarterly median of the RMSE ($\mu\text{g}/\text{m}^3$) computed at regulatory air quality monitoring stations for top: daily maximum ozone and bottom: daily mean PM_{10} . The straight yellow line corresponds to the Key Performance Indicator for RMSE of $18\mu\text{g}/\text{m}^3$.

In the European Air Quality regulation, detrimental air quality situations are identified in terms of various exceedance levels depending on the air pollutants. For PM_{10} , the daily mean concentrations should not exceed $50\mu\text{g}/\text{m}^3$ more than 35 days (EC, 2008). The performance of the CAMS Regional reanalyses in capturing that threshold can be assessed through the performance diagram presented in Figure 4. On the x-axis the success ratio is the number of hits divided by the number of hits and false alarms. On the y-axis, the probability of detection is the number of hits divided by the number of hits and misses. The dashed lines provide the frequency bias defined as the ratio of the total number of predicted exceedances to the total number of observed exceedances. For this example, for the year 2021, the ENSEMBLE median has the best success ratio, but some individual models outperform in terms of probability of detection. It is not possible to point one single model which would outperform systematically the ENSEMBLE (the best performing model will vary depending on the targeted pollutant, threshold, geographic area, etc.). Therefore the reference product remains the median ENSEMBLE which provides the best

1349 scores for conservative annual average metrics, but interested users can refer to the annual evaluation report to select alternative
 1350 depending on their specific needs.



1351
 1352 *Figure 4: Performance of the CAMS Regional ENSEMBLE and individual models reanalyses in capturing air quality threshold detection*
 1353 *for daily mean PM₁₀ above 50µg/m³ in 2021.*

1354 An illustration of the evaluation above the surface is provided in Figure 5. The tropospheric column of NO₂ in the CAMS
 1355 regional ENSEMBLE forecast is compared to the observations from the TROPOMI instrument on board the Sentinel 5p
 1356 satellite. The higher spatial resolution (approximately 5km) available since the launch of the instrument allows reaching out
 1357 to urban level NO₂ concentrations therefore providing an excellent opportunity for the evaluation of spatial patterns of air
 1358 pollution. Beyond surface and total columns, it is also essential to assess the performances of the vertical structure as illustrated
 1359 for the comparison with ozone soundings in Belgium (Uccle). Here both the regional forecast and analyses are compared to
 1360 assess the impact of surface assimilation of air quality measurement on the vertical profiles. The CAMS global model forecast
 1361 is also included along with the CAMS regional ensemble range for the forecast and the analysis. A more detailed analysis of
 1362 the comparison with satellite data can be found in (Douros et al., 2022).

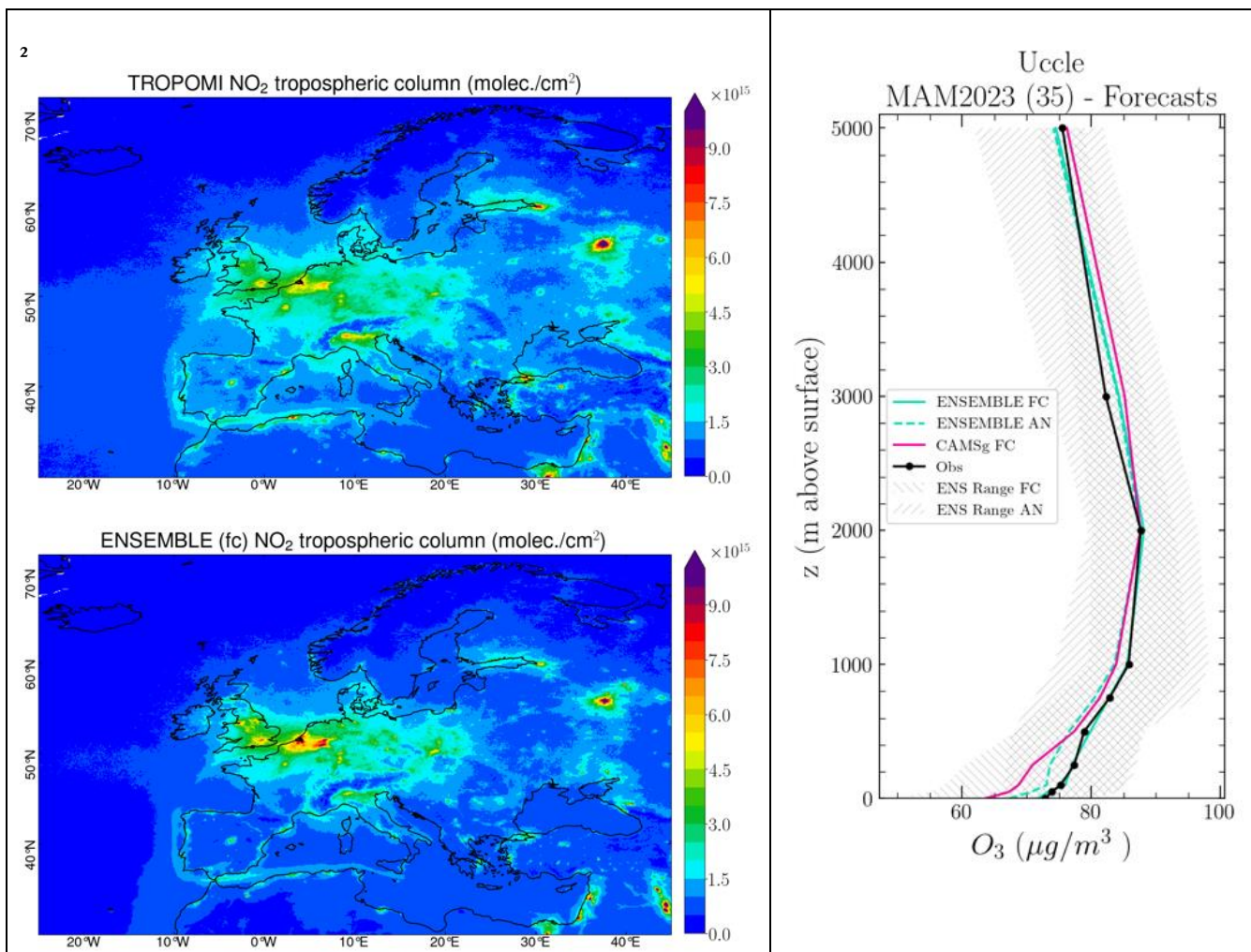


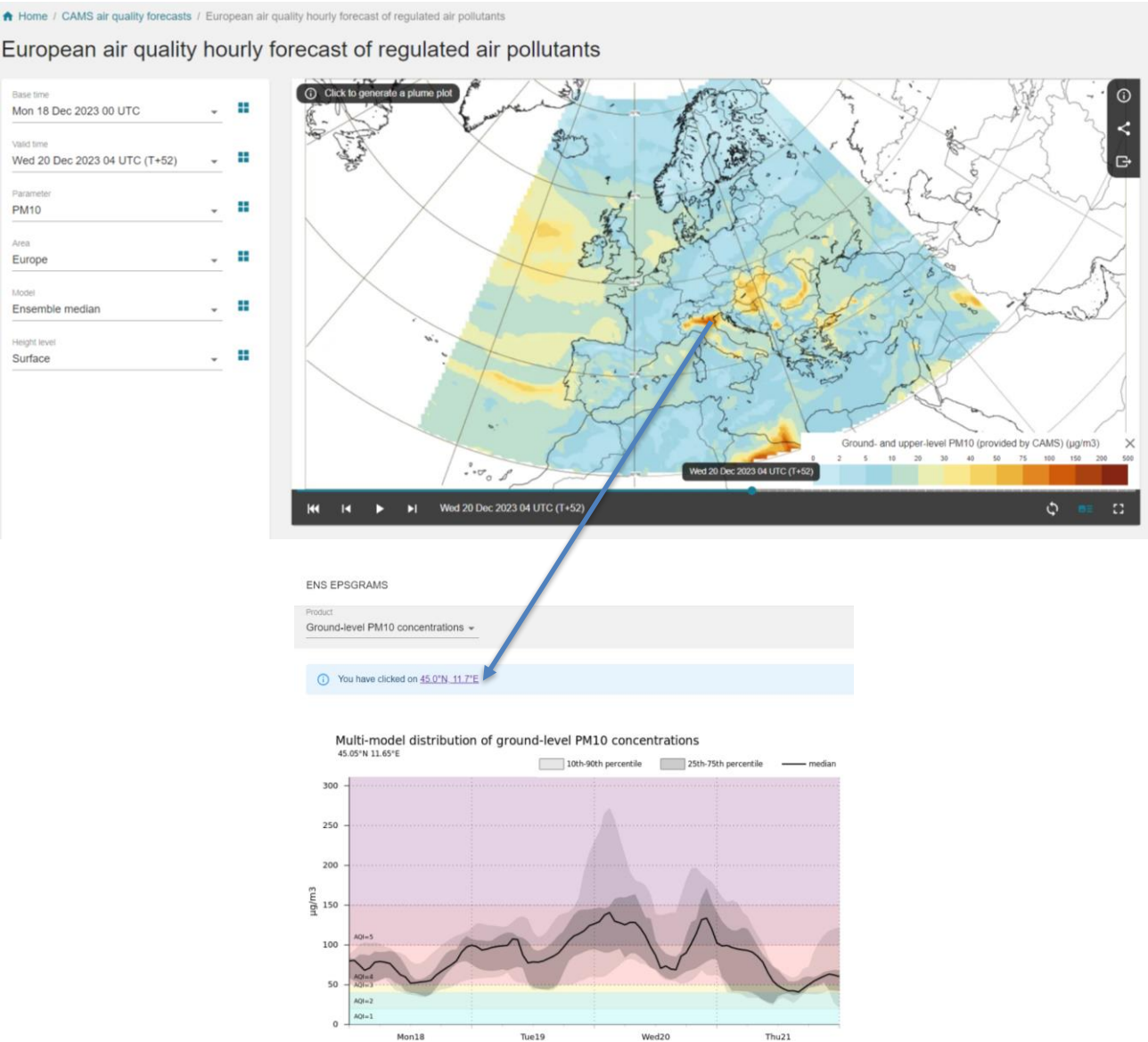
Figure 5: Left: Evaluation over MAM-2023 of the CAMS Regional ensemble forecasts against TROPOMI satellite NO₂ tropospheric columns (10^{15} molecules/cm²). The CAMS NO₂ profiles have been multiplied with the TROPOMI kernels to remove the dependency on the retrieval a-priori profile shape. Right: Regional and global CAMS forecast and regional analyses of ozone compared to vertical profiles measured with ozone sondes over Uccle, Brussels, Belgium for MAM-2023 ($\mu\text{g}/\text{m}^3$). source: CAMS2_83 Evaluation and Quality Control Service, <https://atmosphere.copernicus.eu/regional-services>

4.3 Dissemination and further use of the CAMS Regional Products

The results of the CAMS regional production system are made available publicly on the website <https://atmosphere.copernicus.eu/european-air-quality-forecast-plots> where maps and time series of the various air pollutant and pollen species can be displayed. The results of the median ENSEMBLE as well as each individual model are available for both forecast and analysis products with a three years retention time. Daily means, daily maxima, and hourly fields are available. The list of vertical levels available for interactive plotting on the website is: surface, 100m, 1000m, 3000m and

1374 5000m (note that more vertical levels are available on the ADS). The model spread can also be assessed by selecting any grid
1375 point in the map to display the time series of the 4 day forecast including modelled dispersion which provides an information
1376 on the uncertainty in the ensemble forecast (Figure 6).

1377



1378 Figure 6: Screenshot of the CAMS Regional Production website displaying air quality forecasts over Europe (atmosphere.copernicus.eu6)

1379 The Copernicus Atmosphere Data Store (ADS) constitutes an important dissemination pathway for the CAMS Regional
1380 production system. All the numerical data can be freely retrieved through the website ads.atmosphere.copernicus.eu where
1381 automated requests can be built to download entire fields or custom extractions in either grib or netcdf formats.

1382 The typical use of CAMS Regional forecast product is for national and local air quality management agencies to understand
1383 the day-to-day air quality situation and anticipate major air pollution events. This can be done either by a qualitative analysis
1384 of quicklooks available on the CAMS website or external companies that have developed alternative visualisation tools.

1385 The numerical data obtained on the ADS can also be used as background information for national or local scale air quality
1386 modelling applications. Such uses range from the nesting of a Chemistry Transport Model as three-dimensional and hourly
1387 concentrations of several chemical species are available in the CAMS Regional Forecast. They can also be used to feed
1388 gaussian city-scale surface air quality models. There are also reported uses of the CAMS Regional Forecast to inform machine-
1389 learning air quality statistical prediction tools (Bertrand et al., 2022; Petetin et al., 2022).

1390 The use of CAMS Regional reanalyses is rather to inform longer term air quality applications. They can be used as background
1391 information for land-use regression models used in air quality policy products or exposure assessment for health impact studies
1392 (Horálek et al., 2022). They are also the primary source of information for the Interim Assessment Report produced annually
1393 by the CAMS Policy Service and serves as background information for European Member States in the Regulatory Air Quality
1394 reporting obligations (Hamer et al., 2023).

1395 **5 Conclusion & Perspectives**

1396 The regional production of the Copernicus Atmosphere Monitoring Service is today a well-established reference for air quality
1397 forecast and analysis in Europe and beyond. It is constituted of a unique ensemble of eleven European Chemistry-Transport
1398 models operated in ten countries under the management of a Centralised Regional Production Unit. The system follows strict
1399 requirements in order to produce consistent air quality products through the ensemble of individual CTM. Those requirements
1400 include in particular forcing fields such as meteorology, chemical hemispheric boundary conditions, and surface fluxes of
1401 anthropogenic and wildfire emissions. But the added value of the use of an ensemble of models also lies in the diversity of the
1402 modelling strategy. As of today, the ensemble offers a very wide array of choices in terms of model design and structure, as
1403 well as regarding the formulation of underlying physical and chemical processes or forcing and coupling at the interfaces (land,
1404 sea, biosphere, ...).

1405 In the present paper, we provide a comprehensive scientific documentation of the technical characteristics for the common
1406 forcing requirements as well as the diversity in modelling design brought about by the individual contributing modelling

1407 groups. We also explained how the billions of data produced on a daily basis are aggregated centrally, evaluated and
1408 disseminated for a wide range of air quality applications. The CAMS Service has been operational since the end of 2014 and
1409 has reached today a high level of performance and stability. Since 2017 the spread of model performances has converged and
1410 it continues to improve gradually over the years.

1411 As an operational service, the Regional Production of CAMS follows closely the research developments in the field of air
1412 quality modelling. A substantial part of the model development is undertaken independently by the modelling teams through
1413 various research projects and PhD work at national level. The international benchmarking activities (such as the AQMEII or
1414 Eurodelta initiatives, (Galmarini et al., 2017; Colette et al., 2017)) are also an important source of information to identify
1415 model development priorities. More recently, the European Union has launched a series of research projects devoted to the
1416 Evolution of Copernicus in the Horizon Europe Programme⁸.

1417 In order to ensure a continuous improvement, the system follows a regular development cycle. The individual models are
1418 improved in time so that they remain in the state of the art of chemistry transport modelling. When the progress becomes
1419 mature enough, system upgrades are scheduled on a bi-annual basis to allow individual modelling groups to bring their
1420 development into the operational model version. These bi-annual upgrades are also the opportunity to carry coordinated
1421 changes, such as the regular update of anthropogenic emission fluxes. Through these upgrades, the portfolio of products is also
1422 continuously expanding. For instance, in addition to the 19 chemical species already being delivered, the current plan at the
1423 time of submission of the present article (i.e. for the year 2024) is to include new PM species such as ammonium nitrate and a
1424 tracer of shipping emissions.

1425 A large part of the research effort in relation to the Regional Production is related to Chemistry-Transport deterministic
1426 modelling. But there are also interesting prospects in the coupling between machine learning and physical and chemical
1427 modelling. The Regional Service already produces operationally optimised forecasts at station level on the basis of Model
1428 Output Statistics which relies on Machine Learning to offer unprecedented performance in particular for air quality threshold
1429 detection (Bertrand et al., 2022). Novel methodologies to compute the ENSEMBLE model from the eleven individual
1430 production and move away from the conservative median approach are also under consideration.

1431 Besides the modelling developments, the uptake of innovative observations is also instrumental in the long-term perspective
1432 of CAMS. The production of deposition fluxes is a good illustration of the need to make the best of available observations.
1433 While CTMs are producing by nature deposition fluxes, they are not systematically quality checked and therefore the output
1434 products are limited at present to ambient air concentrations. A mid-term development is therefore ongoing to benchmark wet

⁸ <https://atmosphere.copernicus.eu/copernicus-research-whats-horizon>

1435 and dry deposition fluxes to ensure their robustness. To achieve this, CAMS relies on the network of deposition data collected
1436 in the EMEP network of rural supersites in Europe. But there are also promising prospects in the uptake of near-real-time
1437 advanced observations of atmospheric composition at the supersites of the ACTRIS European Research Infrastructure, in
1438 particular with regards to particulate matter chemical composition and source apportionment. Lastly, in the outlook of the
1439 future perspectives there are also high expectations regarding the uptake of geostationary satellite retrievals with the
1440 perspective of the launch of the Sentinel 4 satellite which will bring unprecedented high-frequency atmospheric composition
1441 information over Europe.

1442 **6 Data Availability**

1443 Copernicus is funded under the Copernicus Regulation and operated by ECMWF under the ECMWF Agreement. Access to
1444 all Copernicus (previously known as GMES or Global Monitoring for Environment and Security) Information and Data is
1445 regulated under Regulation (EU) No 1159/2013 of the European Parliament and of the Council of 12 July 2013 on the European
1446 Earth monitoring programme, under the ECMWF Agreement and under the European Commission's Terms and Conditions.
1447 Access to all Copernicus information is regulated under Regulation (EU) No 1159/2013 and under the ECMWF Agreement.

1448 The Copernicus Licence is free of charge, worldwide, non-exclusive, royalty free and perpetual. Access to Copernicus Products
1449 is given for any purpose in so far as it is lawful, whereas use may include, but is not limited to: reproduction; distribution;
1450 communication to the public; adaptation, modification and combination with other data and information; or any combination
1451 of the foregoing.

1452 The full terms of the Copernicus Licence are available at: [https://ads.atmosphere.copernicus.eu/api/v2/terms/static/licence-to-](https://ads.atmosphere.copernicus.eu/api/v2/terms/static/licence-to-use-copernicus-products.pdf)
1453 [use-copernicus-products.pdf](https://ads.atmosphere.copernicus.eu/api/v2/terms/static/licence-to-use-copernicus-products.pdf)

1454 **7 Code Availability**

1455 Following the Copernicus Programme Data Policy, the Regional Production data and information are available on a full, open,
1456 and free-of-charge basis, subject to limitations concerning registration, dissemination formats, and access restrictions. The
1457 Copernicus Atmosphere Data Store is located at: <https://ads.atmosphere.copernicus.eu/>.

1458 The CHIMERE model is available to registered users through the dedicated website at
1459 <https://www.lmd.polytechnique.fr/chimere/>, the actual version used in CAMS is available at
1460 <https://zenodo.org/records/14724119>.

1461 The DEHM model used in CAMS is available at <https://zenodo.org/records/14628278>.

1462 The EMEP model is available at <https://github.com/metno/emep-ctm> under the GPLv3 licence. The model version for CAMS
1463 is updated once or twice a year in the frame of the regular updates in the CAMS regional service. The current version is
1464 <https://zenodo.org/records/14507729>.

1465 The EURAD-IM version 5.11.1 source code used in CAMS is <https://doi.org/10.5281/zenodo.15198902>.

1466 The GEM model is a free software that can be redistributed and/or modified under the terms of the GNU Lesser General Public
1467 License published by the Free Software Foundation. It is available on a repository administered by Environment and Climate
1468 Change Canada at <https://github.com/ECCC-ASTD-MRD/gem/>. GEM-AQ includes an additional source code tree accessed
1469 via an interface routine in GEM. The GEM-AQ code used in CAMS is available at <https://zenodo.org/records/14720848>.

1470 The LOTOS-EUROS model is available to registered users from the website [https://airqualitymodeling.tno.nl/lotos-](https://airqualitymodeling.tno.nl/lotos-euros/open-source-version/)
1471 [euros/open-source-version/](https://airqualitymodeling.tno.nl/lotos-euros/open-source-version/) the version used in CAMS is available at <https://zenodo.org/records/14711996>.

1472 The MATCH model as used in CAMS is available at <https://zenodo.org/records/14719885>.

1473 The FARM code embedded in the MINNI System as used in CAMS is available at <https://zenodo.org/records/14650298>
1474

1475 The MOCAGE source code used in CAMS is available at <https://doi.org/10.5281/zenodo.14625973>.

1476 The MONARCH model is available at <https://earth.bsc.es/gitlab/es/monarch> under the GPLv3 licence. The version used in
1477 CAMS is <https://zenodo.org/records/5215467>.

1478 The SILAM code is available at <https://github.com/fmidev/silam-model> under the GPLv3 licence. The model is updated
1479 several times a year, including two CAMS-related updates. The version used in CAMS is <https://zenodo.org/records/14608973>.
1480

1481
1482
1483

8 Author Contribution

1484

AC designed and drafted the overall manuscript and coordinated all contributions.

1485
1486

GC, FB, EB, VG, FM, AR, VP, CM, OF, AJ, VHP and LR contributed to drafting the centralised production specifics and general review of the draft.

1487
1488
1489

MA, JA, AB, RB, DB, JB, GB, AC, JHC, FC, IDE, MDI, GD, EDT, JD, JE, HF, YF, JF, EF, LF, MG, CG, GG, MG, AG, JG, RH, MK, JWK, RKo, RKr, ACL, JL, VL, FM, AM, MM, AN, MO, CPGP, JP, AP, BR, LR, AS, MS, PS, DS, MS, AS, JS, CT, RT, TT, ST, ST, AUn, AUp, AV, PvV, LV, ZY contributed to draft the specificities of individual model description.

1490

HE contributed to draft the text on model evaluation

1491

JK, HdVG: contributed to draft the text on emissions.

1492

MR, OF, VP, AR, EB, provided plots and figures

1493

9 Competing Interest

1494

The authors declare that they have no conflict of interest.

1495

10 Acknowledgements

1496
1497
1498

The activities described in this paper have been funded by the Copernicus Atmosphere Monitoring Service. ECMWF implements the Copernicus Atmosphere Monitoring Service and the Copernicus Climate Change Service with funding from the European Union on behalf of the European Commission.

1499
1500

INERIS acknowledged the support of the French Ministry in Charge of Ecology for continuous support in developing the CHIMERE model and related air quality forecasting activities.

1501
1502
1503
1504

BSC acknowledge support from the Department of Research and Universities of the Government of Catalonia via the Research Group Atmospheric Composition (grant no. 2021 SGR 01550) and project PID-2022-140843OB-I00 funded by MCIN/AEI/10.13039/501100011033 for continuous support in developing the MONARCH model and data assimilation system.

1505
1506

FMI acknowledges the support of Academy of Finland projects PS4A (grant 318194) and ALL-Impress (grant 329215) for the pollen module developments.

1507
1508

The computing resources and the related technical support for MINNI forecast are provided by CRESCO/ENEAGRID High Performance Computing infrastructure and its staff. CRESCO/ENEAGRID High Performance Computing infrastructure is

1509 funded by ENEA, the Italian National Agency for New Technologies, Energy and Sustainable Economic Development and by
1510 Italian and European research programmes (see <http://www.cresco.enea.it/english>).
1511

1512

1513

Table 1: Overview of the main characteristics and configurations of the eleven chemistry-transport models as used in the CAMS Regional Production

		CHIMERE	DEHM	EMEP	EURAD-IM	GEM-AQ	LOTOS-EUROS	MATCH	MINNI	MOCAGE	MONARCH	SILAM
Discretisation	Horizontal resolution	0.1° x 0.1° regular lat-lon	0.1° x 0.1° regular lat-lon	0.1° x 0.1° regular lat-lon	9x9 km Lambert conformal	0.1° x 0.1° lat-lon spherical grid	0.1° x 0.1° regular lat-lon	0.1° x 0.1° regular lat-lon	0.15° x 0.1° regular lat-lon	0.1° x 0.1° regular lat-lon	0.15° x 0.15° rotated regular lat-lon	0.1° x 0.1° regular lat-lon
	number of vertical levels	9	29	20	23	28	12	26	14	47	24	10
	top altitude	500hPa	100hPa	100hPa	100hPa	10hPa	200hPa	8000m	7040m	5hPa	50hPa	8700m
	depth of lowermost layer	20m	20m	50m	35m	20m	20m	45m	40m	40m	40m	25m
	number of lower layers	7 below 2km	12 below 1km	10 in PBL	15 below 2km	14 below 5km	7 below 1km	10 below 850hPa	8 below 1km	8 below 2km	7 below 2km	5 below 1km
Initial & boundary conditions & meteorology	Meteorological driver	D-1 00:00 UTC IFS, 3hrly	D-1 12:00 UTC IFS, 3hrly	D-1 12:00 UTC IFS, 3hrly	D-1 12:00 UTC IFS for FC, IFS analysis for AN, 3hrly for FC, 6hrly for AN, downscaled with WRF	D-1 12:00 UTC IFS, 3hrly	D-1 00:00/12:00 UTC IFS, 3hrly	D-1 12:00 UTC IFS, 3hrly	D-1 12:00 UTC IFS, 1hrly	D-1 12:00 UTC IFS for FC, 1hrly (from +00h to +72h), 3hrly (from +72h to +96h) ; D00:00 UTC IFS for AN, 1hrly	D-1 12:00 UTC IFS, 6hrly, downscaled with NMMB	D-1 12:00 UTC IFS, 1hrly (from +00h to +72h), 3hrly (from +72h to +96h)

		CHIMERE	DEHM	EMEP	EURAD-IM	GEM-AQ	LOTOS-EUROS	MATCH	MINNI	MOCAGE	MONARCH	SILAM
	Boundary values	CAMS-Global	CAMS-Global	CAMS-Global	CAMS-Global	CAMS-Global	CAMS-Global	CAMS-Global	CAMS-Global	CAMS-Global + MOCAGE global for additional species	CAMS-Global	CAMS-Global & SILAM
	Initial values	Previous forecast	Previous forecast	Previous analysis	Previous forecast	Previous forecast	Previous forecast	Previous forecast	Previous forecast	Previous forecast	Previous forecast	Previous forecast
Emissions anthropogenic	Inventory	CAMS-REG v6.1 REF2 2022	CAMS-REG v6.1 REF2 2022	CAMS-REG v6.1 REF2 2022	CAMS-REG v6.1 REF2 2022	CAMS-REG v6.1 REF2 2022	CAMS-REG v6.1 REF2 2022	CAMS-REG v6.1 REF2 2022	CAMS-REG v6.1 REF2 2022	CAMS-REG v6.1 REF2 2022	CAMS-REG v6.1 REF2 2022	CAMS-REG v6.1 REF2 2022
	Temporal disaggregation	TNO	CAMS-REG-TEMPO_v4.1	CAMS-REG-TEMPO_v4.1	CAMS-REG-TEMPO_v4.1	CAMS-REG-TEMPO_v4.1	CAMS-REG-TEMPO_v4.1	GENEMIS	CAMS-REG-TEMPO_v3.2	GENEMIS	CAMS-REG-TEMPO_v4.1	TNO
Emissions: natural & biogenic	in-domain soil and road dust emissions	(Marticorena and Bergametti, 1995)	none	(Marticorena and Bergametti, 1995; Marticorena et al., 1997; Dabdub and Seinfeld, 1994; Gomes et al., 2003; Fécan et al., 1998) Road dust emissions currently switched off.	Based on DREAM model	(Marticorena and Bergametti, 1995)	(Marticorena and Bergametti, 1995) and soil moisture inhibition as in (Fécan et al., 1998)	Road dust from (Schaap et al., 2009) and (Omstedt et al., 2005) and mineral dust based on the DEAD model of (Zender et al., 2003) (mainly attributed to the Mediterranean area).	Erosion and resuspension from (Vautard et al., 2005), soil suitable for mobilization parameterized following (Zender et al., 2003)	(Ginoux et al., 2001) and ECOCLI MAP database	Mineral dust scheme based on (Klose et al., 2021) and (Pérez et al., 2011)	SILAM dust source, SILAM sea salt source, Silam BIO-VOC source

		CHIMERE	DEHM	EMEP	EURAD-IM	GEM-AQ	LOTOS-EUROS	MATCH	MINNI	MOCAGE	MONARCH	SILAM
	in-domain sea-salt emissions	(Martensson et al., 2003) (Monahan, 1986)	(Martensson et al., 2003) (Monahan, 1986)	(Martensson et al., 2003) (Monahan, 1986; Tsyro et al., 2011)	(Sofiev et al., 2011)	(Gong et al., 2003)	(Martensson et al., 2003) {Monahan, 1986 #822	(Sofiev et al., 2011)	(Zhang et al., 2005)	(Sič et al., 2015)	(Jaeglé et al., 2011)	(Sofiev et al., 2011)
	Birch, Grass, Olive, Ragweed,	yes	yes	yes	yes	yes	yes	yes	yes	yes	yes	yes
	Biogenic emissions	MEGAN V2.10 (Guenther et al., 2012)	MEGAN v2.04 (Guenther et al., 2006)	(Simpson et al., 2012)	MEGAN V2.10 (Guenther et al., 2012)	MEGAN-MACC climatology	(Guenther et al., 1993) with detailed tree types for Europe	(Simpson et al., 2012)	MEGAN v2.04 (Guenther et al., 2006)	CAMS-GLOB-BIOv3.1 (Sinderalova et al., 2022) isoprene from MEGAN v2.04 (Guenther et al., 2006)	MEGAN v2.04 (Guenther et al., 2006)	Dynamic biogenic, (Poupkou et al., 2010)
	Soil NOx	MEGAN V2.10 (Guenther et al., 2012)	GEIA (Yienger and Levy, 1995)	CAMS-GLOB-SOIL v2.4 (Simpson et al., 2023)	MEGAN V2.10 (Guenther et al., 2012)	none	(Yienger and Levy, 1995)	none	(Williams et al., 1992)	CAMS-GLOB-SOILv2.2 (Simpson et al., 2021)	MEGAN v2.04 (Guenther et al., 2006)	none
	Wildfires emissions	Hourly emissions from D-2 cycled for AN (D-1) and FC (D+0 and D+1, zero for the remaining days)	last available 24h cycle over D-2 and D-1 cycled for AN (D-1) and FC (D+0 and D+1, zero for the remaining days)	Hourly emissions from D-2 cycled for AN (D-1) and FC (D+0 and D+1, zero for the remaining days)	last available 24h cycle over D-2 and D-1 cycled for AN (D-1) and FC (D+0 and D+1, zero for the remaining days)	last available 24h cycle over D-2 and D-1 cycled for AN (D-1) and FC (D+0 and D+1, zero for the remaining days)	Hourly emissions from D-2 cycled for AN (D-1) and FC (D+0 and D+1, zero for the remaining days)	Hourly emissions from D-1 for AN (D-1) and last available 24h from D-2 and D-1 cycled for FC (D+0 to D+4)	Hourly emissions from D-1 for AN (D-1) and FC (D+0 and D+1, zero for the remaining days)	Hourly emissions from D-2 cycled for AN (D-1) and FC (D+0 and D+1, zero for the remaining days)	Hourly emissions from D-2 cycled for AN (D-1) and FC (D+0 and D+1, zero for the remaining days)	Hourly emissions from D-2 cycled for AN (D-1) and FC (D+0 and D+1, zero for the remaining days)

		CHIMERE	DEHM	EMEP	EURAD-IM	GEM-AQ	LOTOS-EUROS	MATCH	MINNI	MOCAGE	MONARCH	SILAM
Chemistry/Physics	Gas phase chemistry	MELCHIOR2 (Derognat et al., 2003), 44 gaseous species and 120 reactions	Modified (Strand and Hov, 1994), 74 species and 158 reactions	EmChem 19a, (Bergström et al., 2022) 127 species and 198 reactions (Simpson et al., 2020a)	RACM-MM (Geiger et al., 2003)	Modified ADOM IIB mechanism, 51 species and 120 reactions	Modified CBM-IV (Schaap et al., 2004)	EmChem 09 (Simpson et al., 2012) and (Langner et al., 1998)	SAPRC 99 (Carter, 2000)	RACM (tropospheric) and REPROB US (stratospheric)	CB05 (Yarwood, G. et al., 2005)	CBM-IV
	Heterogeneous chemistry	Conversion of NO2 into HNO3 and N2O5 and Conversion of HO2 into H2O2	Oxidation of NO2 by O3 on aerosols	Aerosol-uptake of HNO3, HO2 and to NO3 and O3 and hydrolysis of N2O5 (Stadler et al., 2018)	Hydrolysis of N2O5	Hydrolysis of N2O5	Hydrolysis of N2O5	Hydrolysis of N2O5, aerosol uptake of HNO3 and CH3O2H	none	only relevant for polar stratospheric clouds	Hydrolysis of N2O5 and aerosol uptake of HNO3 on dust and sea salt	Sofiev (2000)
	Aerosol size distribution	10 bins from 10 nm to 40 µm	2 size fractions: PM2.5 and coarse fraction of PM10	2 size fractions: PM2.5 and coarse fraction of PM10	3 log-normal modes: 2 fine + 1 coarse	12 bins from 10nm to 20.5µm	5 size bins for dust and sea-salt, 2 size bins for other aerosols	2 size fractions: PM2.5 and coarse fraction of PM10	3 log-normal model: Aitken, accumulation and coarse	6 bins	8 bins for dust and sea salt. Fine mode for BC, OM, SO4 and NH4. Coarse and fine mode for NO3	2 bins, except for dust (4 bins from 10nm to 30µm) and sea salt (5 bins from 10nm to 30µm)

		CHIMERE	DEHM	EMEP	EURAD-IM	GEM-AQ	LOTOS-EUROS	MATCH	MINNI	MOCAGE	MONARCH	SILAM
	Inorganic aerosols	(Couvidat et al., 2018): Thermodynamic equilibrium for particles under 1 µm and a dynamic approach for particles above 1 µm. Thermodynamic for the H ⁺ -NH ₄ ⁺ -SO ₄ ²⁻ -Na ⁺ -Cl ⁻ -H ₂ O system is based on ISORROPIA 2.1.	(Frohn, 2004)	MARS (Binkowski and Shankar, 1995), thermodynamic equilibrium for the SO ₄ -HNO ₃ -NO ₃ -NH ₃ -NH ₄ -H ₂ O system	thermodynamic equilibrium for the H ⁺ -NH ₄ ⁺ -SO ₄ ²⁻ -NO ₃ -H ₂ O system (Frieese and Ebel, 2010)	(Gong et al., 2003)	ISORROPIA-2 (Fountoukis and Nenes, 2007)	(Mozurkewich, 1993)	ISORROPIA v1.7 (Nenes et al., 1998)	ISORROPIA-2 (Guth et al., 2016)	EQSAM (Metzger et al., 2002)	(Sofiev, 2000)
	Secondary organic aerosols	(Bessagnet et al., 2009)	VBS approach (NPAS scheme of (Bergström et al., 2012a))	VBS approach (NPAS scheme, (Bergström et al., 2012a; Simpson et al., 2012))	updated SORGAM module (Li et al., 2013)	(Jiang, 2003)	not included	VBS schemes for ASOA and BSOA (Bergström et al., 2012a) (Hodzic et al., 2016)	SORGAM (Schell et al., 2001b)	(Castro et al., 1999)	non-volatile scheme for anthropogenic, biogenic and pyrogenic precursors (Pai et al., 2020)	VBS
	Aqueous phase chemistry	SO ₂ oxidation by O ₃ and H ₂ O ₂	SO ₂ oxidation by O ₃ and H ₂ O ₂ (Jonson et al., 2000)	SO ₂ oxidation by ozone and H ₂ O ₂ and metal ion-catalyzed O ₂ (Jonson et al., 2000)	10 gas/aqueous phase equilibria, 5 irreversible S(IV) → S(VI) transformations	SO ₂ oxidation	SO ₂ oxidation	SO ₂ oxidation	SO ₂ oxidation (Seinfeld and Pandis, 1998)	SO ₂ oxidation	SO ₂ oxidation by ozone and H ₂ O ₂	SO ₂ oxidation, nitrate formation (Sofiev, 2000), heterogeneous nitrate formation on sea salt particles

		CHIMERE	DEHM	EMEP	EURAD-IM	GEM-AQ	LOTOS-EUROS	MATCH	MINNI	MOCAGE	MONARCH	SILAM
	Dry deposition: gases	resistance approach (Wesely, 1989)	resistance approach (Simpson et al., 2003; Emberson et al., 2000a)	resistance approach, including non-stomatal deposition of NH ₃ (Simpson et al., 2012)	resistance approach (Zhang et al., 2003)	resistance approach	resistance approach (Erisman et al., 1994)	resistance approach (Simpson et al., 2012)	resistance approach (Michou et al., 2005) (Wesely, 1989)	resistance approach (Michou et al., 2005)	resistance approach (Wesely, 1989)	resistance approach (Wesely, 1989)
	Dry deposition: aerosols	gravitational settling	gravitational settling (Simpson et al., 2003; Emberson et al., 2000a)	(Simpson et al., 2012; Venkatram and Pleim, 1999)	resistance approach (Petroff and Zhang, 2010)	gravitational settling	(Zhang et al., 2001)	resistance approach (Simpson et al., 2012)	gravitational settling (Binkowski and Shankar, 1995)	(Sič et al., 2015)	(Zhang et al., 2001; Pérez et al., 2011)	(Kouznetsov and Sofiev, 2012)
	Wet deposition	In-cloud scavenging for all gas/aerosols is taken into account. Below cloud by rain and snow falls is taken into account for soluble gas (HNO ₃ , H ₂ O ₂) and particles	(Simpson et al., 2003)	In-cloud and sub-cloud scavenging ratios for gases; in-cloud scavenging ratios and sub-cloud scavenging efficiencies for aerosols. (Berge, 1993; Simpson et al., 2012)	CMAQ (Salameh et al., 2007)	Below cloud scavenging for soluble gas species and aerosols	(Banzhaf et al., 2012)	gases: species dependent in-cloud and sub-cloud scavenging ratios; particles: in-cloud scavenging ratio, sub-cloud scavenging (Berge, 1993) and (Simpson et al., 2012)	(Simpson et al., 2003)	Convective: (Mari et al., 2000) Stratiform: (Giorgi and Chameides, 1986), (Slinn et al., 1978; Slinn, 1983)	(Foley et al., 2010; Pérez et al., 2011)	SILAM
Assimilation	Assimilation method	Kriging-based analysis	3D-Var	Intermittent 3d-var	Intermittent 3d-var	Optimal Interpolation	ENKF	Intermittent 3d-var	Optimal Interpolation	3D VAR	LETKF (Di Tomaso et al., 2017)	Intermittent 3d-var

		CHIMERE	DEHM	EMEP	EURAD-IM	GEM-AQ	LOTOS-EUROS	MATCH	MINNI	MOCAGE	MONARCH	SILAM
	Assimilated surface pollutants	NO2, O3, PM2.5, PM10, CO, SO2	NO2, O3, CO, SO2, PM2.5, PM10	NO2, O3, SO2, CO, PM2.5, PM10	NO2, O3, CO, SO2, PM2.5, PM10	NO2, O3, PM2.5, PM10, CO, SO2	NO2, O3, PM2.5, PM10	NO2, O3, CO, SO2, PM2.5, PM10	NO2, O3, CO, SO2, PM2.5, PM10	NO2, O3, PM2.5, PM10	NO2, O3, CO, SO2, PM2.5, PM10	NO2, O3, CO, SO2, PM2.5, PM10
	assimilated satellite	none	none	NO2 (OMI) until 2021, currently disabled	currently none	none	NO2 (OMI) until 2021	none	none	ground-based lidars from French network, ceilometers from e-profile, SO2 Tropomi	none	none
	Assimilation of concentrations	Yes	Yes	Yes	Yes	Yes	None	Yes	Yes	Yes	Yes	Yes
	Assimilation of emissions	None	None	None	None	None	Yes	None	None	None	None	None
	Assimilation of deposition	None	None	None	None	None	Yes	None	None	None	None	None
	Assimilation of other processes	None	None	None	None	None	Ozone top boundary	None	None	None	None	None

		CHIMERE	DEHM	EMEP	EURAD-IM	GEM-AQ	LOTOS-EUROS	MATCH	MINNI	MOCAGE	MONARCH	SILAM
	Frequency of assimilation	Hourly	Hourly	Hourly	Hourly	Hourly	Hourly	Hourly	Hourly	Hourly	Hourly	Hourly

1514

1515
1516

Table 2: Overview of the matching between chemical species used as boundary conditions from the CAMS-Global model and the eleven regional models of the CAMS Regional production

CAMS-Global	CHIME RE	DEHM	EMEP	EURAD	GEM-AQ	LOTOS EUROS	MATCH	MINNI	MOCAGE	MONARCH	SILAM
aermr01 (wet) (sea salt 0.03-0.5 µm radius)	sea salt bins 3 to 5	SS_25= aermr01/4.3+ 0.5*aermr02/4.3	SS_25= aermr01/4.3+ 0.5*aermr02/4.3	not used	not used	SS bins 1=aermr01/4.3 (where SS_25 = SS bin 1 and 2)	SS_25=aermr01/4.3+0.4*aermr02/4.3	SS bin [1-2.5µm] = aermr01/4.3+0.40*aermr02/4.3	SS bins 1-6 = aermr01/4.3	SS bin 1=0.34*aermr01/4.3 + 0.02*aermr02/4.3	SS bin 0.5µm = aermr01/4.3
aermr02 (wet) (sea salt 0.5-5 µm radius)	sea salt bins 6 to 8	SS_co= 0.5*aermr02/4.3	SS_co=0.5*aermr02/4.3	not used	not used	SS bins 2=0.1*aermr02/4.3 SS bins 3=0.2*aermr02/4.3 SS bins 4=0.4*aermr02/4.3 SS bins 5=0.3*aermr02/4.3	SS_co=0.6*aermr02/4.3	SS bin [2.5-10µm] = 0.60*aermr02/4.3	SS bins 1-6 = aermr02/4.3	SS bin 3=0.13*aermr02/4.3 SS bin 4=0.18*aermr02/4.3 SS bin 5=0.35*aermr02/4.3 SS bin 6=0.32*aermr02/4.3+ 0.06*aermr03/4.3	SS bin 3µm = aermr02/4.3
aermr03 (wet) (sea salt 5-20 µm radius)	sea salt bin 9	not used	not used	not used	not used	not used	not used	not used	SS bins 1-6 = aermr03/4.3	SS bin 7=0.40*aermr03/4.3 SS bin 8=0.54*aermr03/4.3	SS bin 9µm = 0.5*aermr02/4.3 SS bin 20µm = 0.5*aermr02/4.3
aermr04 (dust 0.03-0.55 µm radius)	dust bins 4 to 6	DUST_25=aermr04+ aermr05	DUST_25= aermr04+ aermr05	DUST_a cc=0.05 total CAMS-Global dust, DUST_c oa=0.95 total CAMS-Global dust	dust bins 3-7	dust bin 1 = 0.2*aermr04+ 0.2*aermr05 dust bin 2 = 0.8*aermr04+ 0.8*aermr05	dust_25= aermr04+ aermr05+ 0.11*aermr06	dust bin [1-2.5µm] = aermr04+ aermr05+ aermr06*0.11	Dust bins 1-6	DUST bin 1 = 0.03 * aermr04 DUST bin 2 = 0.14 * aermr04	Dust 0.3µm = 0.4*aermr04 Dust 1.5µm = 0.6*aermr04

aermr05 (dust 0.55-0.9 μm radius)	dust bin 7	not used	DUST_2 5= aermr04+ aermr05	DUST_a cc=0.05 total CAMSGlobal dust, DUST_c oa=0.95 total CAMSGlobal dust	dust bins 8		dust_25= aermr04+ aermr05+ 0.11*aer mr06	used above in dust bin [1- 2.5um]	Dust bins 1-6	DUST bin 3 = 0.82 * aermr04 + 0.11 * aermr05	Dust 6μm = aermr05
aermr06 (dust 0.9- 20 μm radius)	dust bins 7 to 10	DUST_c o = 0,4*aerm r06	DUST_c o =0,4*aer mr06	DUST_a cc=0.05 total CAMSGlobal dust, DUST_c oa=0.95 total CAMSGlobal dust	dust bins 9-12	dust bin 3 = 0.08*aer mr06 dust bin 4 = 0.16*aer mr06 dust bin 5 = 0.16*aer mr06	dust_co= 0.44*aer mr06	dust bin [2.5- 10μm] = aermr06* 0,44	Dust bins 1-6	DUST bin 4 = 0.89 * aermr05 + 0.01 * aermr06 DUST bin 5 = 0.11 * aermr06 DUST bin 6 = 0.23 * aermr06 DUST bin 7 = 0.50 * aermr06 DUST bin 8 = 0.14 * aermr06	Dust 6μm = 0.4*aerm r06 Dust 20μm = 0.6*aerm r06
aermr07 hydrophil ic OM	PPM bins 3 to 6	not used	not used	80% accumula tion mode, 20% Aitken mode	OC bins 1-12	POM_25	EC_25=0 .7*aermr 07; EC_co=0 .15*aerm r07	AORPA bin 0- 1μm = 0,00050* aermr07+ 0,00050* aermr08 AORPA bin 1- 2.5μm = 0,44955* aermr07+ 0,44955* aermr08 AORA bin 0- 1μm = 0,00050* aermr07 + 0,00050* aermr08 AORA	OC bins 1-6	hydrophil ic POM	Non- volatile bin of organic aerosol

								bin 1-2.5µm = 0,49950*aermr07 + 0,49950*aermr08			
aermr08 hydrophobic OM	PPM bins 3 to 6	not used	not used	80% accumulation mode, 20% Aitken mode	OC bins 1-12	POM_25	EC_25=0.7*aermr08; EC_co=0.15*aermr08	AORB bin 0-1µm = 0,00010*aermr07 + 0,00010*aermr08 AORB bin 1-2.5µm = 0,09990*aermr07 + 0,09990*aermr08	OC bins 1-6	hydrophobic POM	Non-volatile bin of organic aerosol
aermr09 hydrophilic BC	PPM bins 3 to 6	BCfresh	not used	70% accumulation mode, 30% Aitken mode	BC bins 1-12	EC_25	OC_25=0.7*aermr09 OC_co=0.15*aermr09	AEC bin 0-1µm = 0,0011*aermr09+0.001*aermr10	BC bins 1-6	hydrophilic BC	EC
aermr10 hydrophobic BC	PPM bins 3 to 6	BCaged	not used	70% accumulation mode, 30% Aitken mode	BC bins 1-12	EC_25	OC_25=0.7*aermr10 OC_co=0.15*aermr10	AEC bin 1-2.5µm = 0,999*aermr09+0,999*aermr10	BC bins 1-6	hydrophobic BC	EC
aermr11 Sulphate Aerosol	SO4 bins 3 to 6	SO4	SO4	90% accumulation mode, 10% Aitken mode	SO4 bins 1-12	SO4_25	SO4	SO4 bin 0-1µm = 0,001*aermr11 SO4 bin 1-2,5µm = 0,999*aermr11	MOCAG E-global	SO4	SO4 split equally on 2 modes
aermr16 Nitrate fine mode	not used	not used	NO3_F (0-2.5 µm)	90% accumulation mode, 10%	not used	NO3_25	NO3_f	NO3 bin 0-1µm = 0,001*aermr16 NO3 bin	MOCAG E-global	not used	not used

				Aitken mode				1-2,5µm = 0,999*ae rmr16 + 0,55*ae mr17			
aermr17 Nitrate coarse mode	not used	not used	NO3_C (2.5-10 µm)	not used	not used	NO3_co	NITRAT E(coarse)	Coarse unspecifi ed =0.45*ae rmr17	MOCAG E-global	not used	not used
aermr18 Ammoni um	not used	not used	NH4_F (0-2.5 µm)	90% accumula tion mode, 10% Aitken mode	not used	NH4_25	NH4_f	NH4 bin 0-1µm = 0,001*ae rmr18 NH4 bin 1-2,5µm = 0,999*ae rmr18	MOCAG E-global	not used	not used
aerm19 Biogenic SOA	OM	OM	not used	not used	BSOA	not used	SOA	BSOA	BSOA	not used	BSOA
aerm20 Anthropo genic SOA	OM	OM	not used	not used	ASOA	not used	SOA	ASOA	ASOA	not used	ASOA
CHOCH O (Glyoxal)	CHOCH O	not used	CHOCH O	CHOCH O	CHOCH O	not used	CHOCH O	CHOCH O	CHOCH O	not used	CHOCH O
C2H6 (ethane)	C2H6	C2H6	C2H6	C2H6	C2H6	not used	C2H6	ALK1	MOCAG E-global	C2H6	2xPAR5
C5H8 (isoprene)	C5H8	C5H8	C5H8	C5H8	C5H8	C5H8	C5H8	C5H8	MOCAG E-global	C5H8	C5H8
CH4_c (methane)	CH4	not used	CH4	not used	CH4	CH4	CH4	CH4	MOCAG E-global	not used	not used

CO (carbon monoxide)	CO	CO	CO	CO	CO	CO	CO	CO	CO	CO	CO
GO3 (ozone)	O3	O3	O3	O3	O3	O3	O3	O3	O3	O3	O3
H2O2 (hydrogen peroxide)	not used	not used	not used	H2O2	H2O2	not used	seasonal climatological conc used	not used	MOCAG E-global	H2O2	not used
HCHO (formaldehyde)	HCHO	HCHO	HCHO	HCHO	HCHO	HCHO	HCHO	HCHO	MOCAG E-global	HCHO	HCHO
HNO3 (nitric acid)	HNO3	HNO3	HNO3	HNO3	HNO3	HNO3	HNO3	HNO3	MOCAG E-global	HNO3	HNO3
NO (nitrogen monoxide)	not used	NO	NO	NO	NO	NO	NO	NO	MOCAG E-global	NO	NO
NO2 (nitrogen dioxide)	NO2	NO2	NO2	NO2	NO2	NO2	NO2	NO2	MOCAG E-global	NO2	NO2
PAN (Peroxycetyl nitrate)	PAN	PAN	PAN	PAN	PAN	PAN	PAN	PAN	MOCAG E-global	PAN	PAN
SO2 (Sulphur dioxide)	SO2	SO2	SO2	SO2	SO2	SO2	SO2	SO2	SO2	SO2	SO2

1517

1518

1519

1520 **References**

1521

1522 Aamaas, B., Peters, G. P., and Fuglestad, J. S.: Simple emission metrics for climate impacts, *Earth Syst. Dynam.*, 4, 145-
1523 170, 2013.

1524 Ackermann, I. J., Hass, H., Memmesheimer, M., Ebel, A., Binkowski, F. S., and Shankar, U.: Modal aerosol dynamics
1525 model for Europe: development and first applications, *Atmospheric Environment*, 32, 2981-2999,
1526 [http://dx.doi.org/10.1016/S1352-2310\(98\)00006-5](http://dx.doi.org/10.1016/S1352-2310(98)00006-5), 1998.

1527 Adani, M. and Uboldi, F.: Data assimilation experiments over Europe with the Chemical Transport Model FARM,
1528 *Atmospheric Environment*, 306, 119806, 2023.

1529 Alfaro, S. C. and Gomes, L.: Modeling mineral aerosol production by wind erosion: Emission intensities and aerosol size
1530 distributions in source areas, *Journal of Geophysical Research: Atmospheres*, 106, 18075-18084, 2001.

1531 Andersson-Sköld, Y. and Simpson, D.: Comparison of the chemical schemes of the EMEP MSC-W and IVL photochemical
1532 trajectory models, *Atmospheric Environment*, 33, 1111-1129, 1999.

1533 Atkinson, R., Baulch, D. L., Cox, R. A., Crowley, J. N., Hampson, R. F., Hynes, R. G., Jenkin, M. E., Rossi, M. J., and Troe,
1534 J.: Evaluated kinetic and photochemical data for atmospheric chemistry: Volume I - gas phase reactions of Ox, HOx, NOx
1535 and SOx species, *Atmos. Chem. Phys.*, 4, 1461-1738, 10.5194/acp-4-1461-2004, 2004.

1536 Badia, A. and Jorba, O.: Gas-phase evaluation of the online NMMB/BSC-CTM model over Europe for 2010 in the
1537 framework of the AQMEII-Phase2 project, *Atmospheric Environment*, 115, 657-669, 2015.

1538 Badia, A., Jorba, O., Voulgarakis, A., Dabdub, D., Pérez García-Pando, C., Hilboll, A., Gonçalves, M., and Janjic, Z.:
1539 Description and evaluation of the Multiscale Online Nonhydrostatic Atmosphere Chemistry model (NMMB-MONARCH)
1540 version 1.0: gas-phase chemistry at global scale, *Geoscientific Model Development*, 10, 609-638, 2017.

1541 Baklanov, A. and Sørensen, J.: Parameterisation of radionuclide deposition in atmospheric long-range transport modelling,
1542 *Physics and Chemistry of the Earth, Part B: Hydrology, Oceans and Atmosphere*, 26, 787-799, 2001.

1543 Banzhaf, S., Schaap, M., Kerschbaumer, A., Reimer, E., Stern, R., van der Swaluw, E., and Bultjes, P. J. H.:
1544 Implementation and evaluation of pH-dependent cloud chemistry and wet deposition in the chemical transport model REM-
1545 Calgrid, *Atmos. Environ.*, 49, 2012.

1546 Barbu, A., Segers, A., Schaap, M., Heemink, A., and Bultjes, P.: A multi-component data assimilation experiment directed
1547 to sulphur dioxide and sulphate over Europe, *Atmospheric Environment*, 43, 1622-1631, 2009.

1548 Bechtold, P., Bazile, E., Guichard, F., Mascart, P., and Richard, E.: A mass-flux convection scheme for regional and global
1549 models, *Quarterly Journal of the Royal Meteorological Society*, 127, 869-886, 2001.

1550 Berge, E.: Coupling of wet scavenging of sulphur to clouds in a numerical weather prediction model, *Tellus B: Chemical and*
1551 *Physical Meteorology*, 45, 1-22, 1993.

1552 Bergström, R., Hayman, G. D., Jenkin, M. E., and Simpson, D.: Update and comparison of atmospheric chemistry
1553 mechanisms for the EMEP MSC-W model system — EmChem19a, EmChem19X, CRIv2R5Em, CB6r2Em, and
1554 MCMv3.3Em, The Norwegian Meteorological Institute, Oslo, Norway, 2022.

1555 Bergström, R., Denier Van Der Gon, H., Prévôt, A. S., Yttri, K. E., and Simpson, D.: Modelling of organic aerosols over
1556 Europe (2002–2007) using a volatility basis set (VBS) framework: application of different assumptions regarding the
1557 formation of secondary organic aerosol, *Atmospheric Chemistry and Physics*, 12, 8499-8527, 2012a.

1558 Bergström, R., Denier van der Gon, H. A. C., Prévôt, A. S. H., Yttri, K. E., and Simpson, D.: Modelling of organic aerosols
1559 over Europe (2002–2007) using a volatility basis set (VBS) framework: application of different assumptions regarding the
1560 formation of secondary organic aerosol, *Atmos. Chem. Phys.*, 12, 8499-8527, doi:10.5194/acp-12-8499-2012, 2012b.

1561 Bertrand, J. M., Meleux, F., Ung, A., Descombes, G., and Colette, A.: Technical note: Improving the European air quality
1562 forecast of Copernicus Atmosphere Monitoring Service using machine learning techniques, *Atmos. Chem. Phys. Discuss.*,
1563 2022, 1-28, 10.5194/acp-2022-767, 2022.

1564 Bessagnet, B., Brignon, J.-M., Le Gall, A.-C., Meleux, F., Schucht, S., and Rouïl, L.: Politiques combinées de gestion de la
1565 qualité de l'air et du changement climatique (partie 1): enjeux, synergies et antagonismes, INERIS, Verneuil en Halatte,
1566 2009.

1567 Bessagnet, B., Menut, L., Colette, A., Couvidat, F., Dan, M., Mailler, S., Létinois, L., Pont, V., and Rouïl, L.: An Evaluation
1568 of the CHIMERE Chemistry Transport Model to Simulate Dust Outbreaks across the Northern Hemisphere in March 2014,
1569 *Atmosphere*, 8, 251, 2017.

1570 Bessagnet, B., Menut, L., Curci, G., Hodzic, A., Guillaume, B., Lioussé, C., Moukhtar, S., Pun, B., Seigneur, C., and Schulz,
1571 M.: Regional modeling of carbonaceous aerosols over Europe—focus on secondary organic aerosols, *Journal of*
1572 *Atmospheric Chemistry*, 61, 175-202, 2008.

1573 Bieser, J., Aulinger, A., Matthias, V., Quante, M., and Van Der Gon, H. D.: Vertical emission profiles for Europe based on
1574 plume rise calculations, *Environmental Pollution*, 159, 2935-2946, 2011.

1575 Binkowski, F. and Shankar, U.: The Regional Particulate Matter Model .1. Model description and preliminary results, *J.*
1576 *Geophys. Res.*, 100, 26191–26209, 1995.

1577 Binkowski, F. S.: The aerosol portion of Models-3 CMAQ. In *Science Algorithms of the EPA Models-3 Community*
1578 *Multiscale Air Quality (CMAQ) Modeling System. Part II: Chapters 9-18*, National Exposure Research Laboratory, U.S.
1579 Environmental Protection Agency, Research Triangle Park, NC, 1999.

1580 Bott, A.: A Positive Definite Advection Scheme Obtained by Nonlinear Renormalization of the Advective Fluxes, *Mon.*
1581 *Wea. Rev.*, 117, 1006-1015, 1989.

1582 Brandt, J., Silver, J. D., Frohn, L. M., Geels, C., Gross, A., Hansen, A. B., Hansen, K. M., Hedegaard, G. B., Skjoth, C. A.,
1583 Villadsen, H., Zare, A., and Christensen, J. H.: An integrated model study for Europe and North America using the Danish
1584 Eulerian Hemispheric Model with focus on intercontinental transport of air pollution, *Atmospheric Environment*, 53, 156-
1585 176, 2012.

1586 Brasseur, G. P., Xie, Y., Petersen, A. K., Bouarar, I., Flemming, J., Gauss, M., Jiang, F., Kouznetsov, R., Kranenburg, R.,
1587 and Mijling, B.: Ensemble forecasts of air quality in eastern China—Part 1: Model description and implementation of the
1588 MarcoPolo–Panda prediction system, version 1, *Geoscientific Model Development*, 12, 33-67, 2019.

1589 Burridge, D.: THE METEOROLOGICAL OFFICE OPERATIONAL 10-LEVEL NUMERICAL WEATHER
1590 PREDICTION MODEL (DECEMBER 1975), 1977.

1591 Cariolle, D. and Teyssedre, H.: A revised linear ozone photochemistry parameterization for use in transport and general
1592 circulation models: multi-annual simulations, *Atmospheric chemistry and physics*, 7, 2183-2196, 2007.

1593 Carslaw, K. S., Luo, B., and Peter, T.: An analytic expression for the composition of aqueous HNO₃-H₂SO₄ stratospheric
1594 aerosols including gas phase removal of HNO₃, *Geophysical Research Letters*, 22, 1877-1880, 1995.

1595 Carson, D.: The development of a dry inversion-capped convectively unstable boundary layer, *Quarterly Journal of the*
1596 *Royal Meteorological Society*, 99, 450-467, 1973.

1597 Carter, W. P. L.: Condensed atmospheric photooxidation mechanisms for isoprene, *Atmospheric Environment*, 30, 4275-
1598 4290, [http://dx.doi.org/10.1016/1352-2310\(96\)00088-X](http://dx.doi.org/10.1016/1352-2310(96)00088-X), 1996.

1599 Carter, W. P. L.: Documentation of the SAPRC-99 Chemical Mechanism for VOC Reactivity Assessment, 2000.

1600 Castro, L., Pio, C., Harrison, R. M., and Smith, D.: Carbonaceous aerosol in urban and rural European atmospheres:
1601 estimation of secondary organic carbon concentrations, *Atmospheric Environment*, 33, 2771-2781, 1999.

1602 Chang, T.: Rain and snow scavenging of HNO₃ vapor in the atmosphere, *Atmospheric Environment* (1967), 18, 191-197,
1603 1984.

1604 Christensen, J., Brandt, J., Frohn, L., and Skov, H.: Modelling of mercury in the Arctic with the Danish Eulerian
1605 Hemispheric Model, *Atmospheric Chemistry and Physics*, 4, 2251-2257, 2004.

1606 Christensen, J. H.: The Danish Eulerian hemispheric model—A three-dimensional air pollution model used for the Arctic,
1607 *Atmospheric Environment*, 31, 4169-4191, 1997.

1608 Colella, P. and Woodward, P. R.: The piecewise parabolic method (PPM) for gas-dynamical simulations, *Journal of*
1609 *computational physics*, 54, 174-201, 1984.

1610 Colette, A., Bessagnet, B., Meleux, F., Terrenoire, E., and Rouïl, L.: Frontiers in air quality modelling, *Geosci. Model Dev.*,
1611 7, 203-210, 2014.

1612 Colette, A., Bessagnet, B., Vautard, R., Szopa, S., Rao, S., Schucht, S., Klimont, Z., Menut, L., Clain, G., Meleux, F., Curci,
1613 G., and Rouïl, L.: European atmosphere in 2050, a regional air quality and climate perspective under CMIP5 scenarios,
1614 *Atmos. Chem. Phys.*, 13, 7451-7471, 2013.

1615 Colette, A., Andersson, C., Baklanov, A., Bessagnet, B., Brandt, J., Christensen, J. H., Doherty, R., Engardt, M., Geels, C.,
1616 Giannakopoulos, C., Hedegaard, G. H., Katragkou, E., Langner, J., Lei, H., Manders, A., Melas, D., Meleux, F., Rouïl, L.,
1617 Sofiev, M., Soares, J., Stevenson, D. S., Tombrou-Tzella, M., Varotsos, K. V., and Young, P.: Is the ozone climate penalty
1618 robust in Europe?, *Environmental Research Letters*, 10, 084015, 2015.

1619 Colette, A., Andersson, C., Manders, A., Mar, K., Mircea, M., Pay, M. T., Raffort, V., Tsyro, S., Cuvelier, C., Adani, M.,
1620 Bessagnet, B., Bergström, R., Briganti, G., Butler, T., Cappelletti, A., Couvidat, F., D'Isidoro, M., Doumbia, T., Fagerli, H.,
1621 Granier, C., Heyes, C., Klimont, Z., Ojha, N., Otero, N., Schaap, M., Sindelarova, K., Stegehuis, A. I., Roustan, Y., Vautard,
1622 R., van Meijgaard, E., Vivanco, M. G., and Wind, P.: EURODELTA-Trends, a multi-model experiment of air quality
1623 hindcast in Europe over 1990–2010, *Geosci. Model Dev.*, 10, 3255–3276, 10.5194/gmd-10-3255-2017, 2017.

1624 Côté, J., Gravel, S., Méthot, A., Patoine, A., Roch, M., and Staniforth, A.: The operational CMC–MRB global environmental
1625 multiscale (GEM) model. Part I: Design considerations and formulation, *Monthly Weather Review*, 126, 1373–1395, 1998a.

1626 Côté, J., Desmarais, J.-G., Gravel, S., Méthot, A., Patoine, A., Roch, M., and Staniforth, A.: The operational CMC–MRB
1627 global environmental multiscale (GEM) model. Part II: Results, *Monthly Weather Review*, 126, 1397–1418, 1998b.

1628 Couvidat, F., Bessagnet, B., Garcia-Vivanco, M., Real, E., Menut, L., and Colette, A.: Development of an inorganic and
1629 organic aerosol model (CHIMERE 2017 β v1.0): seasonal and spatial evaluation over Europe, *Geosci. Model Dev.*, 11, 165–
1630 194, 10.5194/gmd-11-165-2018, 2018.

1631 Curier, R., Timmermans, R., Calabretta-Jongen, S., Eskes, H., Segers, A., Swart, D., and Schaap, M.: Improving ozone
1632 forecasts over Europe by synergistic use of the LOTOS-EUROS chemical transport model and in-situ measurements,
1633 *Atmospheric environment*, 60, 217–226, 2012.

1634 Cussac, M., Marécal, V., Thouret, V., Josse, B., and Sauvage, B.: The impact of biomass burning on upper tropospheric
1635 carbon monoxide: a study using MOCAGE global model and IAGOS airborne data, *Atmospheric Chemistry and Physics*,
1636 20, 9393–9417, 2020.

1637 D'Elia, I., Briganti, G., Vitali, L., Piersanti, A., Righini, G., D'Isidoro, M., Cappelletti, A., Mircea, M., Adani, M., and
1638 Zanini, G.: Measured and modelled air quality trends in Italy over the period 2003–2010, *Atmospheric Chemistry and*
1639 *Physics*, 21, 10825–10849, 2021.

1640 Dabdub, D. and Seinfeld, J. H.: Numerical advective schemes used in air quality models—sequential and parallel
1641 implementation, *Atmospheric Environment*, 28, 3369–3385, 1994.

1642 Damski, J., Thölix, L., Backman, L., Taalas, P., and Kulmala, M.: FinRose--middle atmospheric chemistry transport model,
1643 *Boreal environment research*, 12, 2007.

1644 Denier van der Gon, H. A. C., Bergström, R., Fountoukis, C., Johansson, C., Pandis, S. N., Simpson, D., and Visschedijk, A.
1645 J. H.: Particulate emissions from residential wood combustion in Europe – revised estimates and an evaluation, *Atmos.*
1646 *Chem. Phys.*, 15, 6503–6519, 10.5194/acp-15-6503-2015, 2015.

1647 Derognat, C., Beekmann, M., Baeumle, M., Martin, D., and Schmidt, H.: Effect of biogenic volatile organic compound
1648 emissions on tropospheric chemistry during the Atmospheric Pollution Over the Paris Area (ESQUIF) campaign in the Ile-
1649 de-France region, *Journal of Geophysical Research: Atmospheres*, 108, 2003.

1650 Di Tomaso, E., Schutgens, N. A. J., Jorba, O., and Pérez García-Pando, C.: Assimilation of MODIS Dark Target and Deep
1651 Blue observations in the dust aerosol component of NMMB-MONARCH version 1.0, *Geoscientific Model Development*, 10,
1652 1107–1129, 2017.

1653 Di Tomaso, E., Escribano, J., Basart, S., Ginoux, P., Macchia, F., Barnaba, F., Benincasa, F., Bretonnière, P. A., Buñuel, A.,
1654 Castrillo, M., Cuevas, E., Formenti, P., Gonçalves, M., Jorba, O., Klose, M., Mona, L., Montané Pinto, G., Mytilinaios, M.,

1655 Obiso, V., Olid, M., Schutgens, N., Votsis, A., Werner, E., and Pérez García-Pando, C.: The MONARCH high-resolution
1656 reanalysis of desert dust aerosol over Northern Africa, the Middle East and Europe (2007–2016), *Earth Syst. Sci. Data*, 14,
1657 2785-2816, 10.5194/essd-14-2785-2022, 2022.

1658 Douros, J., Eskes, H., van Geffen, J., Boersma, K. F., Compernelle, S., Pinardi, G., Blechschmidt, A. M., Peuch, V. H.,
1659 Colette, A., and Veeckind, P.: Comparing Sentinel-5P TROPOMI NO₂ column observations with the CAMS-regional air
1660 quality ensemble, *EGUsphere*, 2022, 1-40, 10.5194/egusphere-2022-365, 2022.

1661 Ebel, A., Friedrich, R., and Rodhe, H.: GENEMIS: Assessment, improvement, and temporal and spatial disaggregation of
1662 European emission data, in: *Tropospheric modelling and emission estimation*, Springer, 181-214, 1997.

1663 EC: Directive 2008/50/EC of the European Parliament and of the Council of 21 May 2008 on ambient air quality and cleaner
1664 air for Europe, European Commission, Brussels, 2008.

1665 ECMWF: IFS Documentation CY47R3 - Part IV Physical processes, Reading, doi: 10.21957/eyrpir4vj, 2021.

1666 Elbern, H., Strunk, A., Schmidt, H., and Talagrand, O.: Emission rate and chemical state estimation by 4-dimensional
1667 variational inversion, *Atmospheric Chemistry and Physics*, 7, 3749-3769, 2007.

1668 Emberson, L., Ashmore, M., Cambridge, H., Simpson, D., and Tuovinen, J.-P.: Modelling stomatal ozone flux across
1669 Europe, *Environmental Pollution*, 109, 403-413, 2000a.

1670 Emberson, L. D., Ashmore, M. R., Simpson, D., Tuovinen, J.-P., and Cambridge, H. M.: Towards a model of ozone
1671 deposition and stomatal uptake over Europe, *Norwegian Meteorological Institute, Oslo, Norway*, 57, 2000b.

1672 EMEP: Transboundary particulate matter, photo-oxydants, acidifying and eutrophying components, EMEP, Oslo, Norway,
1673 2023.

1674 Erisman, J. W., Van Pul, A., and Wyers, P.: Parametrization of surface resistance for the quantification of atmospheric
1675 deposition of acidifying pollutants and ozone, *Atmospheric Environment*, 28, 2595-2607, [http://dx.doi.org/10.1016/1352-](http://dx.doi.org/10.1016/1352-2310(94)90433-2)
1676 [2310\(94\)90433-2](http://dx.doi.org/10.1016/1352-2310(94)90433-2), 1994.

1677 Escribano, J., Di Tomaso, E., Jorba, O., Klose, M., Gonçalves Ageitos, M., Macchia, F., Amiridis, V., Baars, H., Marinou,
1678 E., Proestakis, E., Urbanneck, C., Althausen, D., Bühl, J., Mamouri, R. E., and Pérez García-Pando, C.: Assimilating
1679 spaceborne lidar dust extinction can improve dust forecasts, *Atmos. Chem. Phys.*, 22, 535-560, 10.5194/acp-22-535-2022,
1680 2022.

1681 Fécan, F., Marticorena, B., and Bergametti, G.: Parametrization of the increase of the aeolian erosion threshold wind friction
1682 velocity due to soil moisture for arid and semi-arid areas, *Annales Geophysicae*, 149-157,

1683 Flemming, J., Huijnen, V., Arteta, J., Bechtold, P., Beljaars, A., Blechschmidt, A. M., Diamantakis, M., Engelen, R. J.,
1684 Gaudel, A., Inness, A., Jones, L., Josse, B., Katragkou, E., Marecal, V., Peuch, V. H., Richter, A., Schultz, M. G., Stein, O.,
1685 and Tsikerdekis, A.: Tropospheric chemistry in the Integrated Forecasting System of ECMWF, *Geosci. Model Dev.*, 8, 975-
1686 1003, 10.5194/gmd-8-975-2015, 2015.

1687 Foley, K., Roselle, S., Appel, K., Bhawe, P., Pleim, J., Otte, T., Mathur, R., Sarwar, G., Young, J., and Gilliam, R.:
1688 Incremental testing of the Community Multiscale Air Quality (CMAQ) modeling system version 4.7, *Geoscientific Model*
1689 *Development*, 3, 205-226, 2010.

1690 Forester, C.: Higher order monotonic convective difference schemes, *Journal of Computational Physics*, 23, 1-22, 1977.

1691 Fountoukis, C. and Nenes, A.: ISORROPIA II: a computationally efficient thermodynamic equilibrium model for K^+ –
1692 Ca^{2+} – Mg^{2+} – NH_4^+ – Na^+ – SO_4^{2-} – NO_3^- – Cl^- – H_2O aerosols, *Atmos. Chem. Phys.*, 7, 4639-4659, doi:10.5194/acp-7-4639-
1693 2007, 2007.

1694 Friese, E. and Ebel, A.: Temperature dependent thermodynamic model of the system H^+ – NH_4^+ – Na^+ – SO_4^{2-} – NO_3^- –
1695 Cl^- – H_2O , *The Journal of Physical Chemistry A*, 114, 11595-11631, 2010.

1696 Frohn, L.: A study of long-term high-resolution air pollution modelling, Ministry of the Environment, National
1697 Environmental Research Institute, Roskilde, Denmark, 2004.

1698 Galmarini, S., Kioutsioukis, I., and Solazzo, E.: E pluribus unum*: ensemble air quality predictions, *Atmos. Chem. Phys.*,
1699 13, 7153-7182, 10.5194/acp-13-7153-2013, 2013.

1700 Galmarini, S., Bianconi, R., Addis, R., Andronopoulos, S., Astrup, P., Bartzis, J., Bellasio, R., Buckley, R., Champion, H.,
1701 and Chino, M.: Ensemble dispersion forecasting—Part II: Application and evaluation, *Atmospheric Environment*, 38, 4619-
1702 4632, 2004.

1703 Galmarini, S., Koffi, B., Solazzo, E., Keating, T., Hogrefe, C., Schulz, M., Benedictow, A., Griesfeller, J. J., Janssens-
1704 Maenhout, G., Carmichael, G., Fu, J., and Dentener, F.: Technical note: Coordination and harmonization of the multi-scale,
1705 multi-model activities HTAP2, AQMEII3, and MICS-Asia3: simulations, emission inventories, boundary conditions, and
1706 model output formats, *Atmos. Chem. Phys.*, 17, 1543-1555, 10.5194/acp-17-1543-2017, 2017.

1707 Galperin, M. and Sofiev, M.: Errors in the validation of models for long-range transport and critical loads stipulated by
1708 stochastic properties of pollution fields., *EMEP Chemical Coordinating Centre, Lillestrom, Passau*, 162–179, 1994.

1709 Geels, C., Winther, M., Andersson, C., Jalkanen, J.-P., Brandt, J., Frohn, L. M., Im, U., Leung, W., and Christensen, J. H.:
1710 Projections of shipping emissions and the related impact on air pollution and human health in the Nordic region,
1711 *Atmospheric Chemistry and Physics*, 21, 12495-12519, 2021.

1712 Geiger, H., Barnes, I., Bejan, I., Benter, T., and Spittler, M.: The tropospheric degradation of isoprene: an updated module
1713 for the regional atmospheric chemistry mechanism, *Atmospheric Environment*, 37, 1503-1519, 2003.

1714 Gery, M. W., Whitten, G. Z., Killus, J. P., and Dodge, M. C.: A photochemical kinetics mechanism for urban and regional
1715 scale computer modeling, *Journal of Geophysical Research: Atmospheres*, 94, 12925-12956, 1989.

1716 Ginoux, P., Chin, M., Tegen, I., Prospero, J. M., Holben, B., Dubovik, O., and Lin, S. J.: Sources and distributions of dust
1717 aerosols simulated with the GOCART model, *Journal of Geophysical Research: Atmospheres*, 106, 20255-20273, 2001.

1718 Giorgi, F. and Chameides, W. L.: Rainout lifetimes of highly soluble aerosols and gases as inferred from simulations with a
1719 general circulation model, *Journal of Geophysical Research: Atmospheres*, 91, 14367-14376, 1986.

1720 Gomes, L., Rajot, J., Alfaro, S., and Gaudichet, A.: Validation of a dust production model from measurements performed in
1721 semi-arid agricultural areas of Spain and Niger, *Catena*, 52, 257-271, 2003.

1722 Gong, S., Barrie, L., Blanchet, J. P., Von Salzen, K., Lohmann, U., Lesins, G., Spacek, L., Zhang, L., Girard, E., and Lin, H.:
 1723 Canadian Aerosol Module: A size-segregated simulation of atmospheric aerosol processes for climate and air quality models
 1724 1. Module development, *Journal of Geophysical Research: Atmospheres*, 108, AAC 3-1-AAC 3-16, 2003.

1725 Granier, C., Darras, S., van der Gon, H. D., Doubalova, J., Elguindi, N., Galle, B., Gauss, M., Guevara, M., Jalkanen, J. P.,
 1726 and Kuenen, J.: The Copernicus Atmosphere Monitoring Service global and regional emissions (April 2019 version),
 1727 Copernicus Atmosphere Monitoring Service, 10.24380/d0bn-kx16, 2019.

1728 Groisman, P. Y. and Genikhovich, E. L.: Assessing surface–atmosphere interactions using former Soviet Union standard
 1729 meteorological network data. Part I: Method, *Journal of climate*, 10, 2154-2183, 1997.

1730 Guenther, A., Zimmerman, P., Harley, P., Monson, R., and Fall, R.: Isoprene and monoterpene rate variability: model
 1731 evaluations and sensitivity analyses, *J. Geophys. Res.*, 98, 12609–12617, 1993.

1732 Guenther, A., Karl, T., Harley, P., Wiedinmyer, C., Palmer, P. I., and Geron, C.: Estimates of global terrestrial isoprene
 1733 emissions using MEGAN (Model of Emissions of Gases and Aerosols from Nature), *Atmos. Chem. Phys.*, 6, 3181-3210,
 1734 2006.

1735 Guenther, A., Jiang, X., Heald, C. L., Sakulyanontvittaya, T., Duhl, T. a., Emmons, L., and Wang, X.: The Model of
 1736 Emissions of Gases and Aerosols from Nature version 2.1 (MEGAN2. 1): an extended and updated framework for modeling
 1737 biogenic emissions, *Geoscientific Model Development*, 5, 1471-1492, 2012.

1738 Guevara, M., Tena, C., Porquet, M., Jorba, O., and Pérez García-Pando, C.: HERMESv3, a stand-alone multi-scale
 1739 atmospheric emission modelling framework–Part 1: global and regional module, *Geoscientific Model Development*, 12,
 1740 1885-1907, 2019.

1741 Guevara, M., Jorba, O., Tena, C., Denier van der Gon, H., Kuenen, J., Elguindi, N., Darras, S., Granier, C., and Pérez
 1742 García-Pando, C.: Copernicus Atmosphere Monitoring Service TEMPORal profiles (CAMs-TEMPO): global and European
 1743 emission temporal profile maps for atmospheric chemistry modelling, *Earth Syst. Sci. Data*, 13, 367-404, 10.5194/essd-13-
 1744 367-2021, 2021.

1745 Guth, J., Josse, B., Marécal, V., Joly, M., and Hamer, P.: First implementation of secondary inorganic aerosols in the
 1746 MOCAGE version 2.15.0 chemistry transport model, *Geosci. Model Dev.*, 9, 137-160, 10.5194/gmd-9-137-2016, 2016.

1747 Guth, J., Marécal, V., Josse, B., Arteta, J., and Hamer, P.: Primary aerosol and secondary inorganic aerosol budget over the
 1748 Mediterranean Basin during 2012 and 2013, *Atmospheric Chemistry and Physics*, 18, 4911-4934, 2018.

1749 Hamer, P., Fjaeraa, A.-M., Soares, J., Meleux, F., Colette, A., Ung, A., Raux, B., and Tarrason, L.: Copernicus Atmosphere
 1750 Monitoring Service Interim Annual Assessment Report on European Air Quality in 2022, ECMWF, Bonn,
 1751 [https://policy.atmosphere.copernicus.eu/reports/CAMS271_2021SCx_D1.1.1_202306_2022_Interim_Assessment_Report_v](https://policy.atmosphere.copernicus.eu/reports/CAMS271_2021SCx_D1.1.1_202306_2022_Interim_Assessment_Report_v1.pdf)
 1752 [1.pdf](https://policy.atmosphere.copernicus.eu/reports/CAMS271_2021SCx_D1.1.1_202306_2022_Interim_Assessment_Report_v1.pdf), 2023.

1753 Hansen, K. M., Christensen, J. H., Brandt, J., Frohn, L. M., Geels, C., Skjøth, C. A., and Li, Y. F.: Modeling short-term
 1754 variability of α -hexachlorocyclohexane in Northern Hemispheric air, *Journal of Geophysical Research: Atmospheres*, 113,
 1755 2008.

1756 Hass, H., Jakobs, H., and Memmesheimer, M.: Analysis of a regional model (EURAD) near surface gas concentration
 1757 predictions using observations from networks, *Meteorology and Atmospheric Physics*, 57, 173-200, 1995.

1758 Heidam, N. Z., Christensen, J., Wählin, P., and Skov, H.: Arctic atmospheric contaminants in NE Greenland: levels,
1759 variations, origins, transport, transformations and trends 1990–2001, *Science of the Total Environment*, 331, 5-28, 2004.

1760 Heimann, M. and Keeling, C. D.: A three-dimensional model of atmospheric CO₂ transport based on observed winds: 2.
1761 Model description and simulated tracer experiments, Max-Planck-Institut für Meteorologie 1989.

1762 Hendriks, C., Forsell, N., Kieseewetter, G., Schaap, M., and Schöpp, W.: Ozone concentrations and damage for realistic
1763 future European climate and air quality scenarios, *Atmospheric Environment*, 144, 208-219, 2016.

1764 Hertel, O., Christensen, J., Runge, E. H., Asman, W. A., Berkowicz, R., Hovmand, M. F., and Hov, Ø.: Development and
1765 testing of a new variable scale air pollution model—ACDEP, *Atmospheric Environment*, 29, 1267-1290, 1995.

1766 Hicks, B., Baldocchi, D., Meyers, T., Hosker, R., and Matt, D.: A preliminary multiple resistance routine for deriving dry
1767 deposition velocities from measured quantities, *Water, Air, and Soil Pollution*, 36, 311-330, 1987.

1768 Hodzic, A., Kasibhatla, P. S., Jo, D. S., Cappa, C. D., Jimenez, J. L., Madronich, S., and Park, R. J.: Rethinking the global
1769 secondary organic aerosol (SOA) budget: stronger production, faster removal, shorter lifetime, *Atmospheric Chemistry and
1770 Physics*, 16, 7917-7941, 2016.

1771 Hollingsworth, A.: Toward a monitoring and forecasting system for atmospheric composition: The GEMS Project, *Bull.
1772 Amer. Meteor. Soc.*, 89, 1147-1164, <https://doi.org/10.1175/2008BAMS2355.1>, 2008.

1773 Hollingsworth, A. and Lönnberg, P.: The statistical structure of short-range forecast errors as determined from radiosonde
1774 data. Part I: The wind field, *Tellus A*, 38, 111-136, 1986.

1775 Holtslag, A., Van Meijgaard, E., and De Rooy, W.: A comparison of boundary layer diffusion schemes in unstable
1776 conditions over land, *Boundary-Layer Meteorology*, 76, 69-95, 1995.

1777 Holtslag, A. A. and Nieuwstadt, F. T.: Scaling the atmospheric boundary layer, *Boundary-Layer Meteorology*, 36, 201-209,
1778 1986.

1779 Honoré, C., Vautard, R., and Beekmann, M.: Photochemical regimes in urban atmospheres: The influence of dispersion,
1780 *Geophysical Research Letters*, 27, 1895-1898, 2000.

1781 Horálek, J., Schreiberová, M., Vlasáková, L., Hamer, P., Schneider, P., and Marková, J.: Interim European air quality maps
1782 for 2020. PM₁₀, NO₂ and ozone spatial estimates based on non-validated UTD data., NILU, Oslo,
1783 [https://www.eionet.europa.eu/etcs/etc-atni/products/etc-atni-report-19-2021-interim-european-air-quality-maps-for-2020-
1784 pm10-no2-and-ozone-spatial-estimates-based-on-non-validated-utd-data](https://www.eionet.europa.eu/etcs/etc-atni/products/etc-atni-report-19-2021-interim-european-air-quality-maps-for-2020-pm10-no2-and-ozone-spatial-estimates-based-on-non-validated-utd-data), 2022.

1785 Huang, G., Brook, R., Crippa, M., Janssens-Maenhout, G., Schieberle, C., Dore, C., Guizzardi, D., Muntean, M., Schaaf, E.,
1786 and Friedrich, R.: Speciation of anthropogenic emissions of non-methane volatile organic compounds: a global gridded data
1787 set for 1970–2012, *Atmospheric Chemistry and Physics*, 17, 7683-7701, 2017.

1788 Huijnen, V., Eskes, H., Poupkou, A., Elbern, H., Boersma, K., Foret, G., Sofiev, M., Valdebenito, A., Flemming, J., and
1789 Stein, O.: Comparison of OMI NO₂ tropospheric columns with an ensemble of global and European regional air quality
1790 models, *Atmospheric Chemistry and Physics*, 10, 3273-3296, 2010.

1791 Hunt, B. R., Kostelich, E. J., and Szunyogh, I.: Efficient data assimilation for spatiotemporal chaos: A local ensemble
1792 transform Kalman filter, *Physica D: Nonlinear Phenomena*, 230, 112-126, <https://doi.org/10.1016/j.physd.2006.11.008>,
1793 2007.

1794 Jaeglé, L., Quinn, P. K., Bates, T. S., Alexander, B., and Lin, J.-T.: Global distribution of sea salt aerosols: new constraints
1795 from in situ and remote sensing observations, *Atmospheric Chemistry and Physics*, 11, 3137, 2011.

1796 Janjic, Z. and Gall, L.: Scientific documentation of the NCEP nonhydrostatic multiscale model on the B grid (NMMB). Part
1797 1 Dynamics, NCAR/TN-489+STR, 2012.

1798 Jöckel, P., Tost, H., Pozzer, A., Brühl, C., Buchholz, J., Ganzeveld, L., Hoor, P., Kerkweg, A., Lawrence, M., and Sander,
1799 R.: The atmospheric chemistry general circulation model ECHAM5/MESSy1: consistent simulation of ozone from the
1800 surface to the mesosphere, *Atmospheric Chemistry and Physics*, 6, 5067-5104, 2006.

1801 Joly, M. and Peuch, V.-H.: Objective classification of air quality monitoring sites over Europe, *Atmospheric Environment*,
1802 47, 111-123, 2012.

1803 Jonson, J., Kylling, A., Berntsen, T., Isaksen, I., Zerefos, C., and Kourtidis, K.: Chemical effects of UV fluctuations inferred
1804 from total ozone and tropospheric aerosol variations, *Journal of Geophysical Research: Atmospheres*, 105, 14561-14574,
1805 2000.

1806 Jorba, O., Dabdub, D., Blaszcak-Boxe, C., Pérez, C., Janjic, Z., Baldasano, J., Spada, M., Badia, A., and Gonçalves, M.:
1807 Potential significance of photoexcited NO₂ on global air quality with the NMMB/BSC chemical transport model, *Journal of*
1808 *Geophysical Research: Atmospheres*, 117, 2012.

1809 Kahnert, M.: Variational data analysis of aerosol species in a regional CTM: background error covariance constraint and
1810 aerosol optical observation operators, *Tellus B: Chemical and Physical Meteorology*, 60, 753-770, 2008.

1811 Kain, J. S. and Fritsch, J. M.: A one-dimensional entraining/detraining plume model and its application in convective
1812 parameterization, *Journal of Atmospheric Sciences*, 47, 2784-2802, 1990.

1813 Kaiser, J., Heil, A., Andreae, M., Benedetti, A., Chubarova, N., Jones, L., Morcrette, J.-J., Razinger, M., Schultz, M., and
1814 Suttie, M.: Biomass burning emissions estimated with a global fire assimilation system based on observed fire radiative
1815 power, *Biogeosciences*, 9, 527-554, 2012.

1816 Klose, M., Jorba, O., Gonçalves Ageitos, M., Escibano, J., Dawson, M. L., Obiso, V., Di Tomaso, E., Basart, S., Montané
1817 Pinto, G., and Macchia, F.: Mineral dust cycle in the Multiscale Online Nonhydrostatic Atmosphere Chemistry model
1818 (MONARCH) version 2.0, *Geoscientific Model Development*, 14, 6403-6444, 2021.

1819 Köble, R. and Seufert, G.: Novel maps for forest tree species in Europe, *Proceedings of the 8th European symposium on the*
1820 *physico-chemical behaviour of air pollutants: “a changing atmosphere*, 17-20,

1821 Korhonen, H., Carslaw, K. S., Spracklen, D. V., Mann, G. W., and Woodhouse, M. T.: Influence of oceanic dimethyl sulfide
1822 emissions on cloud condensation nuclei concentrations and seasonality over the remote Southern Hemisphere oceans: A
1823 global model study, *Journal of Geophysical Research: Atmospheres*, 113, 2008.

1824 Kouznetsov, R. and Sofiev, M.: A methodology for evaluation of vertical dispersion and dry deposition of atmospheric
1825 aerosols, *Journal of Geophysical Research: Atmospheres*, 117, 2012.

1826 Kouznetsov, R., Sofiev, M., Vira, J., and Stiller, G.: Simulating age of air and the distribution of SF 6 in the stratosphere
1827 with the SILAM model, *Atmospheric Chemistry and Physics*, 20, 5837-5859, 2020.

1828 Kuenen, J., Visschedijk, A., Jozwicka, M., and Denier Van Der Gon, H.: TNO-MACC_II emission inventory; a multi-year
1829 (2003–2009) consistent high-resolution European emission inventory for air quality modelling, *Atmospheric Chemistry and*
1830 *Physics*, 14, 10963-10976, 2014.

1831 Kuenen, J., Dellaert, S., Visschedijk, A., Jalkanen, J.-P., Super, I., and Denier van der Gon, H.: CAMS-REG-v4: a state-of-
1832 the-art high-resolution European emission inventory for air quality modelling, *Earth System Science Data*, 14, 491-515,
1833 2022.

1834 Kukkonen, J., Savolahti, M., Palamarchuk, Y., Lanki, T., Nurmi, V., Paunu, V.-V., Kangas, L., Sofiev, M., Karppinen, A.,
1835 and Maragkidou, A.: Modelling of the public health costs of fine particulate matter and results for Finland in 2015,
1836 *Atmospheric Chemistry and Physics*, 20, 9371-9391, 2020.

1837 Kylling, A., Stamnes, K., and Tsay, S.-C.: A reliable and efficient two-stream algorithm for spherical radiative transfer:
1838 Documentation of accuracy in realistic layered media, *Journal of Atmospheric Chemistry*, 21, 115-150, 1995.

1839 Lahoz, W., Geer, A., Bekki, S., Bormann, N., Ceccherini, S., Elbern, H., Errera, Q., Eskes, H., Fonteyn, D., and Jackson, D.:
1840 The Assimilation of Envisat data (ASSET) project, *Atmospheric Chemistry and Physics*, 7, 1773-1796, 2007.

1841 Lambert, J. D.: Numerical methods for ordinary differential systems, Wiley New York 1991.

1842 Lana, A., Bell, T., Simó, R., Vallina, S., Ballabrera-Poy, J., Kettle, A., Dachs, J., Bopp, L., Saltzman, E., and Stefels, J.: An
1843 updated climatology of surface dimethylsulfide concentrations and emission fluxes in the global ocean, *Global*
1844 *Biogeochemical Cycles*, 25, 2011.

1845 Landgraf, J. and Crutzen, P.: An efficient method for online calculations of photolysis and heating rates, *Journal of the*
1846 *atmospheric sciences*, 55, 863-878, 1998.

1847 Lange, R.: Transferability of a three-dimensional air quality model between two different sites in complex terrain, *Journal of*
1848 *Applied Meteorology and Climatology*, 28, 665-679, 1989.

1849 Langner, J., Bergström, R., and Pleijel, K.: European scale modeling of sulphur, oxidized nitrogen and photochemical
1850 oxidants. Model development and evaluation for the 1994 growing season, *Swedish Met. and Hydrol. Inst., Norrköping,*
1851 *Sweden*, 1998.

1852 Lansø, A. S., Smallman, T. L., Christensen, J. H., Williams, M., Pilegaard, K., Sørensen, L.-L., and Geels, C.: Simulating the
1853 atmospheric CO 2 concentration across the heterogeneous landscape of Denmark using a coupled atmosphere–biosphere
1854 mesoscale model system, *Biogeosciences*, 16, 1505-1524, 2019.

1855 Lefevre, F., Brasseur, G., Folkins, I., Smith, A., and Simon, P.: Chemistry of the 1991–1992 stratospheric winter: Three-
1856 dimensional model simulations, *Journal of Geophysical Research: Atmospheres*, 99, 8183-8195, 1994.

1857 Lehtomäki, H., Korhonen, A., Asikainen, A., Karvosenoja, N., Kupiainen, K., Paunu, V.-V., Savolahti, M., Sofiev, M.,
1858 Palamarchuk, Y., and Karppinen, A.: Health impacts of ambient air pollution in Finland, *International journal of*
1859 *environmental research and public health*, 15, 736, 2018.

1860 Li, Y., Elbern, H., Lu, K., Friese, E., Kiendler-Scharr, A., Mentel, T. F., Wang, X., Wahner, A., and Zhang, Y.: Updated
1861 aerosol module and its application to simulate secondary organic aerosols during IMPACT campaign May 2008,
1862 Atmospheric chemistry and physics, 13, 6289-6304, 2013.

1863 Liu, D. C. and Nocedal, J.: On the limited memory BFGS method for large scale optimization, Mathematical programming,
1864 45, 503-528, 1989.

1865 Louis, J.-F.: A parametric model of vertical eddy fluxes in the atmosphere, Boundary-Layer Meteorology, 17, 187-202,
1866 1979.

1867 Lurmann, F. W., Lloyd, A. C., and Atkinson, R.: A chemical mechanism for use in long-range transport/acid deposition
1868 computer modeling, Journal of Geophysical Research: Atmospheres, 91, 10905-10936, 1986.

1869 Maas, R. and Grennfelt, P.: Towards Cleaner Air - Scientific Assessment Report 2016, EMEP-Steering body and Working
1870 Group on Effects - Convention on Long-Range Transboundary Air Pollution 2016.

1871 Madronich, S.: Photodissociation in the atmosphere: 1. Actinic flux and the effects of ground reflections and clouds, Journal
1872 of Geophysical Research: Atmospheres, 92, 9740-9752, 1987.

1873 Madronich, S. and Weller, G.: Numerical integration errors in calculated tropospheric photodissociation rate coefficients,
1874 Journal of atmospheric chemistry, 10, 289-300, 1990.

1875 Mailler, S., Menut, L., di Sarra, A. G., Becagli, S., Di Iorio, T., Bessagnet, B., Briant, R., Formenti, P., Doussin, J. F.,
1876 Gómez-Amo, J. L., Mallet, M., Rea, G., Siour, G., Sferlazzo, D. M., Traversi, R., Udisti, R., and Turquety, S.: On the
1877 radiative impact of aerosols on photolysis rates: comparison of simulations and observations in the Lampedusa island during
1878 the ChArMEx/ADRIED campaign, Atmos. Chem. Phys., 16, 1219-1244, 10.5194/acp-16-1219-2016, 2016.

1879 Manders, A. M. M., Builtjes, P. J. H., Curier, L., Denier van der Gon, H. A. C., Hendriks, C., Jonkers, S., Kranenburg, R.,
1880 Kuenen, J., Segers, A. J., Timmermans, R. M. A., Visschedijk, A., Wichink Kruit, R. J., Van Pul, W. A. J., Sauter, F. J., van
1881 der Swaluw, E., Swart, D. P. J., Douros, J., Eskes, H., van Meijgaard, E., van Ulft, B., van Velthoven, P., Banzhaf, S., Mues,
1882 A., Stern, R., Fu, G., Lu, S., Heemink, A., van Velzen, N., and Schaap, M.: Curriculum Vitae of the LOTOS-EUROS (v2.0)
1883 chemistry transport model, Geosci. Model Dev. Discuss., 2017, 1-53, 10.5194/gmd-2017-88, 2017.

1884 Marécal, V., Peuch, V. H., Andersson, C., Andersson, S., Arteta, J., Beekmann, M., Benedictow, A., Bergstrom, R.,
1885 Bessagnet, B., Cansado, A., Chéroux, F., Colette, A., Coman, A., Curier, R. L., Denier van der Gon, H. A. C., Drouin, A.,
1886 Elbern, H., Emili, E., Engelen, R. J., Eskes, H. J., Foret, G., Friese, E., Gauss, M., Giannaros, C., Guth, J., Joly, M.,
1887 Jaumouilla, E., Josse, B., Kadyrov, N., Kaiser, J. W., Krajsek, K., Kuenen, J., Kumar, U., Liora, N., Lopez, E., Malherbe,
1888 L., Martinez, I., Melas, D., Meleux, F., Menut, L., Moinat, P., Morales, T., Parmentier, J., Piacentini, A., Plu, M., Poupkou,
1889 A., Queguiner, S., Robertson, L., Rouil, L., Schaap, M., Segers, A., Sofiev, M., Tarasson, L., Thomas, M., Timmermans, R.,
1890 Valdebenito, A., van Velthoven, P., van Versendaal, R., Vira, J., and Ung, A.: A regional air quality forecasting system over
1891 Europe: the MACC-II daily ensemble production, Geosci. Model Dev., 8, 2777-2813, 2015.

1892 Mari, C., Jacob, D. J., and Bechtold, P.: Transport and scavenging of soluble gases in a deep convective cloud, Journal of
1893 Geophysical Research: Atmospheres, 105, 22255-22267, 2000.

1894 Martensson, E., Nilsson, E., de Leeuw, G., Cohen, L., and Hansson, H.-C.: Laboratory simulations and parameterisation of
1895 the primary marine aerosol production, J. Geophys. Res., 108, 4297, doi:10.1029/2002JD002263, 2003.

1896 Martet, M., Peuch, V., Laurent, B., Marticorena, B., and Bergametti, G.: Evaluation of long-range transport and deposition
1897 of desert dust with the CTM MOCAGE, *Tellus B: Chemical and Physical Meteorology*, 61, 449-463, 2009.

1898 Marticorena, B. and Bergametti, G.: Modeling the atmospheric dust cycle: 1. Design of a soil-derived dust emission scheme,
1899 *Journal of geophysical research: atmospheres*, 100, 16415-16430, 1995.

1900 Marticorena, B., Bergametti, G., Aumont, B., Callot, Y., N'Doumé, C., and Legrand, M.: Modeling the atmospheric dust
1901 cycle: 2. Simulation of Saharan dust sources, *Journal of Geophysical Research: Atmospheres*, 102, 4387-4404, 1997.

1902 Maul, P., Barber, F., and Martin, A.: Some observations of the meso-scale transport of sulphur compounds in the rural East
1903 Midlands, *Atmospheric Environment (1967)*, 14, 339-354, 1980.

1904 McRae, G. J., Goodin, W. R., and Seinfeld, J. H.: Numerical solution of the atmospheric diffusion equation for chemically
1905 reacting flows, *Journal of Computational Physics*, 45, 1-42, 1982.

1906 Meleux, F., Solmon, F., and Giorgi, F.: Increase in summer European ozone amounts due to climate change, *Atmospheric
1907 Environment*, 41, 7577-7587, 2007.

1908 Memmesheimer, M., Friese, E., Ebel, A., Jakobs, H., Feldmann, H., Kessler, C., and Piekorz, G.: Long-term simulations of
1909 particulate matter in Europe on different scales using sequential nesting of a regional model, *International Journal of
1910 Environment and Pollution*, 22, 108-132, 2004.

1911 Ménégoz, M., Salas y Melia, D., Legrand, M., Teyssède, H., Michou, M., Peuch, V.-H., Martet, M., Josse, B., and
1912 Dombrowski-Etchevers, I.: Equilibrium of sinks and sources of sulphate over Europe: comparison between a six-year
1913 simulation and EMEP observations, *Atmospheric Chemistry and Physics*, 9, 4505-4519, 2009.

1914 Menut, L., Schmechtig, C., and Marticorena, B.: Sensitivity of the sandblasting flux calculations to the soil size distribution
1915 accuracy, *Journal of Atmospheric and Oceanic Technology*, 22, 1875-1884, 2005.

1916 Menut, L., Vautard, R., Beekmann, M., and Honore, C.: Sensitivity of photochemical pollution using the adjoint of a
1917 simplified chemistry-transport model, *Journal of geophysical research*, 105, 2000.

1918 Menut, L., Bessagnet, B., Briant, R., Cholakian, A., Couvidat, F., Mailler, S., Pennel, R., Siour, G., Tuccella, P., and
1919 Turquety, S.: The CHIMERE v2020r1 online chemistry-transport model, *Geoscientific Model Development*, 14, 6781-6811,
1920 2021.

1921 Metzger, S., Dentener, F., Pandis, S., and Lelieveld, J.: Gas/aerosol partitioning: 1. A computationally efficient model, *J.
1922 Geophys. Res.*, 107, 4312, 2002.

1923 Michou, M., Laville, P., Serça, D., Fotiadi, A., Bouchou, P., and Peuch, V.-H.: Measured and modeled dry deposition
1924 velocities over the ESCOMPTE area, *Atmospheric Research*, 74, 89-116, 2005.

1925 Mircea, M., Ciancarella, L., Briganti, G., Calori, G., Cappelletti, A., Cionni, I., Costa, M., Cremona, G., D'Isidoro, M.,
1926 Finardi, S., Pace, G., Piersanti, A., Righini, G., Silibello, C., Vitali, L., and Zanini, G.: Assessment of the AMS-MINNI
1927 system capabilities to simulate air quality over Italy for the calendar year 2005, *Atmospheric Environment*, 84, 178-188,
1928 <https://doi.org/10.1016/j.atmosenv.2013.11.006>, 2014.

- 1929 Miyoshi, T. and Yamane, S.: Local Ensemble Transform Kalman Filtering with an AGCM at a T159/L48 Resolution,
1930 Monthly Weather Review, 135, 3841-3861, 10.1175/2007MWR1873.1, 2007.
- 1931 Monahan, E. C.: The ocean as a source of atmospheric particles, in: The Role of Air-Sea Exchange in Geochemical Cycling,
1932 Kluwer Academic Publishers, Dordrecht, Holland, 129–163, 1986.
- 1933 Morcrette, J. J., Boucher, O., Jones, L., Salmond, D., Bechtold, P., Beljaars, A., Benedetti, A., Bonet, A., Kaiser, J., and
1934 Razinger, M.: Aerosol analysis and forecast in the European Centre for medium-range weather forecasts integrated forecast
1935 system: Forward modeling, Journal of Geophysical Research: Atmospheres, 114, 2009.
- 1936 Mozurkewich, M.: The dissociation constant of ammonium nitrate and its dependence on temperature, relative humidity and
1937 particle size, Atmospheric Environment. Part A. General Topics, 27, 261-270, 1993.
- 1938 Nenes, A., Pandis, S., and Pilinis, C.: ISORROPIA: A New Thermodynamic Equilibrium Model for Multiphase
1939 Multicomponent Inorganic Aerosols, Aquatic Geochemistry, 4, 123-152, 1998.
- 1940 Nho-Kim, E.-Y., Michou, M., and Peuch, V.-H.: Parameterization of size-dependent particle dry deposition velocities for
1941 global modeling, Atmospheric Environment, 38, 1933-1942, 2004.
- 1942 Nho-Kim, E., Peuch, V., and Oh, S.: Estimation of the global distribution of Black Carbon aerosols with MOCAGE, the
1943 CTM of Météo-France, J. Korean Meteor. Soc, 41, 587-598, 2005.
- 1944 Nieradzik, L.: Application of a high dimensional model representation on the atmospheric aerosol module MADE of the
1945 EURAD-CTM, Institut für Geophysik und Meteorologie der Universität zu Köln, 2005.
- 1946 Nieuwstadt, F.: The steady-state height and resistance laws of the nocturnal boundary layer: Theory compared with Cabauw
1947 observations, Boundary-Layer Meteorology, 20, 3-17, 1981.
- 1948 Nocedal, J.: Updating quasi-Newton matrices with limited storage, Mathematics of computation, 35, 773-782, 1980.
- 1949 Noilhan, J. and Planton, S.: A simple parameterization of land surface processes for meteorological models, Monthly
1950 weather review, 117, 536-549, 1989.
- 1951 Omstedt, G., Bringfelt, B., and Johansson, C.: A model for vehicle-induced non-tailpipe emissions of particles along
1952 Swedish roads, Atmospheric environment, 39, 6088-6097, 2005.
- 1953 Pai, S. J., Heald, C. L., Pierce, J. R., Farina, S. C., Marais, E. A., Jimenez, J. L., Campuzano-Jost, P., Nault, B. A.,
1954 Middlebrook, A. M., Coe, H., Shilling, J. E., Bahreini, R., Dingle, J. H., and Vu, K.: An evaluation of global organic aerosol
1955 schemes using airborne observations, Atmos. Chem. Phys., 20, 2637-2665, 10.5194/acp-20-2637-2020, 2020.
- 1956 Parrish, D. F. and Derber, J. C.: The National Meteorological Center's spectral statistical-interpolation analysis system,
1957 Monthly Weather Review, 120, 1747-1763, 1992.
- 1958 Passant, N.: Speciation of UK emissions of non-methane volatile organic compounds, AEA Technology2002.
- 1959 Pepper, D., Kern, C., and Long Jr, P.: Modeling the dispersion of atmospheric pollution using cubic splines and chapeau
1960 functions, Atmospheric Environment (1967), 13, 223-237, 1979.

1961 Pérez, C., Haustein, K., Jorba, O., Janjic, Z., Huneeus, N., Baldasano, J. M., Black, T., Basart, S., Nickovic, S., Miller, R. L.,
1962 Perlwitz, J., Schulz, M., and Thomson, M.: Atmospheric dust modeling from meso to global scales with the online
1963 NMMB/BSC-Dust model–Part 1: Model description, annual simulations and evaluation, *Atmospheric Chemistry and*
1964 *Physics*, 11, 13001-13027, 2011.

1965 Petersen, A. K., Brasseur, G. P., Bouarar, I., Flemming, J., Gauss, M., Jiang, F., Kouznetsov, R., Kranenburg, R., Mijling,
1966 B., and Peuch, V.-H.: Ensemble forecasts of air quality in eastern China–Part 2: Evaluation of the MarcoPolo–Panda
1967 prediction system, version 1, *Geoscientific Model Development*, 12, 1241-1266, 2019.

1968 Peterson, J. T.: Calculated actinic fluxes (290-700 nm) for air pollution photochemistry applications, US Environmental
1969 Protection Agency, Office of Research and Development ...1976.

1970 Petroff, A. and Zhang, L.: Development and validation of a size-resolved particle dry deposition scheme for application in
1971 aerosol transport models, *Geoscientific Model Development*, 3, 753-769, 2010.

1972 Peuch, V.-H., Engelen, R., Rixen, M., Dee, D., Flemming, J., Suttie, M., Ades, M., Agustí-Panareda, A., Ananasso, C.,
1973 Andersson, E., Armstrong, D., Barré, J., Bousserez, N., Dominguez, J. J., Garrigues, S., Inness, A., Jones, L., Kipling, Z.,
1974 Letertre-Danczak, J., Parrington, M., Razinger, M., Ribas, R., Vermoote, S., Yang, X., Simmons, A., Garcés de Marcilla, J.,
1975 and Thépaut, J.-N.: The Copernicus Atmosphere Monitoring Service: From Research to Operations, *Bulletin of the*
1976 *American Meteorological Society*, 103, E2650-E2668, <https://doi.org/10.1175/BAMS-D-21-0314.1>, 2022.

1977 Peuch, V., Engelen, R., Simmons, A., Lahoz, W., Laj, P., and Galmarini, S.: Monitoring atmospheric composition and
1978 climate, research in support of the Copernicus/GMES atmospheric service, Special Issue, *Atmos. Chem. Phys.*, [http://www.](http://www.atmos-chem-phys.net/special_issue310.html)
1979 [atmos-chem-phys. net/special_issue310. html](http://www.atmos-chem-phys.net/special_issue310.html), 2014.

1980 Poupkou, A., Giannaros, T., Markakis, K., Kioutsioukis, I., Curci, G., Melas, D., and Zerefos, C.: A model for European
1981 Biogenic Volatile Organic Compound emissions: Software development and first validation, *Environmental Modelling &*
1982 *Software*, 25, 1845-1856, 2010.

1983 Prank, M., Chapman, D. S., Bullock, J. M., Belmonte, J., Berger, U., Dahl, A., Jäger, S., Kovtunen, I., Magyar, D., and
1984 Niemelä, S.: An operational model for forecasting ragweed pollen release and dispersion in Europe, *Agricultural and forest*
1985 *meteorology*, 182, 43-53, 2013.

1986 Price, C., Penner, J., and Prather, M.: NO_x from lightning: 1. Global distribution based on lightning physics, *Journal of*
1987 *Geophysical Research: Atmospheres*, 102, 5929-5941, 1997.

1988 Rabitz, H. and Aliş, Ö. F.: General foundations of high-dimensional model representations, *Journal of Mathematical*
1989 *Chemistry*, 25, 197-233, 1999.

1990 Rappenglück, B., Lubertino, G., Alvarez, S., Golovko, J., Czader, B., and Ackermann, L.: Radical precursors and related
1991 species from traffic as observed and modeled at an urban highway junction, *Journal of the Air & Waste Management*
1992 *Association*, 63, 1270-1286, 2013.

1993 Rémy, S., Kipling, Z., Flemming, J., Boucher, O., Nabat, P., Michou, M., Bozzo, A., Ades, M., Huijnen, V., Benedetti, A.,
1994 Engelen, R., Peuch, V. H., and Morcrette, J. J.: Description and evaluation of the tropospheric aerosol scheme in the
1995 European Centre for Medium-Range Weather Forecasts (ECMWF) Integrated Forecasting System (IFS-AER, cycle 45R1),
1996 *Geosci. Model Dev.*, 12, 4627-4659, 10.5194/gmd-12-4627-2019, 2019.

- 1997 Robertson, L., Langner, J., and Engardt, M.: An Eulerian limited-area atmospheric transport model, *Journal of Applied*
1998 *Meteorology and Climatology*, 38, 190-210, 1999.
- 1999 Robichaud, A. and Ménard, R.: Multi-year objective analyses of warm season ground-level ozone and PM 2.5 over North
2000 America using real-time observations and Canadian operational air quality models, *Atmospheric Chemistry and Physics*, 14,
2001 1769-1800, 2014.
- 2002 Roselle, S. J. and Binkowski, F. S.: Cloud dynamics and chemistry, Science algorithms of the EPA Models-3 Community
2003 multiscale air quality (CMAQ) modeling system, 1999.
- 2004 Rouil, L., Honore, C., Vautard, R., Beekmann, M., Bessagnet, B., Malherbe, L., Meleux, F., Dufour, A., Elichegaray, C.,
2005 Flaud, J. M., Menut, L., Martin, D., Peuch, A., Peuch, V. H., and Poisson, N.: PREV'AIR An Operational Forecasting and
2006 Mapping System for Air Quality in Europe, *Bulletin of the American Meteorological Society*, 90, 73-83,
2007 10.1175/2008bams2390.1, 2009.
- 2008 Salameh, T., Drobinski, P., Menut, L., Bessagnet, B., Flamant, C., Hodzic, A., and Vautard, R.: Aerosol distribution over the
2009 western Mediterranean basin during a Tramontane/Mistral event, *Annales Geophysicae*, 25, 2271-2291, 2007.
- 2010 Sander, S., Golden, D., Kurylo, M., Moortgat, G., Wine, P., Ravishankara, A., Kolb, C., Molina, M., Finlayson-Pitts, B., and
2011 Huie, R.: Chemical kinetics and photochemical data for use in atmospheric studies evaluation number 15, Pasadena, CA: Jet
2012 Propulsion Laboratory, National Aeronautics and Space ..., 2006.
- 2013 Sandu, A. and Sander, R.: Simulating chemical systems in Fortran90 and Matlab with the Kinetic PreProcessor KPP-2.1,
2014 *Atmospheric Chemistry and Physics*, 6, 187-195, 2006.
- 2015 Sarwar, G., Simon, H., Bhave, P., and Yarwood, G.: Examining the impact of heterogeneous nitryl chloride production on
2016 air quality across the United States, *Atmospheric Chemistry and Physics*, 12, 6455-6473, 2012.
- 2017 Schaap, M., Van Loon, M., Ten Brink, H., Dentener, F., and Builtjes, P.: Secondary inorganic aerosol simulations for Europe
2018 with special attention to nitrate, *Atmospheric Chemistry and Physics*, 4, 857-874, 2004.
- 2019 Schaap, M., Kranenburg, R., Curier, L., Jozwicka, M., Dammers, E., and Timmermans, R.: Assessing the sensitivity of the
2020 OMI-NO2 product to emission changes across Europe, *Remote Sensing*, 5, 4187-4208, 2013.
- 2021 Schaap, M., Manders, A. M. M., Hendriks, E. C. J., Cnossen, J. M., Segers, A. J. S., Denier van der Gon, H., Jozwicka, M.,
2022 Sauter, F. J., Velders, G. J. M., Matthijsen, J., and Builtjes, P. J. H.: Regional Modelling of Particulate Matter for the
2023 Netherlands Netherlands Research Program on Particulate Matter, ISSN: 1875-2314, 2009.
- 2024 Schell, B., Ackermann, I. J., Hass, H., Binkowski, F. S., and Ebel, A.: Modeling the formation of secondary organic aerosol
2025 within a comprehensive air quality model system, *Journal of Geophysical Research: Atmospheres*, 106, 28275-28293,
2026 2001a.
- 2027 Schell, B., Ackermann, I. J., Hass, H., Binkowski, F. S., and Ebel, A.: Modelling the formation of secondary organic within a
2028 comprehensive air quality model system, *J. Geophys. Res.*, 106, 28275-28293, 2001b.
- 2029 Schultz, M. G., Backman, L., Balkanski, Y., Bjoerndalsaeter, S., Brand, R., Burrows, J. P., Dalsoeren, S., de Vasconcelos,
2030 M., Grodtmann, B., Hauglustaine, D., Heil, A., Hoelzemann, J., Isaksen, I. S. A., Kaurola, J., Knorr, W., Ladstaetter-
2031 Weißenmayer, A., Mota, B., Oom, D., Pacyna, J., Panasiuk, D., Pereira, J., Pulles, T., Pyle, J., Rast, S., Richter, A., Savage,

2032 N., Schnadt, C., Schulz, M., Spessa, A., Staehelin, J., Sundet, J. K., Szopa, S., Thonicke, K., van het Bolscher, M., van
2033 Noije, T., van Velthoven, P., Vik, A. F., and Wittrock F.: REanalysis of the TROpospheric chemical composition over the
2034 past 40 years (RETRO) — A long-term global modeling study of tropospheric chemistry Final Report, Max Planck Institute
2035 for Meteorology, Jülich/Hamburg, Germany, , ISSN 1614-1199, 2007.

2036 Schutgens, N. A. J., Miyoshi, T., Takemura, T., and Nakajima, T.: Applying an ensemble Kalman filter to the assimilation of
2037 AERONET observations in a global aerosol transport model, *Atmos. Chem. Phys.*, 10, 2561-2576, 10.5194/acp-10-2561-
2038 2010, 2010.

2039 Seinfeld, J. H. and Pandis, S. N.: *Atmospheric Chemistry and Physics, From Air Pollution to Climate Change.*, New York,
2040 USA.1998.

2041 Shaddick, G., Salter, J. M., Peuch, V.-H., Ruggeri, G., Thomas, M. L., Mudu, P., Tarasova, O., Baklanov, A., and Gummy, S.:
2042 Global air quality: An inter-disciplinary approach to exposure assessment for burden of disease analyses, *Atmosphere*, 12,
2043 48, 2020.

2044 Shrivastava, M. K., Lane, T. E., Donahue, N. M., Pandis, S. N., and Robinson, A. L.: Effects of gas particle partitioning and
2045 aging of primary emissions on urban and regional organic aerosol concentrations, *Journal of Geophysical Research:*
2046 *Atmospheres*, 113, 2008.

2047 Sič, B., El Amraoui, L., Marécal, V., Josse, B., Arteta, J., Guth, J., Joly, M., and Hamer, P.: Modelling of primary aerosols in
2048 the chemical transport model MOCAGE: Development and evaluation of aerosol physical parameterizations, *Geoscientific*
2049 *Model Development*, 8, 381-408, 2015.

2050 Silibello, C., Calori, G., Brusasca, G., Giudici, A., Angelino, E., Fossati, G., Peroni, E., and Buganza, E.: Modelling of
2051 PM10 concentrations over Milano urban area using two aerosol modules, *Environmental Modelling & Software*, 23, 333-
2052 343, 2008.

2053 Silver, J. D., Christensen, J. H., Kahnert, M., Robertson, L., Rayner, P. J., and Brandt, J.: Multi-species chemical data
2054 assimilation with the Danish Eulerian hemispheric model: system description and verification, *Journal of Atmospheric*
2055 *Chemistry*, 73, 261-302, 2016.

2056 Simpson, D., Benedictow, A., and Darras, S.: The CAMS soil emissions: CAMS-GLOB-SOIL, in: CAMS2_61 – Global and
2057 European emission inventories., 59–70, <https://doi.org/10.24380/q2si-ti6i>, 2023.

2058 Simpson, D., Guenther, A., Hewitt, C., and Steinbrecher, R.: Biogenic emissions in Europe 1. Estimates and uncertainties, *J.*
2059 *Geophys. Res.*, 100, 22875–22890, 1995.

2060 Simpson, D., Fagerli, H., Jonson, J., Tsyro, S., Wind, P., and Tuovinen, J.-P.: The EMEP Unified Eulerian Model. Model
2061 Description, The Norwegian Meteorological Institute, EMEP, Oslo, 2003.

2062 Simpson, D., Bergström, R., Briolat, A., Imhof, H., Johansson, J., Priestley, M., and Valdebenito, A.: GenChem v1.0—a
2063 chemical pre-processing and testing system for atmospheric modelling, *Geoscientific Model Development*, 13, 6447-6465,
2064 2020a.

2065 Simpson, D., Benedictow, A., Berge, H., Bergstrom, R., Emberson, L. D., Fagerli, H., Flechard, C. R., Hayman, G. D.,
2066 Gauss, M., Jonson, J. E., Jenkin, M. E., Nyiri, A., Richter, C., Semeena, V. S., Tsyro, S., Tuovinen, J. P., Valdebenito, A.,

2067 and Wind, P.: The EMEP MSC-W chemical transport model - technical description, *Atmos. Chem. Phys.*, 12, 7825-7865,
2068 2012.

2069 Simpson, D., Fagerli, H., Colette, A., Denier van der Gon, H., Dore, C., Hallquist, M., Hansson, H.-C., Maas, R., Rouil, L.,
2070 Allemand, N., Bergström, B., Bessagnet, B., Couvidat, F., El Haddad, I., Genberg Safont, J., Goile, F., Grieshop, A.,
2071 Fraboulet, I., Hallquist, A., Hamilton, J., Juhlich, K., Klimont, Z., Kregar, Z., Mawdsely, I., Megaritis, A., Ntziachristos, L.,
2072 Pandis, S., Prévôt, A. S. H., Schindlbacher, S., Seljeskog, M., Sirina-Leboine, N., Sommers, J., and Åström, S.: How should
2073 condensables be included in PM emission inventories reported to EMEP/CLRTAP?, EMEP, Oslo, 2020b.

2074 Sindelarova, K., Granier, C., Bouarar, I., Guenther, A., Tilmes, S., Stavrakou, T., Müller, J. F., Kuhn, U., Stefani, P., and
2075 Knorr, W.: Global data set of biogenic VOC emissions calculated by the MEGAN model over the last 30 years, *Atmos.*
2076 *Chem. Phys.*, 14, 9317-9341, 10.5194/acp-14-9317-2014, 2014.

2077 Slinn, W., Hasse, L., Hicks, B., Hogan, A., Lal, D., Liss, P., Munnich, K., Sehmel, G., and Vittori, O.: Some aspects of the
2078 transfer of atmospheric trace constituents past the air-sea interface, *Atmospheric Environment* (1967), 12, 2055-2087, 1978.

2079 Slinn, W. G. N.: Precipitation scavenging, US. Department of Energy, Washington, D.C., 1983.

2080 Smagorinsky, J.: General circulation experiments with the primitive equations: I. The basic experiment, *Monthly weather*
2081 *review*, 91, 99-164, 1963.

2082 Soares, J., Sofiev, M., Geels, C., Christensen, J. H., Andersson, C., Tsyro, S., and Langner, J.: Impact of climate change on
2083 the production and transport of sea salt aerosol on European seas, *Atmospheric Chemistry and Physics*, 16, 13081-13104,
2084 2016.

2085 Sofiev, M.: A model for the evaluation of long-term airborne pollution transport at regional and continental scales,
2086 *Atmospheric Environment*, 34, 2481-2493, 2000.

2087 Sofiev, M.: Extended resistance analogy for construction of the vertical diffusion scheme for dispersion models, *Journal of*
2088 *Geophysical Research: Atmospheres*, 107, ACH 10-11-ACH 10-18, 2002.

2089 Sofiev, M.: On possibilities of assimilation of near-real-time pollen data by atmospheric composition models, *Aerobiologia*,
2090 35, 523-531, 2019.

2091 Sofiev, M., Galperin, M., and Genikhovich, E.: Construction and evaluation of Eulerian dynamic core for the air quality and
2092 emergency modelling system SILAM

2093 NATO Science for peace and security, Series C: Environmental Security, Air pollution modelling and its application, XIX,
2094 Springer, 699-701 pp.2008.

2095 Sofiev, M., Genikhovich, E., Keronen, P., and Vesala, T.: Diagnosing the surface layer parameters for dispersion models
2096 within the meteorological-to-dispersion modeling interface, *Journal of applied meteorology and climatology*, 49, 221-233,
2097 2010.

2098 Sofiev, M., Soares, J., Prank, M., de Leeuw, G., and Kukkonen, J.: A regional-to-global model of emission and transport of
2099 sea salt particles in the atmosphere, *J. Geophys. Res.*, 116, doi:10.1029/2010JD014713, 2011.

2100 Sofiev, M., Vira, J., Kouznetsov, R., Prank, M., Soares, J., and Genikhovich, E.: Construction of an Eulerian atmospheric
2101 dispersion model based on the advection algorithm of M. Galperin: dynamic cores v. 4 and 5 of SILAM v. 5.5, Geoscientific
2102 Model Development Discussions, 8, 2015a.

2103 Sofiev, M., Siljamo, P., Ranta, H., Linkosalo, T., Jaeger, S., Rasmussen, A., Rantio-Lehtimäki, A., Severova, E., and
2104 Kukkonen, J.: A numerical model of birch pollen emission and dispersion in the atmosphere. Description of the emission
2105 module, International journal of biometeorology, 57, 45-58, 2013.

2106 Sofiev, M., Berger, U., Prank, M., Vira, J., Arteta, J., Belmonte, J., Bergmann, K. C., Chéroux, F., Elbern, H., Friese, E.,
2107 Galan, C., Gehrig, R., Khvorostyanov, D., Kranenburg, R., Kumar, U., Marécal, V., Meleux, F., Menut, L., Pessi, A. M.,
2108 Robertson, L., Rittenberga, O., Rodinkova, V., Saarto, A., Segers, A., Severova, E., Sauliene, I., Siljamo, P., Steensen, B. M.,
2109 Teinmaa, E., Thibaudon, M., and Peuch, V. H.: MACC regional multi-model ensemble simulations of birch pollen
2110 dispersion in Europe, Atmos. Chem. Phys., 15, 8115-8130, 10.5194/acp-15-8115-2015, 2015b.

2111 Sofieva, S., Asmi, E., Atanasova, N. S., Heikkinen, A. E., Vidal, E., Duplissy, J., Romantschuk, M., Kouznetsov, R.,
2112 Kukkonen, J., and Bamford, D. H.: Effects of temperature and salinity on sea-spray-aerosol formation simulated with a
2113 bubble-generating chamber, Atmospheric Measurement Techniques Discussions, 2022, 1-40, 2022.

2114 Spada, M.: Development and evaluation of an atmospheric aerosol module implemented within the NMMB/BSC-CTM,
2115 2015.

2116 Spada, M., Jorba, O., Pérez García-Pando, C., Janjic, Z., and Baldasano, J. M.: Modeling and evaluation of the global sea-
2117 salt aerosol distribution: sensitivity to size-resolved and sea-surface temperature dependent emission schemes, Atmos. Chem.
2118 Phys., 13, 11735-11755, 10.5194/acp-13-11735-2013, 2013.

2119 Stadtler, S., Simpson, D., Schröder, S., Taraborrelli, D., Bott, A., and Schultz, M.: Ozone impacts of gas–aerosol uptake in
2120 global chemistry transport models, Atmospheric Chemistry and Physics, 18, 3147-3171, 2018.

2121 Stockwell, W. R., Kirchner, F., Kuhn, M., and Seefeld, S.: A new mechanism for regional atmospheric chemistry modeling,
2122 Journal of Geophysical Research: Atmospheres, 102, 25847-25879, 1997.

2123 Strand, A. and Hov, O.: A two-dimensional global study of tropospheric ozone production, J Geophys Res 99, 22877-22895,
2124 1994.

2125 Struzewska, J. and Kaminski, J.: Formation and transport of photooxidants over Europe during the July 2006 heat wave–
2126 observations and GEM-AQ model simulations, Atmospheric Chemistry and Physics, 8, 721-736, 2008.

2127 Struzewska, J. and Kaminski, J.: Impact of urban parameterization on high resolution air quality forecast with the GEM–AQ
2128 model, Atmospheric Chemistry and Physics, 12, 10387-10404, 2012.

2129 Struzewska, J., Kaminski, J., and Jefimow, M.: Application of model output statistics to the GEM-AQ high resolution air
2130 quality forecast, Atmospheric Research, 181, 186-199, 2016.

2131 Struzewska, J., Zdunek, M., Kaminski, J., Łobocki, L., Porebska, M., Jefimow, M., and Gawuc, L.: Evaluation of the GEM-
2132 AQ model in the context of the AQMEII Phase 1 project, Atmospheric Chemistry and Physics, 15, 3971-3990, 2015.

2133 Thürkow, M., Kirchner, I., Kranenburg, R., Timmermans, R., and Schaap, M.: A multi-meteorological comparison for
 2134 episodes of PM10 concentrations in the Berlin agglomeration area in Germany with the LOTOS-EUROS CTM, *Atmospheric*
 2135 *Environment*, 244, 117946, 2021.

2136 Tie, X., Madronich, S., Walters, S., Zhang, R., Rasch, P., and Collins, W.: Effect of clouds on photolysis and oxidants in the
 2137 troposphere, *Journal of Geophysical Research: Atmospheres*, 108, 2003.

2138 Timmermans, R., van Pinxteren, D., Kranenburg, R., Hendriks, C., Fomba, K., Herrmann, H., and Schaap, M.: Evaluation of
 2139 modelled LOTOS-EUROS with observational based PM10 source attribution, *Atmospheric Environment: X*, 14, 100173,
 2140 2022.

2141 Troen, I. and Mahrt, L.: A simple model of the atmospheric boundary layer: Sensitivity to surface evaporation, *Bound.-Layer*
 2142 *Meteorol.*, 37, 129-148, 1986.

2143 Tsyro, S., Aas, W., Soares, J., Sofiev, M., Berge, H., and Spindler, G.: Modelling of sea salt concentrations over Europe: key
 2144 uncertainties and comparison with observations, *Atmos. Chem. Phys.*, 11, 10367–10388, doi:10.5194/acp-11-10367-2011,
 2145 2011.

2146 Tuovinen, J.-P., Ashmore, M., Emberson, L., and Simpson, D.: Testing and improving the EMEP ozone deposition module,
 2147 *Atmos. Environ.*, 38, 2373–2385, 2004.

2148 van Leer, B.: Multidimensional explicit difference schemes for hyperbolic conservation laws, in: *Computing Methods in*
 2149 *Applied Sciences and Engineering VI*, edited by: Lions, R. G. a. J. L., Elsevier, Amsterdam, 1984.

2150 Van Ulden, A. and Holtslag, A.: Estimation of atmospheric boundary layer parameters for diffusion applications, *Journal of*
 2151 *Applied Meteorology and Climatology*, 24, 1196-1207, 1985.

2152 Van Zanten, M., Sauter, F., RJ, W. K., Van Jaarsveld, J., and Van Pul, W.: Description of the DEPAC module: Dry
 2153 deposition modelling with DEPAC_GCN2010, RIVM rapport 680180001, 2010.

2154 Vautard, R., Bessagnet, B., Chin, M., and Menut, L.: On the contribution of natural Aeolian sources to particulate matter
 2155 concentrations in Europe: Testing hypotheses with a modelling approach, *Atmospheric Environment*, 39, 3291-3303,
 2156 <https://doi.org/10.1016/j.atmosenv.2005.01.051>, 2005.

2157 Venkatram, A.: Estimating the Monin-Obukhov length in the stable boundary layer for dispersion calculations, *Boundary-*
 2158 *Layer Meteorology*, 19, 481-485, 1980.

2159 Venkatram, A. and Pleim, J.: The electrical analogy does not apply to modelling dry deposition of particles, *Atmos.*
 2160 *Environ.*, 33, 3075-3076, 1999.

2161 Venkatram, A., Karamchandani, P., and Misra, P.: Testing a comprehensive acid deposition model, *Atmospheric*
 2162 *Environment (1967)*, 22, 737-747, 1988.

2163 Vira, J. and Sofiev, M.: On variational data assimilation for estimating the model initial conditions and emission fluxes for
 2164 short-term forecasting of SOx concentrations, *Atmospheric environment*, 46, 318-328, 2012.

2165 Vira, J. and Sofiev, M.: Assimilation of surface NO₂ and O₃ observations into the SILAM chemistry transport model,
 2166 *Geoscientific Model Development*, 8, 191-203, 2015.

2167 Wang, X., Zhang, L., and Moran, M. D.: Development of a new semi-empirical parameterization for below-cloud
2168 scavenging of size-resolved aerosol particles by both rain and snow, *Geoscientific Model Development*, 7, 799-819, 2014.

2169 Weaver, A. and Courtier, P.: Correlation modelling on the sphere using a generalized diffusion equation, *Quarterly Journal*
2170 *of the Royal Meteorological Society*, 127, 1815-1846, 2001.

2171 Wesely, M. L.: Parameterization of surface resistances to gaseous dry deposition in regional-scale numerical models,
2172 *Atmospheric Environment* (1967), 23, 1293-1304, 1989.

2173 Wild, O., Zhu, X., and Prather, M. J.: Fast-J: Accurate Simulation of In- and Below-Cloud Photolysis in Tropospheric
2174 Chemical Models, *Journal of Atmospheric Chemistry*, 37, 245-282, 10.1023/A:1006415919030, 2000.

2175 Williams, E., Guenther, A., and Fehsenfeld, F.: An inventory of nitric oxide emissions from soils in the United States,
2176 *Journal of Geophysical Research: Atmospheres*, 97, 7511-7519, 1992.

2177 Williamson, D. L. and Rasch, P. J.: Two-dimensional semi-Lagrangian transport with shape-preserving interpolation,
2178 *Monthly Weather Review*, 117, 102-129, 1989.

2179 Willis, P. T. and Tattelman, P.: Drop-size distributions associated with intense rainfall, *Journal of Applied Meteorology and*
2180 *Climatology*, 28, 3-15, 1989.

2181 Xian, P., Reid, J. S., Hyer, E. J., Sampson, C. R., Rubin, J. I., Ades, M., Asencio, N., Basart, S., Benedetti, A., and
2182 Bhattacharjee, P. S.: Current state of the global operational aerosol multi-model ensemble: An update from the International
2183 Cooperative for Aerosol Prediction (ICAP), *Quarterly Journal of the Royal Meteorological Society*, 145, 176-209, 2019.

2184 Yamartino, R., Scire, J., Carmichael, G., and Chang, Y.: The CALGRID mesoscale photochemical grid model—I. Model
2185 formulation, *Atmospheric Environment. Part A. General Topics*, 26, 1493-1512, 1992.

2186 Yamartino, R. J., Flemming, J., and Stern, R.: Adaptation of analytic diffusivity formulations to Eulerian grid model layers
2187 of finite thickness, in: *Air Pollution Modeling and Its Application XVII*, Springer, 468-477, 2007.

2188 Yarwood, G., Rao, S., Yocke, M., and Whitten, G. Z.: Updates to the Carbon Bond chemical mechanism: CB05,
2189 http://www.camx.com/publ/pdfs/CB05_Final_Report_120805.pdf, 2005.

2190 Yienger, J. and Levy, H.: Empirical model of global soil-biogenic NO_x emissions, *Journal of Geophysical Research:*
2191 *Atmospheres*, 100, 11447-11464, 1995.

2192 Yuan, H., Dai, Y., Xiao, Z., Ji, D., and Shangguan, W.: Reprocessing the MODIS Leaf Area Index Products for Land
2193 Surface and Climate Modelling, *Remote Sensing of Environment*, 155, 1171–1187, doi:10.1016/j.rse.2011.01.001, 2011.

2194 Zare, A., Christensen, J., Irannejad, P., and Brandt, J.: Evaluation of two isoprene emission models for use in a long-range
2195 air pollution model, *Atmospheric Chemistry and Physics*, 12, 7399-7412, 2012.

2196 Zare, A., Christensen, J., Gross, A., Irannejad, P., Glasius, M., and Brandt, J.: Quantifying the contributions of natural
2197 emissions to ozone and total fine PM concentrations in the Northern Hemisphere, *Atmospheric Chemistry and Physics*, 14,
2198 2735-2756, 2014.

2199 Zender, C. S., Bian, H., and Newman, D.: Mineral Dust Entrainment and Deposition (DEAD) model: Description and 1990s
2200 dust climatology, *Journal of Geophysical Research: Atmospheres*, 108, 10.1029/2002jd002775, 2003.

2201 Zhang, K. M., Knipping, E. M., Wexler, A. S., Bhawe, P. V., and Tonnesen, G. S.: Size distribution of sea-salt emissions as a
2202 function of relative humidity, *Atmospheric Environment*, 39, 3373-3379, <https://doi.org/10.1016/j.atmosenv.2005.02.032>,
2203 2005.

2204 Zhang, L., Brook, J. R., and Vet, R.: A revised parameterization for gaseous dry deposition in air-quality models, *Atmos.*
2205 *Chem. Phys.*, 3, 2067–2082, 2003.

2206 Zhang, L., Gong, S., Padro, J., and Barrie, L.: A size-segregated particle dry deposition scheme for an atmospheric aerosol
2207 module, *Atmospheric Environment*, 35, 549-560, 2001.

2208 Zhang, Y., Bocquet, M., Mallet, V., Seigneur, C., and Baklanov, A.: Real-time air quality forecasting, part II: State of the
2209 science, current research needs, and future prospects, *Atmospheric Environment*, 60, 656-676,
2210 <https://doi.org/10.1016/j.atmosenv.2012.02.041>, 2012a.

2211 Zhang, Y., Bocquet, M., Mallet, V., Seigneur, C., and Baklanov, A.: Real-time air quality forecasting, part I: History,
2212 techniques, and current status, *Atmospheric Environment*, 60, 632-655, 2012b.

2213 Zilitinkevich, S. and Mironov, D. V.: A multi-limit formulation for the equilibrium depth of a stably stratified boundary
2214 layer, *Boundary-Layer Meteorology*, 81, 325-351, 1996.
2215